CHAPTER 1

INTRODUCTION

This chapter has been divided into three sections. The first focuses on the reasons for conducting this study, mainly consisting of the literature review, the motivation for the research as well as defining the problem statement. It also mentions the approach and methodology used to achieve the aims and goals mentioned, and finally discusses the research contributions. The second section is a general discussion into the multiple access methods and the various cellular standards. The section gives an overview and introduction to the past, present, near-future and future communication systems represented by first, second, third and fourth generation systems respectively. These communication systems are defined by the various agreed cellular standards and multiple access methods according to the International Telecommunications Union. Also, it especially focuses on the WCDMA system description, and in particular, an introduction to the WCDMA receiver and the channel effects associated with it. The last section gives an insight to the following chapters and the overall document structure.

1 AN OVERVIEW OF MULTIPLE ACCESS INTERFERENCE, MULTIUSER DETECTION AND INTERFERENCE CANCELLATION TECHNIQUES

The majority of 3G(Third Generation) cellular systems defined by IMT-2000 use WCDMA (Wide-band Code Division Multiple Access), as the basic radio access technology. According to Nilsson [1], the first generation analogue systems and the subsequent second generation digital systems are mainly oriented towards voice application traffic. Third generation CDMA-based systems represent a significant leap both in applications and capacity from the second generation narrowband CDMA systems. Studies based on performance improvement in 3G WCDMA have been carried out, with the proposal by Alam et al. [2], for the use of MUD and IC techniques to accomplish this. Falahati et al. [3], talked of the need to exploit the structure of MAI to apply MUD using appropriate algorithms, and concluded that due to the relatively low complexity of some IC schemes, they could easily be implemented.

According to Kang et al. [4], the MUDs could be classified as Linear MUDs (where a linear mapping or transformation is done to produce a new set of outputs as part of the iterative process), and Subtractive Interference Cancellation Detectors (where as part of the iterative process, an estimation of the interference is made before subtraction). These latter schemes of sub-optimum detectors differ from optimum detectors, (here schemes too computationally intensive), in that the receivers perform reliably under MAI with a reasonable computational complexity to ensure practical implementation. They can be divided into Successive Interference Cancellation (SIC), Parallel Interference Cancellation (PIC), and Zero-Forcing Decision-Feedback (ZF-DF) detector.

Additional studies, such as by Malik et al. [5], proposed the use of Hybrid Interference Cancellation (HIC) techniques that combined the advantages of both SIC and PIC. This was very important as far as this current study is concerned, in that it did indicate limitations in the latest assortment of IC schemes being investigated and being implemented. An overview is shown in figure 1-1.

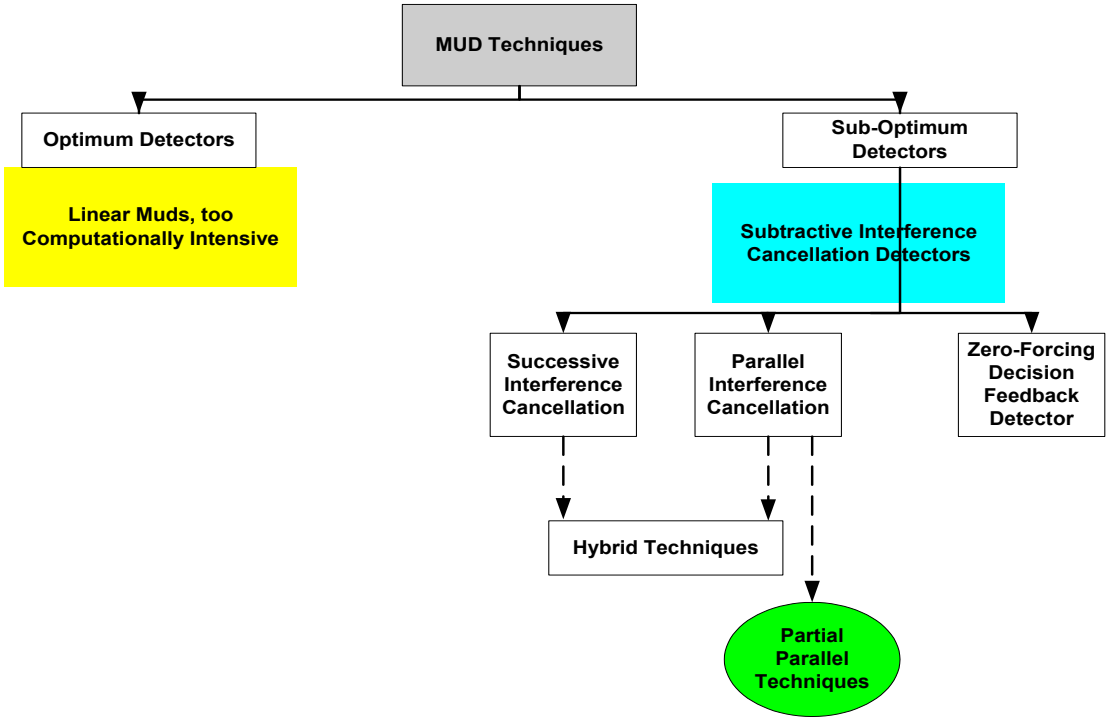

Figure 1-1 : Overview of MUD Techniques

The research of this current study focuses on a proposed hybrid cancellation scheme, in particular, a Partial Parallel Pipelined Multiuser Detector, (P^3MUD), which has come about by incorporating the two techniques of Renucci et al. [6] and Rajagopal et al. [7].

1.1 Motivation for Study and Problem Statement

The overviews and literature studies mentioned above have thus contributed to the overall reasons for conducting the current research study. Some of the most important and extensive research that was done previously was the optimal multiuser receiver algorithm for CDMA derived by Verdu [6]. This work has been used by many researchers as the foundation to their own work.

The original work focused on performing Maximal Likelihood Sequence Estimation (MLSE) over the entire duration of the received signal, followed by using the Viterbi Algorithm in decoding the entire received sequence of symbols within a trellis. This was in order to produce lowest probability of error. Unfortunately, this was a complex procedure with a receiver structure that could not be practically realised. Since then, research has focused on reasonably complex sub-optimal receiver algorithms and iterative detection techniques, Varanasi et al. [8]. These latter methods are the basis of this current study.

Thus the problem statement is centred on stating that, 'There are existing multiuser detection and interference cancellation techniques for processing the number of simultaneous users in a system, but there also appears to be a need to improve these techniques'. The aim of this current study is to take the advantages of the various existing MUD and IC schemes, and use them to formulate a new scheme. To further add, the improved scheme needs to be tested and compared against the existing ones to observe or measure the extent of improvement, if at all. To achieve these aims, the guidelines mentioned next were followed.

1.1.1 Study Guidelines To Achieve Research Aims and Goals

The study is divided into four main modules :

- The Theoretical stage – here, research into the current hybrid IC schemes and related theory and algorithm failures/successes is made.
- The Formulation Stage - where new algorithms and eventually methodologies are adapted and from the current work done.
- The Practical Stage –where the theory is adapted for practical testing. That is, the performance of the hybrid IC is investigated in terms of factors such as complexity of the algorithm used, delay, average Bit Error Rate (BER)…,etc.

- The Conclusion Stage –here, critical evaluation of the proposed Hybrid IC scheme (as compared to existing ones) is made.

1.1.2 Research Contributions

This dissertation analyzes the two research streams which both offer improvements to the parallel interference cancellation receiver originally proposed by Varanasi and Aazhang [8]. The main research contributions of this current study can be summarised as:

- Identifying and proposing the use of a universal Soft Cancellation Factor, SCF_{UNV} and a compensator mechanism.
- Providing a method of determining SCF_{UNV} .
- Incorporating SCF_{UNV} into a conventional parallel interference cancellation algorithm, such as the Bit-streaming parallel interference canceller.
- From the encouraging BER output results, proposing a reduction in the number of algorithm processing stages from three to two, i.e., proposing the 2-stage P^3MUD .
- Optimizing parts of the original code and extending the simulation test-bed to include, a dual output single-screen GUI.

The first stream or technique focuses on the performance gains of interference cancellation over conventional CDMA detection. The multistage parallel interference cancellation CDMA receiver structure proposed by Striglis, et al. [6], consists of a conventional receiver for the first stage of detection, followed by one or more interference cancellation stages. Buehrer et al. [9], discovered that the second stage amplitude estimates were affected by a bias which was in direct proportion to the number of interfering users. This bias had harmful effects as it acted to the detriment of the system BER, particularly under severe loading conditions. When the bias magnitude is small at low system loads, the derived analytical BER is consistent with the simulation BER. In contrast, as the system load grows, there exists a disparity between analytical and simulation BER. The greater bias magnitude results in the simulated BER being less than the analytical rate. The bias reduction exercises that have followed have considered using first stage amplitude estimates, for use in the second stage interference cancellation. The rationale of this

method is based on the premise that if interference estimates are unreliable due to biasing, the partial use of these estimates as opposed to full use tends to improve the performance with lower BER.

This forms the platform for the simulation experiments, Buehrer et al. [9], in finding the optimal scaling factors SCFs, (Soft Cancellation Factors) for a given system. It was found that the SCF varied almost linearly with the system loading: i.e. the greater the system loading, the smaller the SCF and the lower the BER. It is from this background that the contributions of this dissertation are defined. The universal SCF, SCF_{UNV} takes into account the effects of loading at different stages: i.e. the analytically obtained low BER properties across the system loading spectrum are identified and combined in producing this universal SCF. This universal SCF is then used in improving the overall parallel interference cancellation algorithm with the assistance of the SCF_{UNV} Compensator Mechanism, (SCM), as indicated by the BER comparisons. The Bit-Streaming Pipelined Multiuser Detector of Rajagopal [7], was modified to accomplish this. The simulations also indicate the possibility of having at least two cancellation stages after the Matched Filter process as opposed to the conventional three stage algorithm. Comparisons of the improved algorithm simulations with those of the standard parallel cancellation methods are shown and conclusions made.

1.2 Overview of Multiple Access Methods

This is summarised by the diagram in Figure 1-2.

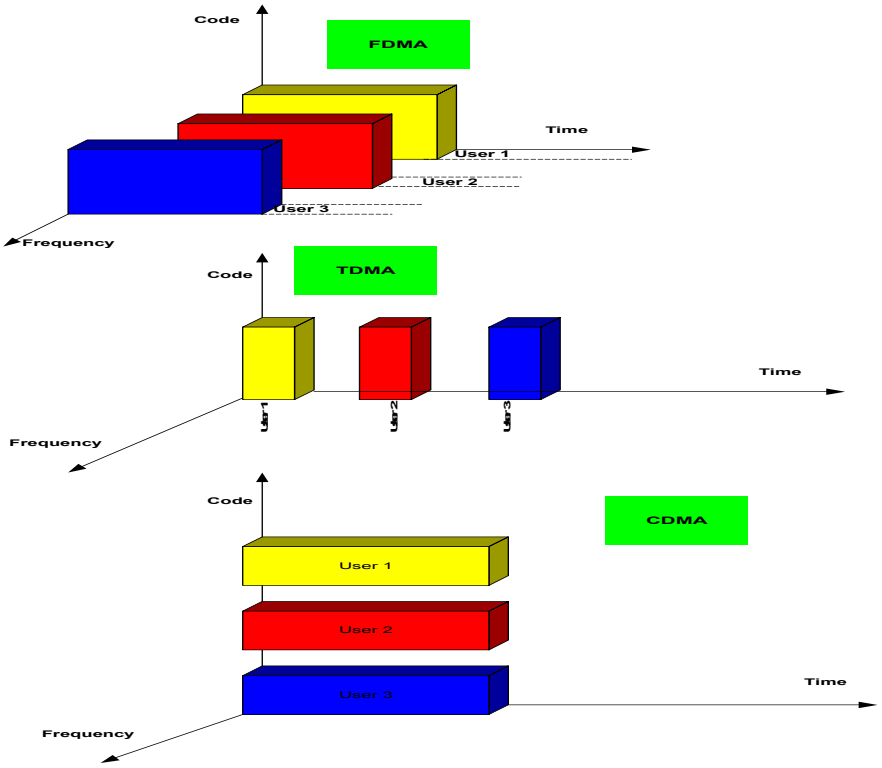

Figure 1-2 : Overview of Multiple Access Methods

In FDMA [10], each transmitter is assigned a distinct frequency channel so that receivers can descriminate among them by tuning to the desired channel. It was deployed in the first generation cellular systems such as the Advanced Mobile Phone Service (AMPS), the Extended European Total Access Cellular System (ETACS), and the Nippon Telephone and Telegraph (NTT) system. TDMA was the most commonly used multiple access technique in early second generation cellular systems. Here, TDMA separates users by assigning each user a short time slot during which only that user's signal is transmitted; during the next time slot another user's signal is transmitted and so forth.

Second generation systems include the Groupe Special Mobile (GSM) standard (which is a TDMA/FDMA system), the Digital Cellular (USDC) standard (also known as the Intermediate Standard-54, or IS-54), and the Pacific Digital Cellular (PDC) standard.

CDMA was the competitor to TDMA that emerged in later second generation cellular systems. CDMA standard is known as Intermediate Standard-95 or IS-95, and is based upon spread spectrum technology. In contrast to FDMA and TDMA where users are orthogonalized along frequency and time, respectively, CDMA signals all overlap in both time and frequency, but are distinguishable by their signature codes (i.e. the codes in Code Division Multiple Access). Here, each user is assigned a unique high rate signature code which isolates it from all other users. For each user, the code signal multiplies the data signal, and since the code rate is much higher than the data rate, the resulting signal bears a higher rate and hence a "spreaded spectrum" compared to the data rate, Scholtz [11]. A timeline diagram on the introduction of the standards and technologies is shown in Figure 1-3.

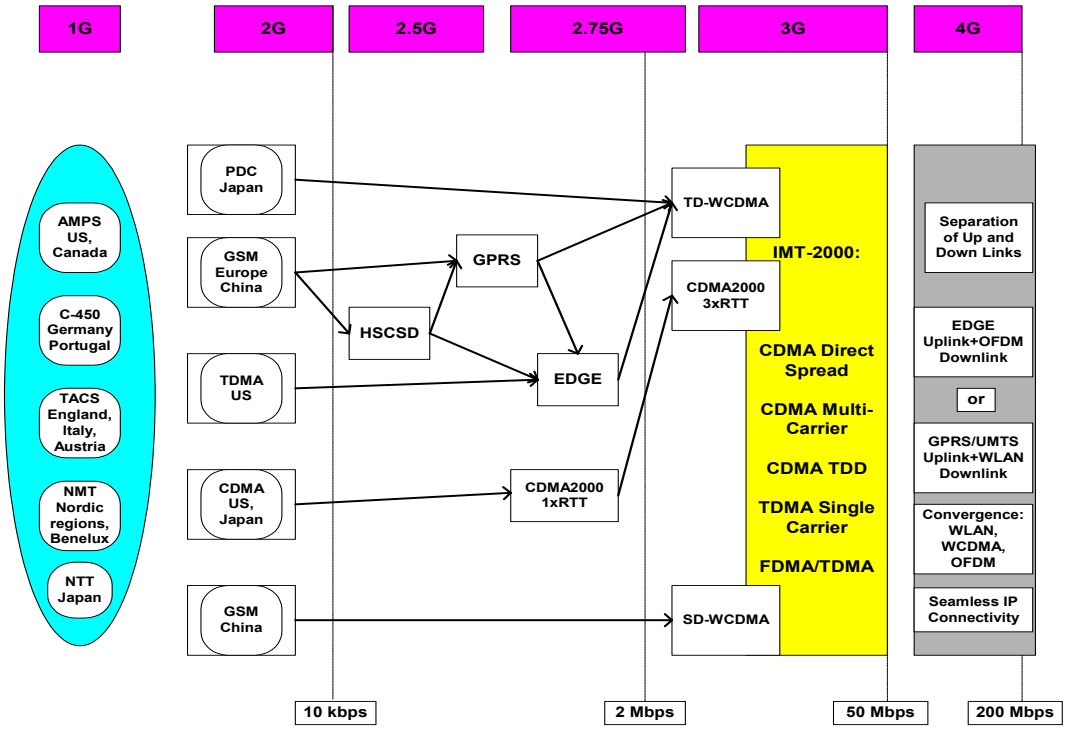

Figure 1-3 : Timeline diagram of introduction of analogue/digital communication standards and technologies.

Figure1-3, also indicates intermediate standards such as HSCSD, GPRS, EDGE and CDMA2000 1xRTT, which have been introduced with two main advantages:

- Providing alternative routes for cellular service providers to migrate from 2G to 3G services, usually on a "Pay as you Grow" basis,

- Introducing pre-3G data rates to users as a form of gauging the forecasted demand for 3G services and handsets.

1.2.1 Overview of Cellular Standards

The aim of the Personal Communications industry is currently focusing on the implementation and enhancement of third generation systems in different parts of the world. Optimisation of the second generation systems is seen as an important challenge by the current cellular service providers the world-over, especially by those that have tight financial budgets. Research is also underway on future generation (4^{th} generation) systems, widely favoured to be fully IP-based [12]. The life-cycle of the development of the past and present generation communications systems is still far from a complete circle, as advances in technology indicate the importance of these systems as platforms to launch future systems, and also the fact that they can still be optimised to offer improved performance, quality and grade of service. Thus, network performance monitoring and optimisation is being promoted by both equipment vendors and cellular network service providers, especially those that need to recoup the costs incurred when they invested in 3G licences.

The ITU requires that IMT-2000 (3G) networks, among other capabilities, deliver improved system capacity and spectrum efficiency over the 2G systems and supports data services at a minimum transmission rates of 144 kb/s in mobile (outdoor) and 2 Mb/s in fixed (indoor) environments. Figure 1-4, shows the five radio interfaces approved for IMT-2000 standards as part of the ITU-R M[1].1457-2-200304 Recommendation [13].

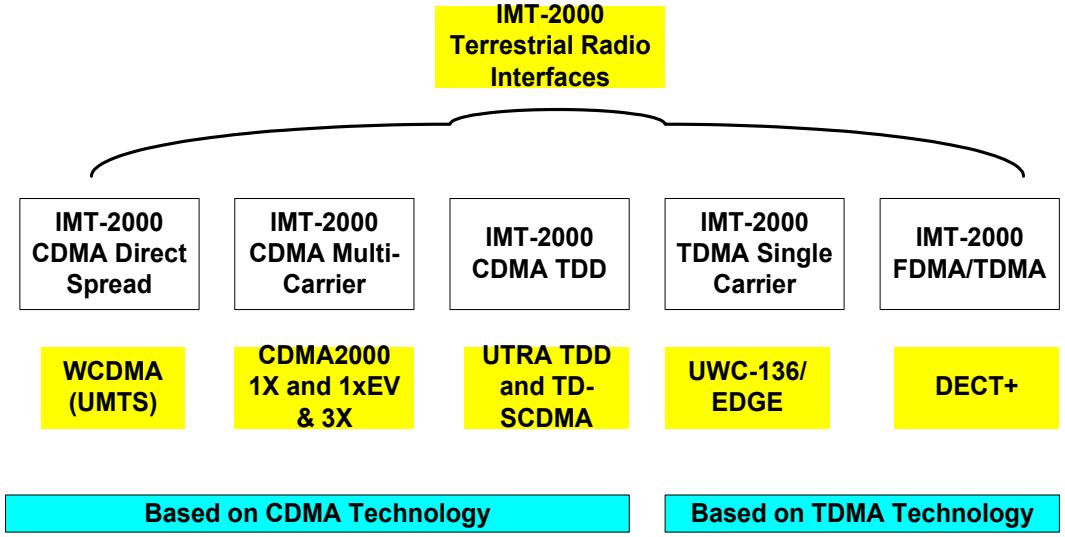

Figure 1-4 : The IMT-2000 Terrestrial Radio Interfaces

Since the 1990s, the wireless telecommunications sector has seen the standardization of third generation mobile communications systems in all major regions of the world. The Universal name for 3G is IMT-2000, with the 3GPP(2) branch as the joint standardisation project of the standardisation bodies from USA, Japan, Europe, Korea and China. The European ETSI based 3G systems go under the name of UMTS (Universal Mobile Telecommunications System), and use UTRA as the WCDMA Radio Interface, see 3GPP TS 25.211 [14] and ETSI TS 125 221[15]. The aim of these systems is to govern the introduction of high-rate data services by extending the services provided by current second generation systems such as GSM, PDC, IS-136, and IS-95. The main applications for these high-rate data services will be wireless packet transfer, as well as circuit-switched services such as video. WCDMA has been widely favoured as the basic radio-access technology for UMTS/IMT-2000 in both Europe and Japan. Compared to second generation narrowband CDMA, the WCDMA radio interface offers significant improvements, in addition to the support of higher-rate services. These include: improved coverage and capacity due to a higher bandwidth and coherent uplink detection; support of inter-frequency handover necessary for high-capacity Hierarchical Cell Structures (HCS); support for capacity improving technologies such as adaptive antennas and multi-user detection; as well as support for a fast and efficient packet-access protocol.

WCDMA supports two basic modes of operation: Frequency Division Duplex (FDD) and Time Division Duplex (TDD). In the FDD mode, separate 5 MHz carrier frequencies are used for the uplink and downlink respectively, whereas in TDD only one 5 MHz band is time-shared between uplink and downlink. Uplink is the connection from the mobile to the base station, and downlink is that from the base station to the mobile. The TDD mode is added to operate in the unpaired spectrum allocations of the ITU IMT-2000 systems. The multiple access method used for WCDMA is DS-CDMA. The base station synchronisation is of asynchronous type, with a chip rate of 3.84 Mcps and a frame length of 10ms. This standard offers multiple services with different quality of service requirements multiplexed on one connection. The multirate concept is achieved through variable spreading and the use of multiparallel codes. Coherent detection is offered using pilot symbols or a common pilot. Multiuser detection and smart antennas are supported by the standard, which is a big leap in an attempt to introduce system-improving techniques as compared to the second generation systems.

Considering the IS-95 standard, the bandwidth of the CDMA signal is 1.25 MHz, and that of WCDMA 5 MHz. The allocation of bandwidth in WCDMA in the time-frequency-code space is shown in Figure 1-5 [16].

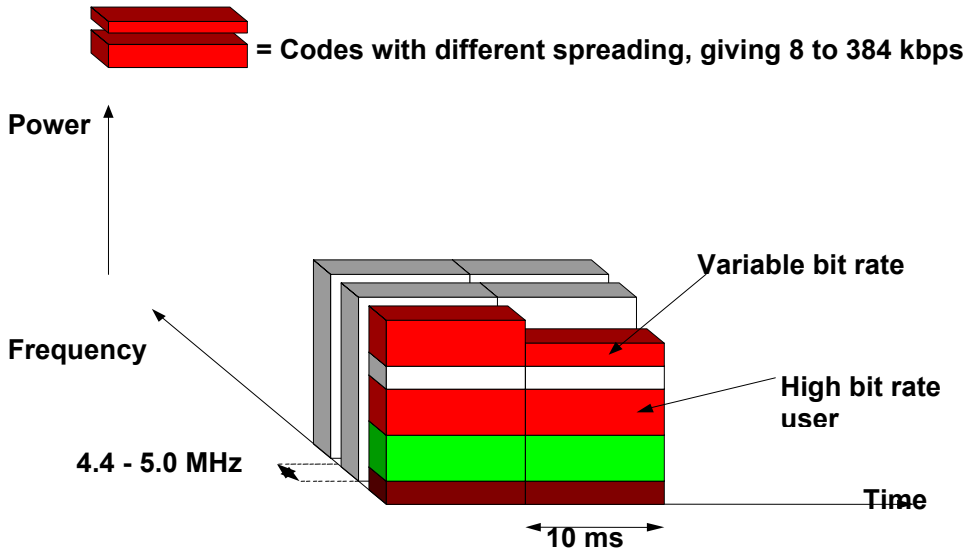

Figure 1-5 : Bandwidth allocation in WCDMA in the time-frequency-code space

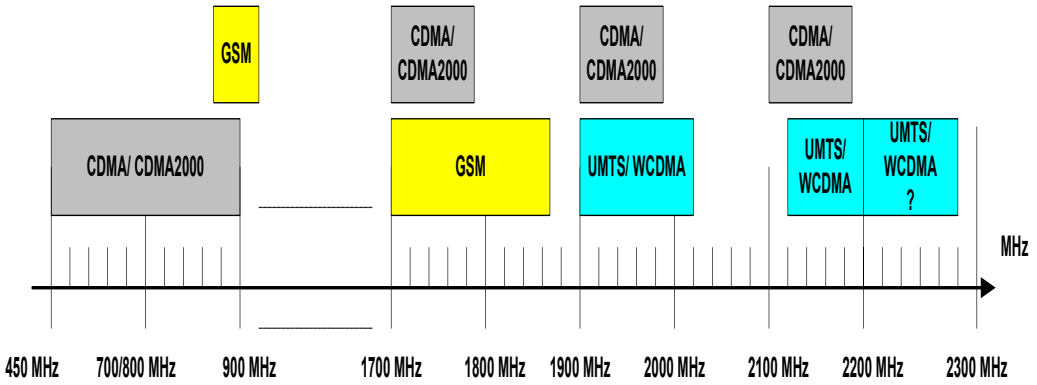

Figure 1-6 : Spectrum use for CDMA, GSM and WCDMA systems

1.2.2 WCDMA System Description

An extensive summary of WCDMA systems is given in Holma et al. [16].

The *Direct-Sequence characteristic* as well as supporting features such as variable spreading factor as well as multicode connections, gives WCDMA (a wideband Direct-Sequence Code Division Multiple Access or DS-CDMA system), the ability to support very high bit rates such as 2 Mb/s and above. The user information bits are spread over a 5MHz bandwidth by multiplying the user data with quasi-random bits (called chips) derived from CDMA spreading codes.

The *Wideband characteristic* is a result of the chip rate of 3.84 Mcps used leading to a carrier spacing of approximately 5 MHz. The advantage of this, is the ability to support high user data rates, as well as posses certain performance benefits, such as increased multi-path diversity.

The *Bandwidth on Demand (BoD) characteristic* is well supported for highly variable user data rates. Each user is allocated frames of 10ms duration, during which the user data rate is kept constant. However, the data capacity among the users can change from frame to frame as shown in Figure 1-5. This can be made to achieve optimum throughput for services such as packet data.

The *optional non-global time reference characteristic* of WCDMA is due to the fact that it supports the operation of asynchronous base stations,(unlike the synchronous IS-95 system requiring a global time reference, such as GPS). In indoor radio base station design, where micro base stations are deployed, the lack of GPS signals make this characteristic an implementation advantage.

The *uplink coherent detection characteristic* of WCDMA results in an overall increase of coverage and capacity on the uplink.

The *advanced receiver concepts characteristic* of the WCDMA air interface, means CDMA receiver concepts, such as multiuser detection and smart adaptive antennas, can be deployed by the network operator as a system option to increase capacity and/or coverage. Such concepts are hardly used in second generation systems.

The *interoperability characteristic* with systems such as GSM means handovers between GSM and WCDMA are supported. This very important requirement has been accomplished by Alsenmyr et al [17], who in their procedure to overcome the challenges of interworking between WCDMA and GSM, use dual-mode mobile terminals. This entails compressed mode channel measurements where gaps or idle spaces are created in time so that WCDMA mobile terminals can perform measurements on GSM cells.

Cell re-selection between WCDMA and GSM is affected where the WCDMA and GSM cells are ranked together according to signal strength and monitoring the fall in serving cell quality below a certain threshold. The WCDMA-to-GSM cell change order is then initiated by the network, based on mobile terminal measurement reports, and finally the actual handover process between WCDMA and GSM [17] takes place.

A short mention of the types of spread spectrum techniques is in order here, as they give an insight into the transmitted signal (spreading) encapsulation techniques. The received signal (de-spreading) decapsulation techniques are the inverse of this.

There are four principle types of spectrum spreading techniques, Direct Sequence, Frequency Hopped and Time Hopped and Chirp.

Direct Sequence Spread Spectrum (DS-SS) based systems will be the focus in this current study. A detailed explanation of the various techniques can be found in Rennuci, [6].

1.2.3 Introduction to WCDMA Receiver Architecture

The WCDMA receiver architecture is based on that of the CDMA receiver. It has been suggested by ETSI [18] that the Rake receiver be employed in the first generation UMTS handsets due to its efficiency and affordable single-user detection. The Rake receiver structure is derived directly from the multi-path channel model [19], ideally with one Rake finger being allocated to each multi-path, in order to maximise the amount of received signal energy. Thus, in each finger of the Rake receiver, the amplitude, the phase shift, and the propagation delay of the selected multi-path have to be compensated for, in a task called synchronisation [18]. The basic structure and operation process of the RAKE receiver is described in Chapter 2. The WCDMA Channel is basically the set of channels transmitted between the base station and mobile stations within a given WCDMA frequency assignment, which is typically a 5MHz segment of spectrum. Two important channel entities, *Multi-path propagation* and *Multiuser Interference* that occur and affect the WCDMA system performance are mentioned next.

1.2.4 Channel Effects

1.2.4.1 Multi-path Propagation

Multi-path propagation is characterised by multiple reflections, diffractions and attenuation of the signal energy, i.e. by natural obstacles such as buildings, hills,..etc. Consequently, there are two effects which arise due to this, if it is assumed that the duration for a chip at 3.84 Mcps is 0.26us. Thus, if the signal energy pertaining to a single chip of a WCDMA waveform arrives at the receiver, when the time difference of the multi-path components is at least 0.26us, the WCDMA receiver can separate those multi-path components and combine them coherently to obtain multi-path diversity [16]. This indicates the advantage that 5MHz WCDMA has over IS-95 in that it can provide multi-path diversity in small cells, by virtue of the former systems' higher temporal discrimination ability.

The other occurrence is of signal cancellation (*fast fading*), which arises as the receiver moves across even short distances, due to the presence of many paths of nearly equal lengths for a certain time delay position. Countermeasures used against fading in WCDMA are:

- Using *multiple RAKE fingers* allocated to those delay positions on which significant energy arrives, to combine the delay dispersive energy.
- Mitigating the fading signal power problem by using *fast power control* and the inherent diversity reception feature of the RAKE receiver.
- Adding redundancy and time diversity, (help receiver recover user bits), by using *strong coding and interleaving* and *retransmission* protocols.

However, it must be noted that the expected multi-path propagation conditions for UMTS are less than ideal. This is due to the orthogonal spreading codes suffering severely because of loss of orthogonality brought about by multi-path propagation. This results in MAI which reduces the performances of Rake-based receivers. Studies such as by Knoche et al, [20] are looking for ways to mitigate this MAI effect.

1.2.4.2 Multiuser Interference (MUI)

Another receiver phenomenon is that of interference, specifically Multiuser Interference [6]. The greater the level of interference, the less capacity the system can support. It has been found that the Bit-Error-Rate (BER) in CDMA increases approximately linearly with the percent of capacity overload [6], and any suppression of interference translates linearly into a capacity increase. This observation holds true for WCDMA systems. Interference-free CDMA (WCDMA) would be possible if the codes were ideal, but this is hampered by the practical impossibility to be able to design perfectly orthogonal codes for an asynchronous uplink. Ideally, if the codes were all orthogonal, (correlation value = 0), and there would be no MAI term. However, since in practice most channels contain some degree of asynchronism, it is not possible to design codes that maintain orthogonality over all possible delays.

So instead we look for codes that are nearly orthogonal, i.e., have as low correlation as possible, (relative to autocorrelation), Moshavi, [21]. Another inhibitor is the near-far problem which could still harm performance despite the design of nearly optimal PN codes. Thus, more effort has been focused into research and designing of WCDMA receiver algorithms capable of reducing the effects of interference, and in particular, the effect of interference due to multiple access by several simultaneous users in the uplink of a WCDMA system.

1.3 Organisation of Dissertation

The structure of the dissertation is as follows.

Chapter 2 focuses on the 3GPP2 Physical Layer Standard for CDMA and WCDMA. The WCDMA channel structure as well as spread spectrum systems are discussed. The multiuser detectors as well as the various receiver structures are encountered.

Chapter 3 deals more with the PIC techniques, especially the need to use soft cancellation to mitigate bias. The initial stages (Methodology I), required to determine the Universal SCF, are mentioned. This is centred around obtaining the optimal SCFs.

Chapter 4 presents the probability of error analysis for conventional as well as partial interference cancellation. The second part (Methodology II), which carries on from Chapter 3, Methodology I, in the Universal SCF determination, is also mentioned here. This involves analysing the optimal SCFs and deriving the Universal SCF.

Chapter 5, focuses on the background of the proposed Partial Parallel Pipelined Multiuser Detector or P^3MUD. Channel estimation and pipelined Multistage Detection of the conventional pipelined multiuser detector is discussed, as well as the description of the system model.

Chapter 6, Brings together the two main lines of research of this study, in order to incorporate the respective advantages to create the P^3MUD algorithm. The simulation software implementation is mentioned, as well as Methodology III, which describes the method used to analyse the algorithm. The compensator mechanism is also mentioned.

Chapter 7, Discusses the proposed 2-Stage P^3MUD algorithm implementation as a result of the analysis work in Chapter 6. It motivates for a 2-Stage implementation as opposed to a 3-Stage algorithm system.

Chapter 8, Consists of the Summary, Conclusions and Recommendations. Possible future work or improvements as regards the proposed P^3MUD Algorithm are mentioned.

CHAPTER 2

WCDMA PHYSICAL LAYER & SPREAD SPECTRUM SYSTEM

The 3GPP2 Physical Layer Standard for CDMA Spread Spectrum Systems is briefly described as an introduction to the WCDMA Channel structure for a system operating in FDD mode. This focuses on the spreading and modulation operation for the Dedicated Physical Channels (DPCH), including the uplink and downlink data structure descriptions. The spreading and scrambling codes used in mainly the uplink are mentioned, followed by a comparison description of the WCDMA air interface features. The mathematical description for DS-SS transmitter and receiver systems is given, with mention of the Matched Filter, Correlator and RAKE receivers. The chapter ends with a short discussion on the various multiuser detectors.

2 3GPP2 PHYSICAL LAYER STANDARD FOR CDMA SPREAD SPECTRUM SYSTEMS

The physical layer standard described here for CDMA2000 spread spectrum systems is based on the 3GPP2 specification C.S0002-C, [22]. It describes the physical layer requirements for mobiles and base stations operating in the CDMA mode. A mobile station complying with these requirements will be able to operate with CDMA base stations complying with this Standard. Thus, the physical layer may be defined as the part of the communication protocol between the mobile station and the base station that is responsible for the transmission and reception of data. The physical layer in the transmitting station is presented a frame and transforms it into an over-the-air waveform. The physical layer in the receiving station transforms the waveform back into a frame. In regards to this study, the reverse CDMA channel is of interest, and is the CDMA channel from the mobile to the base station. From the base station's perspective, the Reverse CDMA Channel is the sum of all mobile station transmissions on a CDMA frequency assignment. An overview of the modulation characteristics is mentioned next.

2.1 Reverse CDMA Channel Signals

The Reverse CDMA channel is made up of portions of other channels as described in Figure 2-1. This shows the structure of the code channels transmitted by a mobile station. The spreading rates 1 and 3 refer to "1X" and "3X" respectively. Here, Spreading Rate 1 Reverse CDMA Channel uses a single direct-sequence spread carrier with a chip rate of 1.2288 Mcps, and Spreading rate 3 Reverse CDMA Channel uses a single direct-sequence spread carrier with a chip rate of 3.6864 Mcps, 3GPP2 [22]. The signals transmitted on the Reverse CDMA Channel are governed by the six allowable radio configurations.

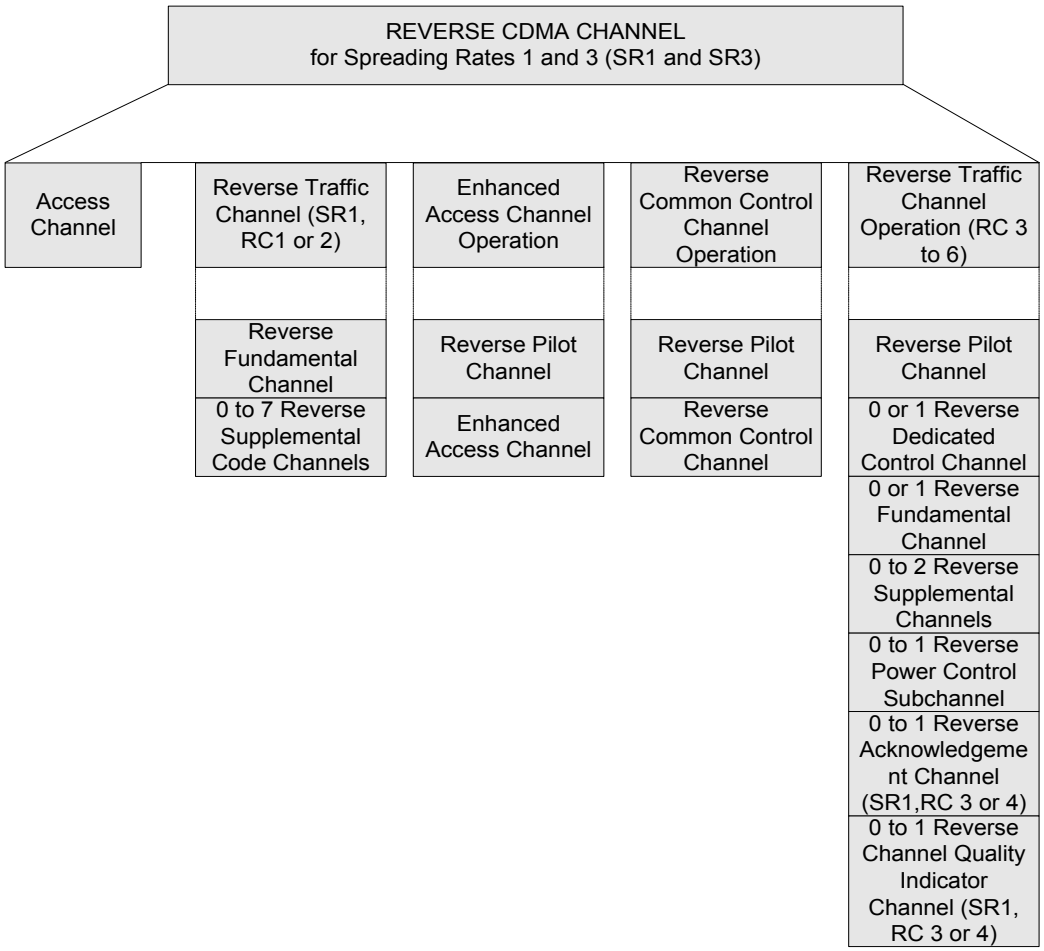

Figure 2-1: The Reverse CDMA Channels received at the base station.

The Radio configurations also govern the orthogonal modulation and spreading on the reverse channels.

2.1.1 Orthogonal Modulation and Spreading

According to 3GPP2, [22], when transmitting on the Access Channel or the Reverse Traffic Channel with Radio Configurations 1 and 2, the mobile station uses 64-ary orthogonal modulation. Conversely, when transmitting on the enhanced Access Channel, the Reverse Common Control Channel, the Reverse Acknowledgement Channel, the Reverse Channel Quality Indicator Channel, or the Reverse Traffic Channel in Radio Configuration 3 through 6, the mobile station employs orthogonal spreading. Table 2-1, indicates the Walsh functions that are applied to the Reverse CDMA Channels.

Channel Type	**Walsh Function**
Reverse Pilot Channel	W_0^{32}
Enhanced Access Channel	W_2^8
Reverse Common Control Channel	W_2^8
Reverse Dedicated Control Channel	W_8^{16}
Reverse Acknowledgement Channel	W_{16}^{64}
Reverse Channel Quality Inicator Channel	W_{12}^{16}
Reverse Fundamenta Channel	W_4^{16}
Reverse Supplement Channel 1	W_1^2 or W_2^4
Reverse Supplement Channel 2	W_2^4 or W_6^8

Table 2-1: Walsh Functions for the Reverse CDMA Channels

The Walsh function W_n^N represents a Walsh function of length N that is serially constructed from the $n-th$ row of an $N \times N$ Hadamard matrix, where the zeroth row is Walsh function 0, the first row being Walsh function 1, etc. Thus, a code channel that is spread using Walsh function n from the $N-ary$ orthogonal set $(0 \le n \le N-1)$ shall be

assigned to Walsh function W_n^N. The spreading sequence repeats with a period of $N/1.2288\mu s$ for Spreading Rate 1, and with a period of $N/3.6864\mu s$ for Spreading Rate 3.

2.1.2 Direct Sequence Spreading

It is specified that Direct sequence spreading using the long code shall be applied to Access Channel and the Reverse Traffic Channel with Radio Configurations 1 and 2, 3GPP2, [22]. For the Access Channel, this spreading operation involves modulo-2 addition of the 64-ary orthogonal modulator output stream and the long code, and for the Reverse Traffic Channel with Radio Configurations 1 and 2, this spreading operation involves modulo-2 addition of the data burst randomizer output stream and the long code. The long code is specified to be periodic with period 2^{42}-1 chips. Each PN chip of the long code shall be generated by the modulo-2 inner product of a 42-bit mask and the 42-bit state vector of the sequence generator.

2.1.3 Quadrature Spreading

The Access Channel and the Reverse Traffic Channel with Radio Configurations 1 and 2 are spread in quadrature where the direct sequence spreading output is modulo-2 added to an in-phase and quadrature-phase sequence. The I and Q components of the spreading sequence are periodic with a period of 2^{15} chips, and after quadrature spreading, the Q-channel data shall be delayed by half a PN chip time (406.901ns) with respect to the I-channel data. With regards to the Enhanced Access Channel, the Reverse Common Control Channel, the Reverse Acknowledgement Channel, the Reverse Channel Quality Indicator Channel, and the Reverse Traffic Channel with Radio Configurations 3 through 6, the I-channel data and Q-channel data shall be multiplied by a complex spreading sequence before baseband filtering as shown in figure 2-2.

Figure 2-2 shows the I and Q mapping for the Reverse Pilot Channel, Enhanced Access Channel, Reverse Common Control Channel, Reverse Acknowledgement Channel, Reverse Channel Quality Indicator Channel, and Reverse Traffic Channel with Radio Configurations 3 and 4.

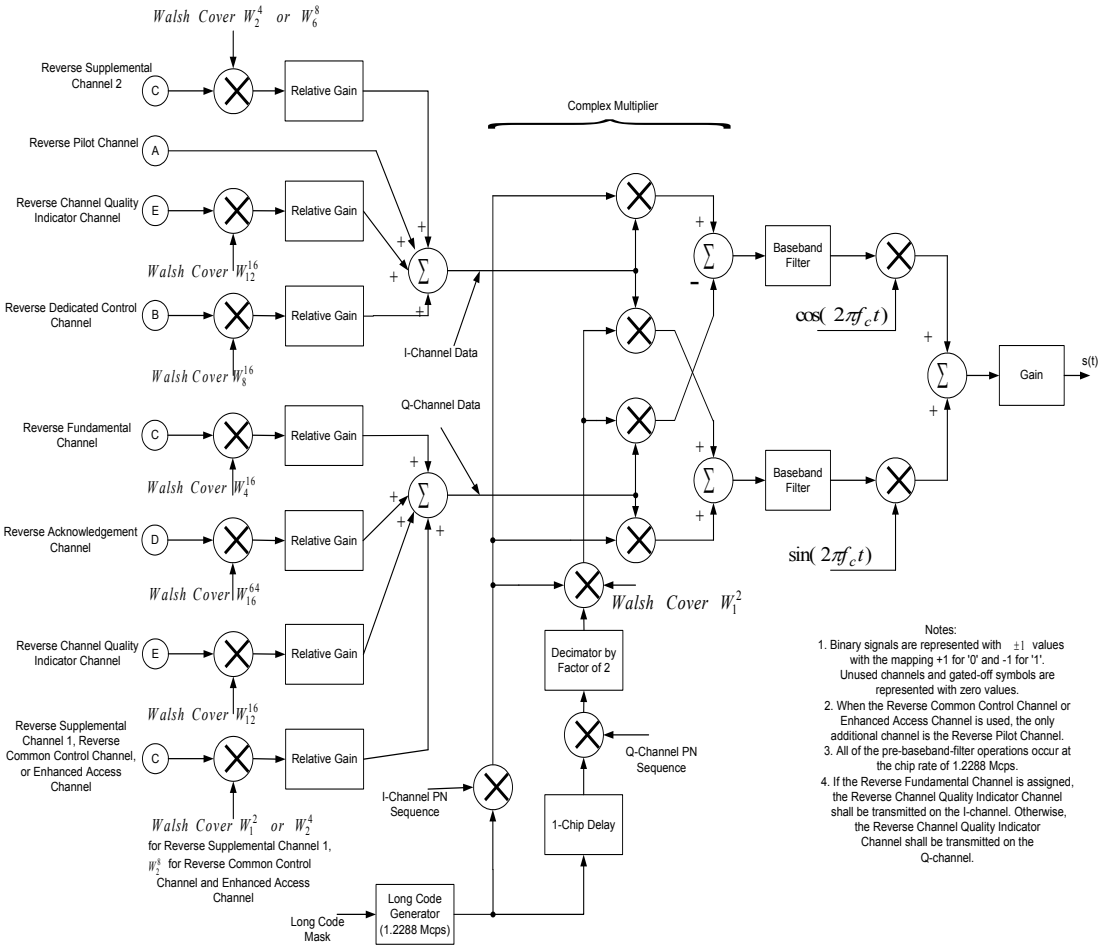

Figure 2-2: I and Q Mapping for the Reverse CDMA Channels for Spreading Rate 1

The detailed specifications and explanations can be found in 3GPP2 C.S0002-C, [22], but some of the entities will be mentioned here. The *Pilot Channel* is an un-modulated, direct-sequence spread spectrum signal transmitted by either the base station or mobile station, whose function is to provide a phase reference for coherent demodulation. It can also provide a means for signal strength comparisons between base stations for determining when to handoff. During normal operation, different base stations are identified by different pilot PN sequence offsets.

These may be described as a pair of modified maximal length PN sequences used to spread the forward CDMA Channel and the Reverse CDMA Channel. Another important entity is the *Power Control Bit*. This is a bit sent on the Forward Power Control Subchannel, Reverse Power Control Subchannel, or Common Power Control Subchannel to signal the mobile or base station to increase or decrease its transmit power.

WCDMA which has evolved from CDMA has similar physical layer channel processes (spreading and modulation), and channel definitions as seen in the following description.

2.2 WCDMA Channel Structure

The WCDMA Structure can be described according to Rajagopal et al. [7]. Layer 1 and 2 are according to the ISO OSI 7-layer Model, 3GPP, [23]. The uplink and downlink both define two dedicated physical channels:

- Dedicated Physical Data Channel (DPDCH), to carry dedicated data generated at layer 2 and above.
- Dedicated Physical Control Channel (DPCCH), to carry layer 1 control information.

As each connection is allocated one DPCCH , one or several DPDCHs, as well as common physical channels defined as:

- Primary and secondary Common Control Physical Channels (CCPCH) to carry downlink common channels
- Synchronization Channels (SCH) for cell search
- Physical Random Access Channel (PRACH)

The Frame Structure for the WCDMA data Transmission is depicted below, Rajagopal [24].

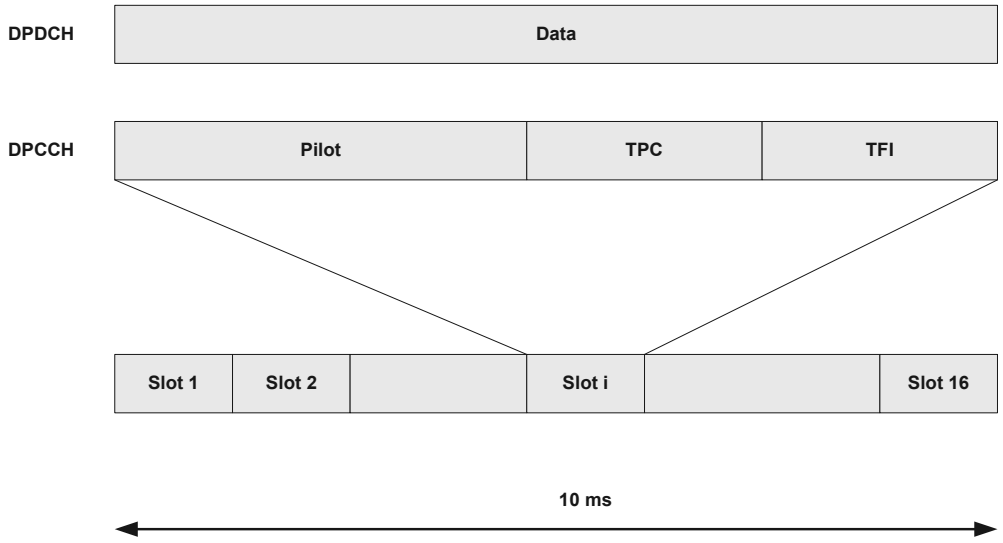

Figure 2-3: Transmission frame structure for the Uplink Data and Control Channels

The data is multiplexed with the control channel in a dual-channel QPSK form. The DPDCH is QPSK-multiplexed with the DPCCH. The actual data transmission is done on the DPDCH, while the DPCCH is used for sending control information.

The control information consists of the Pilot bits, which are used for channel synchronization and estimation, the transmit power control (TPC) commands and an optional Transport Format Indicator (TFI), which contains the data rate information. The data rates achieved by Rajagopal et al. [7], for a typical chip rate of 4.096 Mcps and varying spreading factors between 4 and 256, are shown in Table 2-2.

Spreading Factor (N)	Bits Per Frame	Data Rates (Bits per second)
4	10240	1 Mbps
32	1280	128 Kbps
256	160	16 Kbps

Table 2-2: Proposed Data Rates for 3G Communication Systems

2.2.1 WCDMA Uplink Spreading and Modulation

In general, 3G [25], WCDMA applies a two-layered code structure consisting of orthogonal spreading codes and pseudo-random scrambling codes. The spreading is performed using channelization codes in order to transform every data symbol into a number of chips. The resultant is an increase in the signal bandwidth. The orthogonal codes provide a measure of orthogonality between the different spreading factors. The aim of scrambling is to separate different cells in the downlink, whilst in the uplink, it is of the different users. Uplink signal processing is the main focus of the study, and a brief explanation of the spreading and modulation techniques is given.

The data modulation in the uplink for both the DPDCH and DPCCH is Binary Shift Keying (BPSK). Here, the modulated DPCCH is mapped onto the Q-channel, while the first DPDCH is mapped onto the I-channel, resulting in subsequently added DPDCHs mapped alternatively to the I or the Q-channel. Spreading Modulation (dual channel QPSK) is applied after data modulation and before pulse shaping. Spreading modulation consists of two complementary operations. The first one is spreading where each data symbol is spread to a number of chips given by the spreading factor, to increase the bandwidth of the signal. The second operation is scrambling where a complex valued scrambling code is applied to the spread signal [7].

2.2.1.1 WCDMA Uplink Spreading

The spreading (scrambling) codes used in the uplink are either short or long, (3G), [25]. The short codes are primarily used to easily implement advanced multiuser receiver techniques, otherwise, the long spreading codes are used. The types of short codes are S(2) codes of length 256, whilst the long codes are Gold sequences of length 2^{41} which are truncated to form a cycle of a 10-ms frame. The IQ-code multiplexing used in the uplink results in parallel transmission of two channels (data and control), thus focus is typically

trained on the modulated signal constellation and the related peak-to-average power ratio or crest factor. The uplink spreading of the DPCCH and DPDCH channels is accomplished using different channelization codes, i.e, one DPCCH and up to six parallel DPDCHs can be simultaneously transmitted. The channelization process is followed by the weighting of the real-valued spread signals by gain factors. This is different for DPCCH and DPDCHs, but, is the same for all DPDCHs. This transformation of the signal from real to complex is the required process before scrambling by the complex-valued scrambling code, (long or short) [25].

The two common physical channels, PRACH (Physical Random Access Channel) and PCPCH (Physical Common Packet Channel), also undergo spreading. The PRACH structure consists of the preamble part (complex-valued code), and message parts (data and control), which are spread by similar channelization codes. After the channelization process, the spread signals are weighted by gain factors. The scrambling is performed by a 10-ms long complex valued scrambling code. The PCPCH structure is similar to that of PRACH, but the control and data are spread by different channelization codes. Similarly, after channelization, the spread signals are weighted by gain factors, and scrambling is similar to that of PRACH.

2.2.1.2 WCDMA Modulation

The complex-valued chip sequence generated by the spreading process is QPSK modulated, with a similar modulation principle employed in both the uplink and downlink. The pulse shaping is root-raised cosine with roll-off factor of 0.22. This is the same for the mobile and base stations. This process of employing complex scrambling code with spreading modulation is usually termed as Hybrid Phase Shift Keying (HPSK) [7], and thus reduces the peak-to-average power of the mobile station by generating the complex scrambling sequence in a special way. The 3G systems use HPSK, also known as Orthogonal Complex Quadrature Phase Shift Keying (OCQPSK), to reduce the peak-to-average power ratio of the signal. HPSK is a variation of basic complex scrambling that

eliminates zero-crossings for every second chip point. It accomplishes this by using a specific repeating sequence (or function) as the scrambling signal and by choosing specific orthogonal codes to spread the different channels. The setting of the spreading factor for the control channel to the highest value of 256 takes advantage of the highest possible processing gain by improving the noise immunity at the control channel, at the expense of a reduction of data throughput rate.

A summary of the WCDMA Modulation parameters is shown in Table 2-3 [7].

Spreading Modulation	**Dual Channel QPSK for Uplink**
	Balanced QPSK for Downlink
Data Modulation	**BPSK for Uplink**
	QPSK for Downlink
Spreading	**OVSF codes**
	4-256 spreading factor for Uplink
	4-512 spreading factor for Downlink
Scrambling	**Complex Scrambling**
Frame Length	**10 ms**
Chip Rate	**3.84 Mcps**
Pulse Shaping	**Raised Cosine with 0.22 roll off**

Table 2-3: Parameters of WCDMA Modulation

2.3 Features of the WCDMA Air Interface

The features by which WCDMA differs from GSM and IS-95 (CDMA) is highlighted, Holma et al. [16].

Main differences between WCDMA and GSM and CDMA (IS-95) air interfaces			
	WCDMA	CDMA(IS-95)	GSM
Carrier spacing	5 MHz	1.25 MHz	200 kHz
Frequency reuse factor	1	1	1 to 18
Chip rate	3.84 Mcps	1.2288 Mcps	
Power control frequency	1500 Hz both uplink and	Uplink: 800 Hz,	2 Hz or lower
	downlink	downlink: slow power control	
Quality control	Radio resource management		Network planning (frequency
	algorithms		planning)
Frequency diversity	5 MHz bandwidth gives multipath		Frequency hopping
	diversity with Rake receiver		
Base station synchronisation	Not needed	Yes, typically obtained via GPS	GPS or Switching Centre
Inter-frequency handovers	Yes, measurements with	Possible, but measurement method	
	slotted mode	not specified	
Efficient radio resource management algorithms	Yes, provides required quality	Not needed for speech only	
	of service	networks	
Packet data	Load-based packet scheduling	Packet data transmitted as short	Time slot based scheduling
		circuit switched calls	with GPRS
Downlink transmit diversity	Supported for improving	Not supported by the standard	Not supported by the standard,
	downlink capacity		but can be applied

Table 2-4: Main differences between WCDMA, CDMA(IS-95), and GSM

Thus, in concluding the physical layer description, WCDMA systems are designed to provide reasonable service quality without using complex receivers that use joint detection of multiple user signals. However, if required, short scrambling codes can be used at the uplink to implement multiuser receivers at moderate complexity. This leads us to an analysis of DS-SS systems mentioned above, focusing on the mathematical notation for describing such systems.

2.4 The DS-SS Transmitter For A Single User System

Considering the BPSK digital modulation, for ease of explanation, figure 2-4 outlines the single user BPSK DS-SS transmitter model.

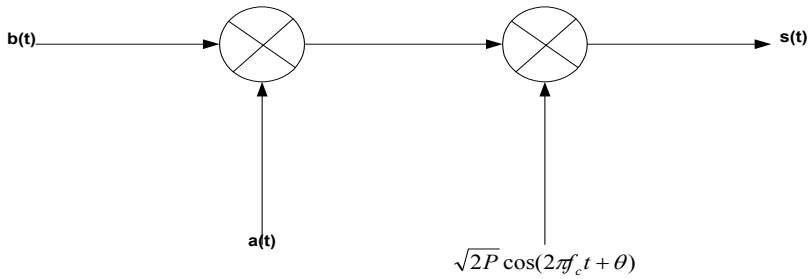

Figure 2-4: The single user BPSK-based DS-SS transmitter model.

The data signal $b(t)$ is written as

$$b(t) = \sum_{i=-\infty}^{\infty} b_i p_T(t - iT), \tag{2-1}$$

where we define $\{b_i\}$ as a set of independent identically distributed bernoulli random variables. Thus, the symbol b_i represents the i^{th} data bit under the conditions:

$$b_i \in \{-1, +1\} \text{ and } \Pr[b_i = -1] = \Pr[b_i = +1] = 1/2. \tag{2-2}$$

Next, the unit rectangular pulse $p_T(t)$ is given by

$$p_T(t) = \begin{cases} 1, & 0 \le t \le T \\ 0, & otherwise, \end{cases} \tag{2-3}$$

where:

T is the duration of the data bit.

Also, the data signal which is spread by the PN code waveform $a(t)$ can be denoted as

$$a(t) = \sum_{j=-\infty}^{\infty} a_j p_{T_c}(t - jT_c), \tag{2-4}$$

where:

a_j is identically distributed to b_i.

Therefore, it is assumed spreading code $\{a_j\}$ is randomly generated, (although known at both the transmitter and the receiver). Where the elements of $\{a_j\}$ are called code chips. Usually, there are many chips per bit given by i.e $T = NT_c$, $T_c << T$.(i.e., N large). Denoting the system processing gain by N, which can also be defined as the ratio of the chip rate to the data rate, i.e. $N = R_c / R$, this can also be expressed as the ratio of the bit duration to the chip duration, i.e. $N = T / T_c$. Many systems' code sequences repeat for each bit of a given user. Such systems are called code on pulse (each bit being a pulse) and their code waveforms are periodic in T. However, many DS-SS system simulations use aperiodic code sequences. The number of studies for such systems have appeared, Xu, [26], such as an iterative method to estimate the FIR channels and the transmitted symbols; the adopting of subspace concepts to identify the multi-path channel; the design of blind receivers to suppress the interference from other cells; or the blind uplink channel estimation method. This is because the time-varying nature of the signatures of aperiodic spreading sequences (long codes), renders the previous channel estimation and multiuser detection methods not directly applicable, as in the periodic,(short codes) case.

The spread data signal $b(t)a(t)$ is modulated onto a radio-frequency,(RF), carrier. If the time-averaged bandpass power of the carrier is P, and the carrier frequency is f_c, with the carrier phase as θ. The resulting transmitted signal $s(t)$ then has the form

$$s(t) = \sqrt{2P}b(t)a(t)\cos(2\pi f_c t + \theta). \tag{2-5}$$

Further insight can be obtained from Ragagopal et al. [7], as regards the multiuser transmitter representations.

As an interlude before the discussion of the DS-SS receivers we briefly mention the PN (Pseudo Noise), sequences and their importance in the coding techniques of CDMA and WCDMA.

2.5 Spreading Sequences

PN sequences are important to the DS-SS system as their characteristics directly impact system performance. Considering ideal conditions, PN sequences would permit multiple users to share bandwidth without interfering with each other. Unfortunately, achieving this ideal level of operation is impossible from a practical perspective. Therefore, codes with near-ideal properties are instead used practically, as mentioned above. Considering the quality aspect of PN codes, this is often gauged by computing their auto- and cross-correlation functions. The aim of PN code design is to minimize auto-correlation for non-zero delay and to minimize cross-correlation over all delays. Ideally, the optimal levels would occur when the auto-correlation would be zero for non-zero delay and the cross-correlation would be zero over all delays. In practice, the degree to which PN code properties approach this operational threshold, determines the degree to which users interfere with one another, and consequently has an impact on the system performance. The low auto-correlation aspect lends its importance in the determination of performance in fading channels as well as low synchronization time. Stating mathematically for a PN code sequence $\{a_j\}$, from which we seek the auto-correlation property to exhibit

$$R_{a_j}[\delta] = \frac{1}{2N-1}\sum_{n=1-N}^{N-1} a_n a_{n+\delta} \approx 0 \qquad \delta \neq 0 \tag{2-6}$$

Considering the requirement of low interference between users, we desire that the cross-correlation between any two distinct $(l \text{ and } m, l \neq m)$ users' PN sequences $\{a_{l,j}\}$ and $\{a_{m,k}\}$ obey

$$Ra_{l,j}a_{m,k}[\delta] = \frac{1}{2N-1}\sum_{n=1-N}^{N-1} a_{l,n}a_{m,n+\delta} \cong 0 \quad \forall \delta, \tag{2-7}$$

where $a_{l,j}$ is the j^{th} chip of the l^{th} user's PN sequence.

Random codes do exhibit good auto- and cross-correlation properties despite their 'almost ideal' characteristic and are widely used in DS-SS system modelling and analysis. The generation of PN codes in real systems, is usually by a finite state machine such as a linear-feedback shift register, i.e. Maximal Length Sequences or m-sequences are a common class of PN codes created by a shift register. Other types of PN sequences can be derived from m-sequences such as Gold codes and Kasami Sequences, Scholtz, [4]. Each type of code has a particular advantage and depending upon system requirements, various performance parameters can be traded-off by the use of one type of code over another.

2.6 Typical DS-SS Receivers

2.6.1 Matched Filter Receiver. (Verdu)

Continuing our discussion from section 2.4, the Matched Filter receiver may be described as the building block of the various receiver structures available. In describing the channel process at the receiver, it begins when the transmitted signal travels across an AWGN channel from the transmitter to the receiver. The receiver's function is to absorb the incoming signal and to recover the transmitted bit stream, while making the least possible amount of incorrect bit decisions. Success in this exercise depends upon the receiver's detection algorithm employed in the previously mentioned PN code properties, as well as the channel conditions.

The transmission system process involves the channel model inserting a finite propagation delay τ into the transmitted signal $s(t)$, producing $s(t-\tau)$, followed by corrupting the transmitted signal with additive white Gaussian noise (AWGN) $n(t)$. Thus, the input to the receiver is the sum of the delayed transmitted signal and the AWGN. In order to exhibit consistency with the previously described BPSK-based DS-SS transmitter, the received signal is modelled by

$$r(t) = s(t-\tau) + n(t) \tag{2-8}$$

which after expansion becomes

$$r(t) = \sqrt{2P}b(t-\tau)a(t-\tau)\cos(2\pi f_c(t-\tau)+\theta)+n(t) \quad (2\text{-}9)$$

The BPSK-based conventional DS-SS receiver representation is shown in Figure 2-5.

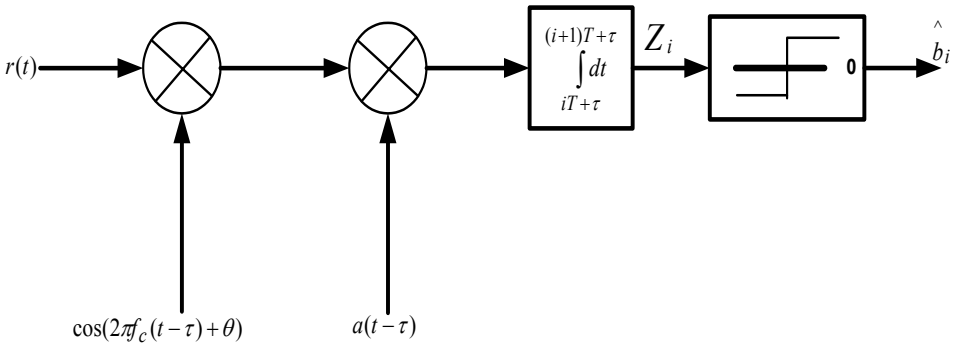

Figure 2-5: A BPSK-based conventional Matched Filter DS-SS receiver representation

The sequence of operations is opposite to those at the transmitter, i.e., demodulation followed by dispreading (and ultimately decision making). For effective demodulation, the receiver's carrier replica must be synchronized with that of the transmitter's. Once the receiver has achieved carrier lock, the receiver must then regenerate a synchronous copy of the PN code waveform $a(t-\tau)$ to fully despread the incoming signal. Once despread, the signal passes through a correlator which produces a decision statistic or metric, Z_i for the i^{th} transmitted data bit, computed as

$$Z_i = \int_{iT+\tau}^{(i+1)T+\tau} r(t)a(t-\tau)\cos(2\pi f_c(t-\tau)+\theta)dt \; . \quad (2\text{-}10)$$

To be recovered from $r(t)$, is the information data, which is embedded along with AWGN. This is accomplished by the above correlation integral gauging the degree of similarity between $a(t-\tau)$ and the base-band version of $r(t)$, similar to an inner product operation. Therefore at reasonable AWGN levels, the correlation operation on $r(t)$ is sufficiently capable of extracting the information data.

Following the correlator, is a non-linear threshold device, modelled as a hard limiter, which yields an estimate of the transmitted bit $\hat{b}_i$, such that

$$\hat{b}_i = \text{sgn}[Z_i] = \begin{cases} -1, & Z_i < 0 \\ +1, & Z_i \geq 0. \end{cases} \quad (2\text{-}11)$$

Such a correlation receiver, which is usually implemented as a matched-filter, exhibits lowest BER when attempting to detect a known signal, Rennuci, [6]. A mention of the various receiver variants follows.

2.6.2 Correlation & RAKE Receivers

Correlation receivers (conventional CDMA receiver), use a bank of single user DS-SS receivers for each user, implemented as a bank of matched-filters. These correlation outputs are fed to decision devices that form transmitted bit estimates. In comparison to other receivers, it offers relatively low complexity at the cost of inferior performance and has been proposed for use in the IS-95 standard. The matched-filters and correlator receivers exhibit almost identical performance in AWGN.

The RAKE receiver introduced by Price and Green [6], takes advantage of the inherent multi-path diversity in a frequency selective fading CDMA channel. Subjected to these conditions, the coherence bandwidth of the channel is significantly smaller than the bandwidth of the transmitted wideband CDMA signal, giving the ability to distinguish the arriving multi-path signal components, Rappaport, [10]. This is done by the RAKE receiver locking onto each arriving multi-path component and, for a given bit, filters the components, hereby producing a final decision statistic corresponding to that particular bit. Figure 2-6 shows the RAKE receiver structure for a given user. The name 'RAKE' given to this receiver structure is analogous to a generic garden RAKE where the M "fingers" of the RAKE receiver track the $\leq M$ multi-path components of each user. The first part of the receiver is similar to the conventional correlation receiver, and then the output of the correlator is searched for multi-path components to be combined, i.e, the correlation detection process is typically followed by RAKE combiner process. In a K user system, there are K such filter banks with M fingers each, one for each user. These correlators produce a set of preliminary decision statistics $\{Z_i\}$ which reflect the strength and

reliability of a given multi-path component. Therefore, based on the multi-path structure of the channel, appropriate FIR filter weights $\{w_i\}$ are chosen to maximize the fidelity of the final decision statistic Z, which is computed as

$$Z = \sum_{i=1}^{M} w_i Z_i . \qquad (2\text{-}12)$$

This is a form of Maximal Ratio Combining (MRC).

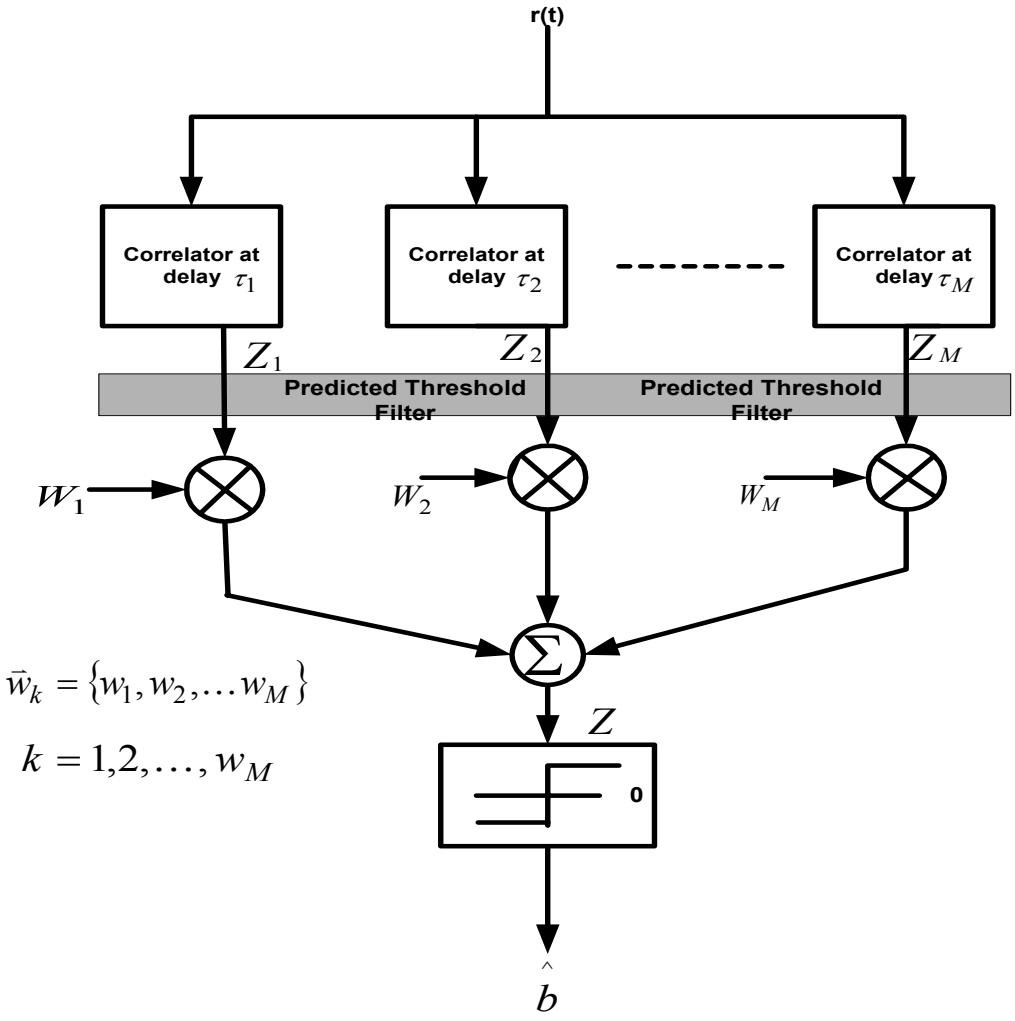

Figure 2-6: BPSK-based RAKE CDMA Receiver for a Given User (given that MUIC has already taken place, with sufficient preservation or restoring of code orthogonality)

2.7 Multiuser Detectors

As mentioned previously, single user detectors are not optimal for CDMA or WCDMA, because they process other users' interference, termed multiple access interference (MAI), as unstructured channel noise. To better design CDMA/WCDMA receivers, the specific structure of MAI needs to be more fully exploited. To such an end, novel receiver structures have been proposed over the years that take advantage of knowledge of MAI signal parameters. Such receivers are termed multiuser receivers. Multiuser receivers are more complex than conventional ones because of their added capability of using MAI signal information to help recover the desired user. For now, multiuser receiver structures are only proposed for use at the base station where additional complexity may be supported.

A description of the advantages and disadvantages of the main MAI Cancellation (MAIC), structures is given below.

2.7.1 Optimal Receiver Structure:The Optimal Detector

Verdu derived the optimal CDMA receiver in 1986 [6]. It had been pre-empted seven years earlier by the introduction of multiuser detection by Schneider in 1979 [6]. The optimal structure consists of a bank of matched-filters providing first order user amplitude estimates to a Viterbi decision algorithm. Verdu mathematically showed that the optimal structure gave significant performance improvement over the conventional structure, but due to its hindered implementation as a result of the expense involved (due to processing complexity), the role of the optimal receiver has been that of a benchmark against which to compare sub-optimal CDMA detectors. These sub-optimal detectors exhibit more reasonable computational complexity. In the following sections, we consider three typical sub-optimal multiuser receivers.

2.7.2 Sub-Optimal Receiver Type I: The Decorrelator-MAIC Receiver

The decorrelator may be described as a linear multiuser detector with a upper bound complexity of K^2, which functions by applying a linear transformation to the set of matched-filter outputs obtained from the first stage. It basically decorrelates or undoes the various inter-user correlations in order to isolate users from one another. This is carried out by computing PN code waveform cross correlation values and storing these in a $K \times K$ matrix, followed by multiplying the inverse of this matrix by the vector of matched-filter outputs from the first stage. Pre- knowledge of signal amplitudes is not required by the detector, and it is completely insensitive to the near-far effect. Though not widely used, it generally provides substantial performance and capacity gains over the conventional receiver [6]. The K^2 complexity is alluded to the $K \times K$ matrix storage requirement. Another disadvantage is the level of noise obtained in decision statistics due to the noise enhancement produced by the decorrelation operation.

2.7.3 Sub-Optimal Receiver Type II: The Minimum Mean Square Error (MMSE) Detector

The MMSE detector operates similarly to the decorrelator by applying a linear transformation to the set of first stage matched-filter outputs. The aim is to minimize the averaged square error between actual data and the soft outputs from the first stage. This makes the MMSE detector able to overcome the decorrelator's shortcoming of enhancing noise, but at an additional cost of requiring knowledge of signal amplitudes. It generally displays better receiver BER than the decorrelator, but in the limit, as the noise level drops to zero, the MMSE detector's performance approaches that of the decorrelator's. It has a near-far resistance slightly less than that of the decorrelator's.

2.7.4 Sub-Optimal Receiver Type III: Interference Cancellation Detectors

The remainder of this dissertation will deal with an interference cancellation algorithm. First proposed by Varanasi and Aazhang [8], interference cancellation detectors seek to remove interference by actually subtracting estimates of interfering signals from the received signal. A general interference cancellation receiver comprises of an initial stage of matched-filters, like the other multiuser receivers, followed by stages of interference

cancellation. Interference cancellation receivers typically come in two flavours: parallel, Varannasi et al. [8], and successive, Renucci, [6]; the parallel scheme is the one originally proposed by Varanasi and Aazhang. In parallel interference cancellation, all interfering users are cancelled (subtracted) concurrently (in parallel) from the received signal. In the successive approach proposed by Holtzman, users are cancelled sequentially in descending order of estimated received power, from strongest to weakest.

Both detectors have been shown to improve performance and capacity over conventional detection, and both have distinct sets of advantages over one another, Moshavi, [21]. From a computational viewpoint, parallel cancellation is more advantageous as it can usually be implemented with complexity proportional to K. Furthermore, since all users are cancelled concurrently, the cancellation process is faster than in the successive cancellation method, which incurs a delay in subtracting out each interferer one after the other. Such ordering of cancellation in the successive case entails an expensive K^2 computational complexity. The parallel scheme also performs better than its successive counterpart under perfect power control. Assuming some form of crude power control in the cellular environment, we henceforth focus on a parallel MAI cancellation method in the following chapters.

2.8 Chapter 2 Summary

The WCDMA physical layer has been described, as well as the uplink spreading and modulation techniques. Also, a short overview of the CDMA receivers, namely conventional single user CDMA detectors as well as multiuser detectors, has been given. The focus in Chapter 3 will be much more on the parallel interference cancellation based approach, specifically, the soft cancellation techniques.

CHAPTER 3

PARALLEL INTERFERENCE CANCELLATION AND BIAS MITIGATION

This chapter focuses on the existing Parallel Interference Cancellation techniques, the conventional and the partial methods. It studies the receiver performance at both the first and second stages of the decision statistic analysis, and shows how the second stage decision statistics become biased. The Bias mitigation techniques in the form of the soft parallel interference cancellation is described around the transmitter and receiver models. Here, the decision statistics are weighted by a soft cancellation factor, SCF and then used in cancellation. This is indicated by the recomputed mean and variance of the second stage metric, generally showing that the partial cancellation process removes more MAI than it enhances noise. The equation for the $BER^{(2)}$ of second stage cancellation is derived in order to obtain the optimal SCF. This is the foundation used to determine the Universal SCF, SCF_{UNV}, which is proposed to produce acceptable cancellation results over the whole range of the system load (simultaneous users).

3 CONVENTIONAL PARALLEL INTERFERENCE CANCELLATION

The parallel interference cancellation originally proposed by Striglis et al. [6], had a receiver structure consisting of an initial stage of matched-filter reception, followed by an arbitrary number of interference cancellation stages,as shown in Figure 3-1.

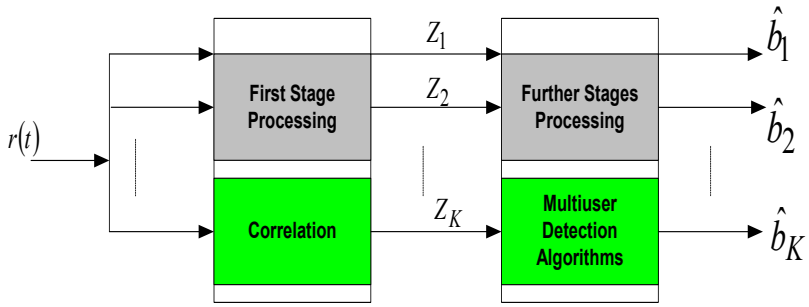

Figure 3-1: Multiuser Receiver Structure

This consists of the first stage providing first order amplitude estimates (decision statistics) of each user, which are then fed to the second stage. The second stage then constructs (MAI) signal estimates based upon first stage amplitude estimates and cancels this reconstructed MAI from the original received signal, with the MAI reconstruction and cancellation process being repeated if preferred, i.e. as many times as may be necessary to meet the same performance (QoS) criterion. Initial analysis, Renucci, [6], assumed that all amplitude estimates were completely unbiased. It was discovered later by work done by Buehrer et al. [9], after extensive analysis of the receiver, that amplitude estimates after cancellation are biased in proportion to the amount of interfering users. This also revealed reasons for analytic BER yielding more promising results, compared to simulation BER results exhibited which bias effects. Early accounts regarding bias in parallel interference cancellation structures can be found in the documentation by Divsalar and Simon [6].

The first stage analysis follows that proposed by Kaul et al. [27], however, the second stage analysis deviates from Kaul [27], as a more accurately modelling of the interference cancellation algorithm was performed, showing the presence of bias in the MAI estimates.

The mean of the second stage statistic demonstrating the bias source, was described, and the effects of the bias on system performance shown. Thus, in a counter-measure effort to mitigate the bias effects, Kaul et. al. carried out simulation experiments where interference estimates were down-scaled by a scalar. Promising initial results of this sort of interference cancellation were documented by Buehrer [9], and later by Correal et al. [28]. Rennuci [1], also performed an analysis of the model of interference estimate down-scaling, ultimately obtaining the down-scaling factors yielding the lowest BER for a given system load.

3.1 Model of Conventional Parallel Interference Cancellation

A detailed mention of the performance of conventional (brute), interference cancellation, where no interference estimate down-scaling is practised, can be found in Renucci [6]. The description of the transmitter and receiver models can be found here. It should be noted that the Gaussian approximation process results in each transmitted signal estimate (MAI signal estimate) becoming an unbiased estimate of the corresponding transmitted signal. Once all signal reconstructions are completed, the second stage proceeded with conventional parallel interference cancellation. The conventional parallel interference cancellation is implemented by the subtraction of interfering user's signal estimates from the received signal $r(t)$, to form a new reconstructed received signal for the k^{th} user $\hat{r}_k^{(2)}(t)$, given by

$$\hat{r}_k^{(2)}(t) = r(t) - \sum_{\substack{\kappa=1 \\ \kappa \neq k}}^{K} \hat{s}_\kappa^{(2)}(t-\tau_\kappa). \qquad (3\text{-}1)$$

Where:

$\hat{s}_\kappa^{(2)}(t-\tau_\kappa)$, is the transmitted delayed signal for each user at second stage.

The new reconstructed received signal is generated for each user, since each user is the desired user at some point so that the new received signals are "cleaner" versions of $r(t)$, for each user respectively.

It is also seen that the level of the effectiveness of the cancellation operation largely lies in the degree of accuracy of the reconstructed MAI signals, meaning that the closer the estimates are to the actual transmitted signals, the better the receiver performance becomes. These new received signals are passed through a bank of correlators similar to those in the first stage in order to produce a second stage decision statistic for each user given by:

$$Z_{k,i}^{(2)} = \frac{1}{T}\int_{iT+\tau_K}^{(i+1)T+\tau_K} \Re\left\{\hat{r}_k^{(2)}(t)a_k(t-\tau_k)e^{-j\phi_K}\right\}dt . \qquad (3\text{-}2)$$

Where:

T, is the bit duration, $\Re$, is the real part operator,

$a_k(t-\tau_k)$, each user's spreading waveform

ϕ_k, denotes received phase of each user

$\hat{r}_k^{(2)}(t)$, is the reconstructed received signal for the k^{th} user

The aim is for $\hat{r}_k^{(2)}(t)$ to contain the least possible amount of MAI, which would enhance the post-cancellation correlator operation as only AWGN is affecting the desired signal. It was observed that the cancellation of interference in first stage metrics enhances the quality of second stage metrics. Interference cancellation could be repeated any number of times, however, most of the performance enhancement is already achieved after the second stage. It was found that the additional performance improvement decreased from stage to stage as the fundamental performance limit imposed by the system processing gain impeded further isolation of the desired signal from MAI. Thus, processing beyond four stages is worth neither the computational burden nor the incurred delay.

3.2 Conventional Parallel Interference Cancellation Receiver Performance

The study of the receiver performance at both the first and second stages involved analysing the decision statistic characteristics. The first stage analysis, based upon 3GPP [14] and Kaul et al. [27], computed both the mean and the variance of the decision statistic, to ultimately obtain the first stage BER. The reasons for this characterization was not only to provide a reference point for comparison with second stage metric moments, but was also to highlight the existence of a bias with potentially harmful effects. This important impediment is discussed further on.

Considering the first stage, the analysis by [6] focuses on user 1 as the desired user, and for convenience as well as to make notation less cumbersome user 1's propagation delay is set to zero, i.e. $\tau_1 = 0$. *(It is however standard practice to consider the reference user to have a propagation delay of $j = 0$, which is the time alignment with respect to the received signals from other users in a CDMA system and not the actual propagation delay between transmitter and receiver).* The correlation integral [6] , is first broken up into its three constituent parts: The desired user, MAI, and noise due to AWGN, as shown in equation (3-3).

$$
\begin{aligned}
Z_{1,i}^{(1)} &= \frac{1}{T}\int_{iT}^{(i+1)T} \Re\left\{ r(t)a_1(t)e^{-j\phi_1} \right\} dt \\
&= \frac{1}{T}\int_{iT}^{(i+1)T} \Re\left\{ \left[\sum_{k=1}^{K} \sqrt{P_k}\, b_k(t-\tau_k)a_k(t-\tau_k)e^{j\phi_K} + n(t) \right] a_1(t)e^{-j\phi_1} \right\} dt \\
&= \underbrace{\frac{1}{T}\int_{iT}^{(i+1)T} \Re\left\{ \sqrt{P_1}\, b_1(t)a_1(t)e^{j\phi_1} a_1(t)e^{-j\phi_1} \right\} dt}_{Desired\,User} \\
&\quad + \underbrace{\frac{i}{T}\int_{iT}^{(i+1)T} \Re\left\{ \left[\sum_{k=2}^{K} \sqrt{P_k}\, b_k(t-\tau_k)a_k(t-\tau_k)e^{j\phi_K} \right] a_1(t)e^{-j\phi_1} \right\} dt}_{MAI} \\
&\quad + \underbrace{\frac{1}{T}\int_{iT}^{(i+1)T} \Re\left\{ n(t)a_1(t)e^{-j\phi_1} \right\} dt}_{Noise} \\
&= A_1 + \sum_{k=2}^{K} I_k^{(1)} + \eta,
\end{aligned}
\tag{3-3}
$$

where A_1, $I_k^{(1)}$, and η are the contributions from the desired user, first stage interference from the k^{th} user, and the noise due to AWGN, respectively.

The first stage amplitude estimates are found to be composed of a desired component, accompanied by MAI and noise due to AWGN. This means that the matched filter's ability to eliminate the effect of MAI from the received signal $r(t)$ is directly affected by the processing gain, with secondary influences due to the relative effect of the desired user's power on MAI.

The analysis process found that the three components in the decision metric are statistically independent random variables, and as a result computation of the first stage's mean and variance yields respectively

$$E\left[Z_{1,i}^{(1)} \mid b_{1,i}\right] = E\left[A_1 \middle| b_{1,i}\right] + E\left[\sum_{k=2}^{K} I_k^{(1)} \middle| b_{1,i}\right] + E\left[\eta \middle| b_{1,i}\right] \tag{3-4}$$

and

$$Var\left[Z_{1,i}^{(1)} \middle| b_{1,i}\right] - Var\left[A_1 \middle| b_{1,i}\right] = Var\left[\sum_{k=2}^{K} I_k^{(1)} \middle| b_{1,i}\right] + Var\left[\eta \middle| b_{1,i}\right]. \tag{3-5}$$

Focusing on the Desired User, this gives:

$$\begin{aligned} E\left[A_1 \middle| b_{1,i}\right] &= E\left[\frac{1}{T}\int_{iT}^{(i+1)T} \Re\left\{\sqrt{P_1} b_{1,i} a_1^2(t) e^{-j\phi_1}\right\} dt\right] \\ &= E\left[\frac{1}{T} T \Re\left\{\sqrt{P_1} b_{1,i}\right\}\right] \\ &= \sqrt{P_1} b_{1,i}. \end{aligned} \tag{3-6}$$

As the conditioning is based upon the desired bit, $b_{1,i}$, the variance of the desired user term becomes zero, yielding

$$Var\left[A_1 \left| b_{1,i} \right.\right] = 0. \tag{3-7}$$

For the MAI it becomes:

$$\begin{aligned} E\left[\sum_{k=2}^{K} I_k^{(1)} \left| b_{(1,i)} \right.\right] &= E\left[\frac{1}{T}\int_{iT}^{(i+1)T} \Re\left\{\left[\sum_{k=2}^{K} \sqrt{P_k} b_k(t-\tau_k) a_k(t-\tau_k) e^{j\phi_k}\right] a_1(t) e^{-j\phi_1}\right\} dt\right] \\ &= E\left[\frac{1}{T}\int_{iT}^{(i+1)T} \Re\left\{\sum_{k=2}^{K} \sqrt{P_k} b_k(t-\tau_k)\, a_k(t-\tau_k)\, a_1(t) e^{j(\phi_k-\phi_1)}\right\} dt\right] \\ &= \frac{1}{T}\int_{iT}^{(i+1)T} \sum_{k=2}^{K} \sqrt{P_k} E\left[b_k(t-\tau_k)\, a_k(t-\tau_k)\, a_1(t-\tau_1)\cos(\phi_k-\phi_1)\right] dt \\ &= 0, \end{aligned} \tag{3-8}$$

(NB: Only true for synchronous case and perfectly orthogonal sequences) as the use of both random bit and signature sequences is assumed.

Focusing on the variance of the MAI term computed in [27] under the Gaussian assumption for MAI with the result stated here, upon adapting it for the baseband model, [6], as well as obtaining normalized decision statistics, gives,

$$Var\left[\sum_{k=2}^{K} I_k^{(1)} \left| b_{1,i} \right.\right] = \frac{1}{3N} \sum_{k=2}^{K} P_k. \tag{3-9}$$

Similarly for the Noise trend we obtain:

$$
\begin{aligned}
E\left[\eta \middle| b_{1,i}\right] &= E\left[\frac{1}{T}\int_{iT}^{(I=1)T} \Re\left\{ n(t)\, a_1(t)\, e^{-j\phi_1} \right\} dt \right] \\
&= \frac{1}{T}\int_{iT}^{(i+1)T} \Re\left\{ E\left[n(t)\, a_1(t)\, e^{-j\phi_1} \right] \right\} dt \\
&= 0,
\end{aligned}
\tag{3-10}
$$

due to modelling AWGN as a zero mean random process. Thus, the noise term variance is computed as

$$
\begin{aligned}
Var\left[\eta \middle| b_{1,i}\right] &= E\left[\eta^2 \middle| b_{1,i}\right] \\
&= E\left[\frac{1}{T}\int_{iT}^{(i+1)T} \Re\left\{ n(t)\, a_1(t) e^{-j\phi_1} \right\} dt \cdot \frac{1}{T}\int_{iT}^{(i+1)T} \Re\left\{ n(\lambda) a_1(\lambda) e^{-j\phi_1} \right\} \right] \\
&= \frac{1}{T^2} E\left[\int_{iT}^{(i+1)T}\int_{iT}^{(i+1)T} a_1(t) a_1(\lambda) \Re\left\{ n(t) e^{-j\phi_1} \right\} \Re\left\{ n(\lambda) e^{-j\phi_1} \right\} dt d\lambda \right] \\
&= \frac{1}{T^2} E\left[\int_{iT}^{(i+1)T}\int_{iT}^{(i+1)T} \left[\frac{n(t) e^{-j\phi_1} + n^*(t) e^{j\phi_1}}{2} \right] \left[\frac{n(\lambda) e^{-j\phi_1} + n^*(\lambda) e^{j\phi_1}}{2} \right] dt d\lambda \right] \\
&= \frac{1}{4T^2}\int_{iT}^{(i+1)T}\int_{iT}^{(i+1)T} E\left[n(t) n^*(\lambda) + n^*(t) n(\lambda) \right] dt d\lambda \\
&= \frac{1}{4T^2}\int_{iT}^{(i+1)T}\int_{iT}^{(i+1)T} 2\delta(t-\lambda)\, dt d\lambda \\
&= \frac{1}{2T^2}\int_{iT}^{(i+1)T} N_o\, dt d\lambda \\
&= \frac{N_o}{2T},
\end{aligned}
\tag{3-11}
$$

where $(\bullet)^*$ denotes complex conjugation. Finally we may write the first stage's mean and variance according to Equation (3-4) and Equation (3-5), as,

$$E\left[Z_{1,i}^{(1)}\,\middle|\,b_{1,i}\right] = \sqrt{P_1}\,b_{1,i}, \tag{3-12}$$

and

$$Var\left[Z_{1,i}^{(1)}\middle|b_{1,i}\right] = \frac{1}{3N}\sum_{k=2}^{K} P_k + \frac{N_0}{2T}. \tag{3-13}$$

Special focus is directed toward Equation (3-12), which indicates that first stage metrics are unbiased amplitude estimates of each user's signal, for a given transmitted bit. This result contrasts the corresponding second stage result described in the following section. Now, Expressing BER for the conventional BPSK-based CDMA system, and on assuming equiprobable signalling, the first stage bit-error-rate $BER^{(1)}$ can be written as

$$\begin{aligned} BER^{(1)} &= \Pr\left[Z_{1,i}^{(1)}\middle|b_{1,i}=+1\right] = \Pr\left[Z_{1,i}^{(1)}\middle|b_{1,i}=-1\right] \\ &= Q\left(\sqrt{\frac{\left(E\left[Z_{1,i}^{(1)}\middle|b_{1,i}\right]\right)^2}{Var\left[Z_{1,i}^{(1)}\middle|b_{1,i}\right]}}\right) \\ &= Q\left(\left[\frac{1}{2\dfrac{E_{b_1}}{N_o}} + \frac{1}{3N}\cdot\frac{\sum_{k=2}^{K}P_k}{P_1}\right]^{-\frac{1}{2}}\right), \end{aligned} \tag{3-14}$$

where $E_{b_1} = P_1 T$ and $Q(z) = \frac{1}{\sqrt{2\pi}}\int_z^{\infty} e^{-\frac{\lambda^2}{2}}\,d\lambda$ (the standard Q-function). It gives the standard "Gaussian Approximation" for the performance of a CDMA system [10], and leads to an analysis of the second stage decision statistic.

Now, consider the analysis of the second stage metrics which show that the decision statistics become biased. It begins by identifying the constituent parts of the second stage correlation integral in Equation (3-2), followed by the development of an expression in terms of first stage metrics. The first stage metrics are re-written in terms of PN code waveform cross-correlation functions to avoid cumbersome elements. Therefore, introducing the PN code waveform cross correlation functions from [6][1], $R_{l,m}(\tau)$ and $\hat{R}_{l,m}(\tau)$, which are the continuous-time partial cross-correlation functions of the first and second signature sequences defined by:

$$R_{l,m}(\tau) = \frac{1}{T}\int_0^{\tau} a_l(t-\tau)\,a_m(t)\,dt \quad \text{and} \quad \hat{R}_{l,m}(\tau)\int_{\tau}^{T} a_l(t-\tau)\,a_m(t)\,dt;\ 0 \le \tau < T. \tag{3-15}$$

Dropping the index k of the delay parameter τ so that τ, from here onwards is considered a general random delay parameter uniformly distributed over [0, T) and attributable to all users.

Where, l, is the desired user and m, the interferer. Interferer m can be any user in $\{1,\ldots,l-1\}\cup\{l+1,\ldots,K\}$, and as such, user m 's bit indeces can be $i-1$, i, or $i+1$, and not just i and $i-1$ as when the interferers are users 2 through K.

With reference to the stochastic properties of $R_{l,m}(\tau)$ and $\hat{R}_{1,m}(\tau)$, and with regard to first moments, it is seen that for random codes the mean could be written as

$$E\left[R_{l,m}(\tau)\right] = E\left[\hat{R}_{l,m}(\tau)\right] = E\left[R_{l,m}(\tau)\hat{R}_{l,m}(\tau)\right] = E\left[R_{l,m}(\tau)\right]\cdot E\left[\hat{R}_{l,m}(\tau)\right] = 0 \tag{3-16}$$

and

$$E\left[\int_0^T a_l(t-\tau)\,a_m(t)\,dt\right] = E\left[R_{l,m}(\tau) + \hat{R}_{l,m}(\tau)\right] = 0. \tag{3-17}$$

It can further be shown, from [1,24], that

[1] Just as with decision statistics, we choose to normalize by the bit duration T here as well so as to remove the dependence upon T of the cross-correlation functions

$$E\left[R_{l,m}^2(\tau)+\hat{R}_{l,m}^2(\tau)\right]=Var\left[\frac{1}{T}\int_0^T a_l(t-\tau)\,a_m(t)\,dt\right]=\frac{2}{3N}. \qquad (3\text{-}18)$$

The detailed illustration as to how PN code cross-correlation functions are used is given in [6], but a diagrammatic explanation is given in Figure3-2. Here, Figure 3-2 depicts the asynchronous time relationship between users in the system.

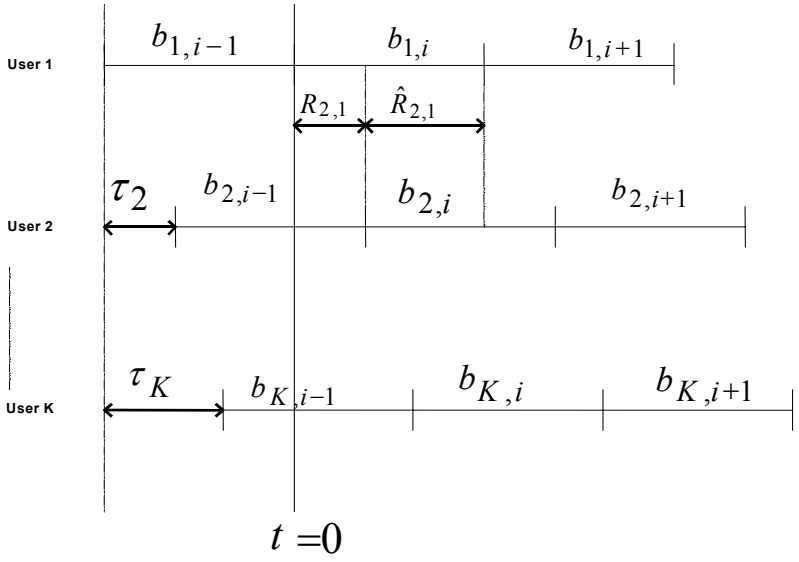

Figure 3-2: The asynchronous time relationship between system users

The $(i-1)^{th}$, i^{th}, and $(i+1)^{th}$ bits of several users are shown, with their respective time delays. Thus, continuing with user 1 as the desired user, and rewriting the first stage decision statistic in terms of PN code cross-correlations, we obtain:

$$
\begin{aligned}
Z_{1,i}^{(1)} &= \frac{1}{T}\int_{iT}^{(i+1)T} \Re\left\{\left[\sum_{l=1}^{K}\sqrt{p_l}\,b_l(t-\tau_l)\times\cdots\right.\right. \\
&\cdots\times a_l(t-\tau_l)e^{j\phi_l}+n(t)\left.\right]a_1(t)e^{-j\phi_1}\left.\right\}dt \\
&= \sqrt{P_1}\,b_{1,i}+\frac{1}{T}\int_{iT}^{(i+1)T}\sum_{l=2}^{K}\sqrt{P_l}\,b_l\times\cdots\cdot \\
&\cdots\times(t-\tau_l)a_l(t-\tau_l)a_1(t)\cos(\phi_l-\phi_1)dt+\eta \\
&= \sqrt{P_1}\,b_{1,i}+\frac{1}{T}\sum_{l}^{K}\sqrt{P_l}\left[\int_{iT}^{iT+\tau_l}b_{l,i-1}\times\cdots\right. \\
&\cdots\times a_l(t-\tau_l)a_1(t)dt+\int_{iT+\tau_l}^{(i+1)T}b_{l,i}\times\cdots \\
&\cdots\times a_l(t-\tau_l)a_1(t)dt\left.\right]\cos(\phi_l-\phi_1)+\eta \\
&= \underbrace{\sqrt{P_1}\,b_{1,i}}_{\text{Desired Use}}+\underbrace{\sum_{l=2}^{K}\sqrt{P_l}\cos(\phi_l-\phi_1)\times\cdots}_{MAI} \\
&\cdots\times\underbrace{\left[b_{l,i-1}R_{l,1}(\tau)+b_{l,i}\hat{R}_{l,1}(\tau)\right]}_{MAI}+\underbrace{\eta}_{Noise}
\end{aligned}
\tag{3-19}
$$

Once the receiver has completed first stage processing and obtained amplitude estimates for all users, MAI signal reconstruction commences as

$$
\hat{s}_l^{(2)}(t-\tau_l)=\left[\sum_{i=-\infty}^{\infty}Z_{l,i}^{(1)}p_T(t-\tau_l-iT)\right]a_l(t-\tau_l)e^{j\phi_l}. \tag{3-20}
$$

MAI is then cancelled according to Equation (3-1), so that, User 1's new reconstructed received signal is written as

$$
\hat{r}_1^{(2)}(t)=r(t)-\sum_{l=2}^{K}\hat{s}_l^{(2)}(t-\tau_l). \tag{3-21}
$$

This gives a set of improved decision statistics, according to Equation (3-2).

User 1's second stage metric is computed according to

$$Z_{1,i}^{(2)} = \frac{1}{T}\int_{iT}^{(i+1)T} \Re\left\{ \hat{r}_1^{(2)}(t)\, a_1(t)\, e^{-j\phi_1} \right\} dt \tag{3-22}$$

So that, substituting Equation (3-21) into Equation (3-22), we obtain:

$$\begin{aligned}
Z_{l,i}^{(2)} &= \frac{1}{T}\int_{iT}^{(i+1)T} \Re\left\{ \left[r(t) - \sum_{l=2}^{K} \hat{s}_l^{(2)}(t-\tau_l) \right] a_1(t) e^{-j\phi_1} \right\} dt \\
&= \frac{1}{T}\int_{iT}^{(i+1)T} \Re\left\{ r(t) a_1(t) e^{-j\phi_1} \right\} dt - \frac{1}{T}\int_{iT}^{(i+1)T} \Re\left\{ \sum_{l=2}^{K} \hat{s}_l^{(2)}(t-\tau_l) a_1(t) e^{-j\phi_1} \right\} dt \\
&= Z_{1,i}^{(1)} - \frac{1}{T}\int_{iT}^{(i+1)T} \Re\left\{ \sum_{l=2}^{K} \left[\left\{ Z_{l,i-1}^{(1)} p_T(t-\tau_l+T) + Z_{l,i}^{(1)} p_T(t-\tau_l) \right\} a_l(t-\tau_l) e^{j\phi_l} \right] a_1(t) e^{-j\phi_1} \right\} dt \\
&= Z_{1,i}^{(1)} - \sum_{l=2}^{K} \cos(\phi_l - \phi_1) \left[Z_{l,i-1}^{(1)} \frac{1}{T}\int_{iT}^{iT+\tau_l} a_l(t-\tau_l) a_1(t) dt + Z_{l,i}^{(1)} \frac{1}{T}\int_{iT+\tau_l}^{(i+1)T} a_l(t-\tau_l) a_1(t) dt \right] \\
&= \underbrace{Z_{1,i}^{(1)}}_{ConvRcver} - \underbrace{\sum_{l=2}^{K} \cos(\phi_l - \phi_1) \left[Z_{l,i-1}^{(1)} R_{l,1}(\tau) + Z_{l,i}^{(1)} \hat{R}_{l,1}(\tau) \right]}_{IC}
\end{aligned} \tag{3-23}$$

Showing the important expression of the second stage statistic in terms of first stage statistics. To obtain the bias produced through conventional parallel interference cancellation, substituting Equation (3-19) into Equation (3-23)[2] yields:

[2] We can only substitute Equation (3-19) in its current written form for the $Z_{1,i}^{(1)}$ term in Equation (3-23). For $Z_{l,i-1}^{(1)}$ and $Z_{l,i}^{(1)}$, l and m are designated as desired user and interferer respectively.

$$
\begin{aligned}
Z_{1,i}^{(2)} &= \sqrt{P_1} b_{1,i} + \sum_{l=2}^{K} \sqrt{P_l} \cos(\phi_l - \phi_1) \left[b_{l,i-1} R_{l,1}(\tau) + b_{l,i} \hat{R}_{l,1}(\tau) \right] + \eta \\
&\quad - \sum_{l=2}^{K} \cos(\phi_l - \phi_1) \left\{ \sqrt{P_1} b_{l,i-1} \right. \\
&\quad + \sum_{m=1}^{l-1} \sqrt{P_m} \cos(\phi_m - \phi_l) \left[b_{m,i-1} \hat{R}_{m,l}(\tau) + b_{m,i} R_{m,l}(\tau) \right] \\
&\quad + \sum_{m=l+1}^{K} \sqrt{P_m} \cos(\phi_m - \phi_l) \left[b_{m,i-2} R_{m,l}(\tau) + b_{m,i-1} \hat{R}_{m,l}(\tau) \right] + \eta \Big] R_{l,1}(\tau) \\
&\quad + \left[\sqrt{P_l} b_{l,i} + \sum_{m=1}^{l-1} \sqrt{P_m} \cos(\phi_m - \phi_l) \left[b_{m,i} \hat{R}_{m,l}(\tau) + b_{m,i+1} R_{m,l}(\tau) \right] \right. \\
&\quad \left. + \sum_{m=l+1}^{K} \sqrt{P_m} \cos(\phi_m - \phi_l) \left[b_{m,i-1} R_{m,l}(\tau) + b_{m,i} \hat{R}_{m,l}(\tau) \right] + \eta \right] \hat{R}_{l,1}(\tau) \Big\}.
\end{aligned}
\tag{3-24}
$$

Following simplification and collection of like terms, yields

$$
\begin{aligned}
Z_{1,i}^{(2)} &= \sqrt{P_1} b_{1,i} - \sum_{l=2}^{K} \sum_{m=1}^{l-1} \sqrt{P_m} \cos(\phi_l - \phi_1) \cos(\phi_m - \phi_l) \left[b_{m,i-1} \hat{R}_{m,l}(\tau) R_{l,1}(\tau) \right. \\
&\quad \left. + b_{m,i} \left[R_{m,l}(\tau) R_{l,1}(\tau) + \hat{R}_{m,l}(\tau) \hat{R}_{l,1}(\tau) \right] + b_{m,i+1} R_{m,l}(\tau) \hat{R}_{l,1}(\tau) \right] \\
&\quad - \sum_{l=2}^{K} \sum_{m=l+1}^{K} \sqrt{P_m} \cos(\phi_l - \phi_1) \cos(\phi_m - \phi_l) \left[b_{m,i-2} \hat{R}_{m,l}(\tau) R_{l,1}(\tau) \right. \\
&\quad \left. + b_{m,i-1} \left[R_{m,l}(\tau) \hat{R}_{l,1}(\tau) + \hat{R}_{m,l}(\tau) \hat{R}_{l,1}(\tau) \right] + b_{m,i} R_{m,l}(\tau) \hat{R}_{l,1}(\tau) \right] \\
&\quad + \eta \left[1 - \sum_{l=2}^{K} \cos(\phi_l - \phi_1) \left[R_{l,1}(\tau) + \hat{R}_{l,1}(\tau) \right] \right].
\end{aligned}
\tag{3-25}
$$

This gives the closed form expression for the second stage statistic.

Then, in taking the conditional expectation (the expectation conditioned upon the desired user's i^{th} transmitted bit $b_{1,i}$), the first term in the expression above remains intact, while the last term, the noise term, vanishes. When considering the two double summation terms, it is realised that the only components that could survive the conditional expectation operator are those with the indices $m = 1$, and $l \in \{2, \ldots, K\}$. Thus, when $m = 1$, the products of cosine terms and the products of PN code cross-correlation terms become

squared terms. It is also noted that when $m=1$, the second double summation does not contribute anything. Therefore, the grouping of like terms gives

$$\begin{aligned} E\left[Z_{1,i}^{(2)}\middle|b_{1,i}\right] &= \sqrt{P_1}b_{1,i} - E\left[\sqrt{P_1}\sum_{l=2}^{K}\cos^2(\phi_l-\phi_1)b_{1,i}\left[R_{l,1}^2(\tau)+\hat{R}_{l,1}^2(\tau)\right]\right] \\ &= \sqrt{P_1}b_{1,i} - \sqrt{P_1}b_{1,i}E\left[\sum_{l=2}^{K}\cos^2(\phi_l-\phi_1)\right]E\left[R_{l,1}^2(\tau)+\hat{R}_{l,1}^2(\tau)\right] \\ &= \sqrt{P_1}b_{1,i} - \sqrt{P_1}b_{1,i}\frac{1}{2}(K-1)\frac{2}{3N} \\ &= \underbrace{\sqrt{P_1}b_{1,i}}_{Des.Amp.Est} \quad \underbrace{-\frac{1}{3N}\sqrt{P_1}b_{1,i}(K-1),}_{BiasTerm} \end{aligned} \tag{3-26}$$

Thus, Equation (3-26) was able to indicate the presence of a bias proportional to the number of interferers in second stage amplitude estimates. This was in contrast to the first stage, as second stage MAI was found not to be zero-mean, but on the ensemble average was observed to corrupt second stage amplitude estimates and ultimately, BER. The conclusion made was that, the more the system was loaded, the more the decision statistic values strayed from the desired user's signal amplitude. It was further noted that the effect of the bias in signal amplitude estimates was to directly cause the received signal points to drift towards the decision boundary and further increase the likelihood of inaccurate detector outputs . Therefore, second stage MAI was seen to corrupt the second stage amplitude estimates, which in turn corrupted MAI signal estimates, ultimately jeopardising second stage BER.

3.3 The harmful effects of bias on system performance

The discussion in Rennuci [6], centred around the fact that while first stage metrics are unbiased, second stage metrics are biased in direct proportion to the system loading,(number of users). The discussion explains the origin of bias, and it was able to gauge the decline in system performance with simulation exercises.

3.3.1 Source of Bias Explained

It was found that the bias emanates from the fact that the second stage's MAI amplitude re-estimation process involves matched-filtering of remnants of previous matched-filter outputs,(i.e. those of first stage MAI). Consequently, the presence of the MAI term in Equation (3-19) indicates the correlation of the interferers'signal with the desired user's signal (user 1's signal) at the first stage. During the second stage, the interferers' first stage decision metrics are used as estimates of their signal amplitudes. This is followed by the reconstruction of the estimates of the interferer's transmitted signals, and finally, subtracting these from the original received signal, to form $\hat{r}_1^{(2)}(t)$. The reconstructed received signal $\hat{r}_1^{(2)}(t)$ is then matched-filtered in an effort to gauge its degree of correlation with user 1's PN sequence. This however means that each interferer's first stage metric itself contains correlation by products from the other $K-1$ users, including user 1. As a result, all $K-1$ reconstructed interfering signals are also correlated with user 1. Importantly, when cancelling MAI, an amount of the desired signal (user 1) is also removed from *r(t)*, resulting in the bias. It is found that the bias exists for all desired users in the system and a similar argument can be substantiated for each of them.

The simulations performed by Rennuci [6], assume a system under perfect power control, and is thus able to view the magnitude of the decision statistic when loading is intensified. It is observed that the degradation in the mean of the second stage decision statistics has a direct impact upon second stage BER. This impact could be particularly severe under heavy system loading (i.e one whose number of users approaches the system gain N). It is found that, as the bias results from the matched-filter estimator, replacing the matched-filter estimator with an equivalent low-complexity unbiased estimator is not a trivial exercise, as the proposed replacement is likely to be more complex, and possibly even non-linear. The answer to this problem is to find an effective low-complexity bias mitigation solution. The reasoning is that, if MAI estimates are unreliable due to biasing, then perhaps using them partially instead of integrally could assist BER reduction. More

specifically, it is postulated that weighting MAI estimates in proportion to their reliability could abate the effects of the bias on BER. Thus, it is proposed to *cancel only a certain percentage of MAI, in order to scale down each interferer prior to cancellation by a soft cancellation factor (SCF), which lay between zero and unity*. The exact down-scaling percentage depends upon the degree of MAI estimate reliability as well as general system parameters (processing gain, signal powers etc…)

3.3.2 Analysis of Soft Parallel Interference Cancellation

The discussion by Rennuci [6], on the proposed bias mitigation technique, termed *soft parallel interference cancellation*, SPIC required the analysis of the soft cancellation system model. Here, the decision statistics were weighted by a *soft cancellation factor (SCF*) and then used in cancellation, resulting in soft interference cancellation. This analysis was based on a bit-synchronous CDMA system, which made it possible to dispense with the modelling of the propagation delay τ through the channel. According to [6], when plotting the BER versus optimal SCF across various system loads for both asynchronous and synchronous systems, it was found that the inter-user asynchronism in time in an asynchronous system decreased the magnitude of MAI, making users interfere with each other less on average, thereby allowing for lower BER, i.e. a higher obtained SCF for the asynchronous case indicated a lower BER. A bit-synchronous system on the other hand did not share this benefit. Therefore, based on these results, [6] concluded that analyzing soft cancellation in a bit-synchronous system would in effect provide a lower bound on the performance improvement that a more realistic asynchronous system would exhibit.

3.4 Transmitter and Receiver Model for Soft Parallel Interference Cancellation

3.4.1 Transmitter Model

The block diagram of the bit-synchronous CDMA transmitter is depicted in Figure 3-3 below.

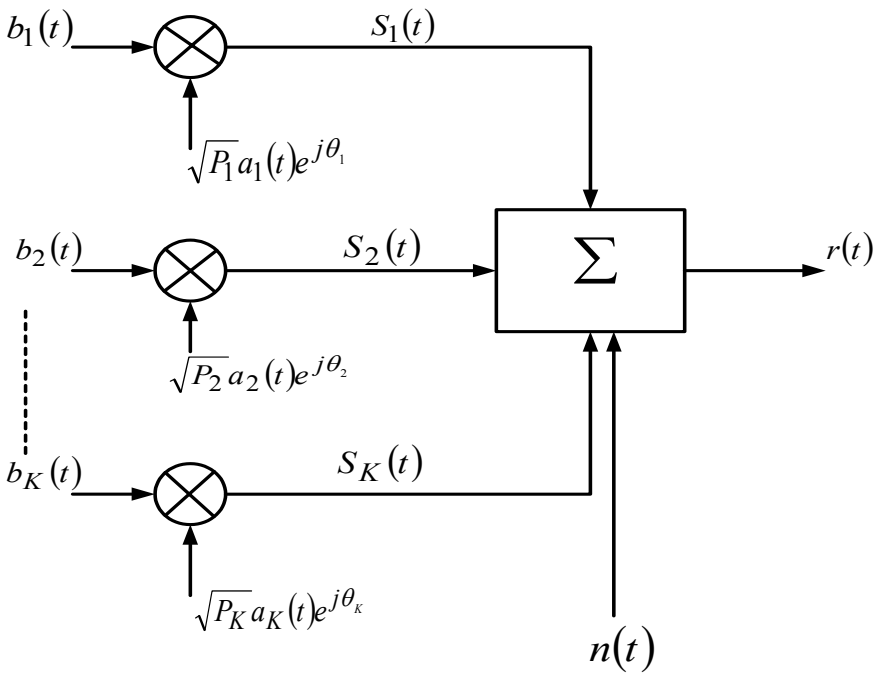

Figure 3-3: CDMA Bit-Synchronous Transmitter Model

Considering K users simultaneously transmitting over a linear AWGN channel a binary data stream modelled as

$$b_k(t) = \sum_{i=-\infty}^{\infty} b_{k,i}\, p_T(t - iT). \tag{3-27}$$

So that each user's data stream is spread by its own high rate PN code waveform, expressed as

$$a_k(t) = \sum_{j=-\infty}^{\infty} a_{k,j}\, p_{T_c}(t - jT_c), \tag{3-28}$$

where $a_k(t) = a_k(t - nT) = a(t - nT_c N)$,i.e. this pseudo-random sequence is usually finite, with period corresponding to $NT_c = T$. It modulates the information signal to generate the transmitted signal, where $\{b_{k,j}\}$ and $\{a_{k,j}\}$ are modelled as $b_{k,i} \in \{-1, +1\}, a_{k,j} \in \{-1, +1\}$, and $\Pr[b_{k,i} = -1] = \Pr[b_{k,i} = +1] = \Pr[a_{k,j} = -1] = \Pr[a_{k,j} = +1] = 1/2$. The bit duration is T and the chip duraction is T_c. The ratio $N = T/T_c$ is defined as the processing gain.

Here, each user transmits a signal given by

$$s_k(t) = \sqrt{P_k}\, b_k(t) a_k(t) e^{j\theta_k}, \tag{3-29}$$

where P_k is the baseband power of the k^{th} user's signal and θ_k is the associated carrier phase, modelled as a random variable uniformly distributed over $[0, 2\pi)$.

Each user's transmitted signal travels through a linear AWGN channel producing a received signal *r(t)* given as

$$\begin{aligned} r(t) &= \sum_{k=1}^{K} s_k(t) + n(t) \\ &= \sum_{k=1}^{K} \sqrt{P_k}\, b_k(t)\, a_k(t)\, e^{j\theta_k} + n(t). \end{aligned} \tag{3-30}$$

Now, the noise *n(t)* is a zero-mean ergodic and stationary complex AWGN process with one-sided power spectrum magnitude N_o. In this bit-synchronous model, the received phase is identical to the transmitted phase.

3.4.2 Receiver Model- Soft Interference Cancellation

The block diagram for the interference cancellation receiver modified for bit-synchronism and soft cancellation is shown in Figure 3-4. The scaling of each reconstructed signal estimate with its own SCF ξ_k represents the soft cancellation.

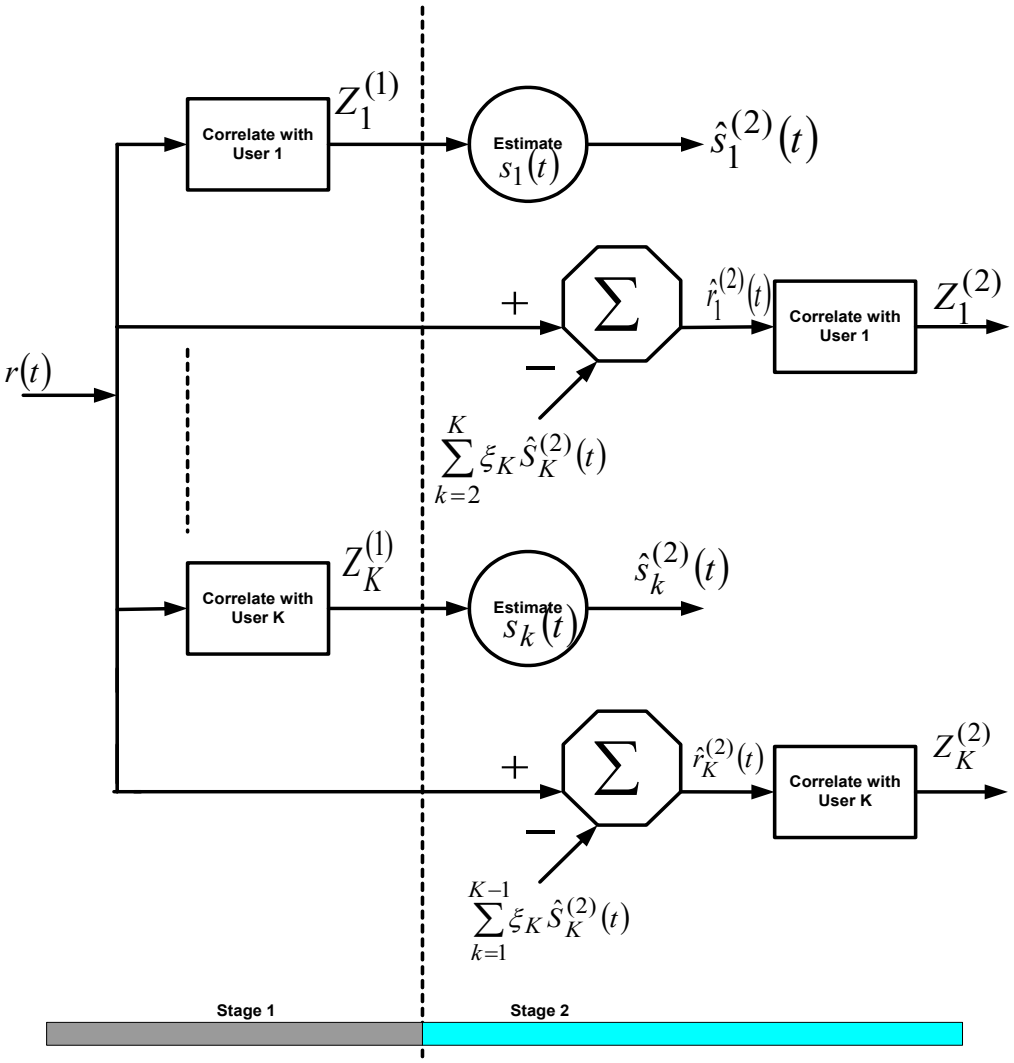

Figure 3-4: The CDMA Bit-Synchronous Soft Cancellation Receiver Model

The first stage is a conventional CDMA correlation receiver. Thus, the decision statistic produced for the k^{th} user's i^{th} bit $Z_{k,i}^{(1)}$ is given as

$$Z_{k.i}^{(1)} = \frac{1}{T}\int_{iT}^{(i+1)T} \Re\left\{ r(t)\, a_k(t)\, e^{-j\theta_k} \right\} dt. \qquad (3\text{-}31)$$

Considering the second stage where the reconstructing of the estimates of transmitted signals also occurs. The form of each reconstructed signal is

$$\hat{s}_k^{(2)}(t) = \left[\sum_{i=-\infty}^{\infty} Z_{k,i}^{(1)} P_T(t - iT) \right] a_k(t) e^{j\theta_k}. \tag{3-32}$$

Then, assigning an SCF ξ_k for each interferer. This is in order to form a new reconstructed received signal for each user which is given by

$$\hat{r}_k^{(2)}(t) = r(t) - \sum_{\substack{\kappa=1 \\ \kappa \neq k}}^{K} \xi_\kappa \hat{s}_\kappa^{(2)}(t) \tag{3-33}$$

The next step involves passing each reconstructed received signal through a bank of correlators identical to that in the first stage, to obtain a cleaner set of decision statistics for each user, given by

$$Z_{k,i}^{(2)} = \frac{1}{T} \int_{iT}^{(i+1)T} \Re \left\{ \hat{r}_k^{(2)}(t) a_k(t) e^{-j\theta_k} \right\} dt. \tag{3-34}$$

The proposed effect of soft cancellation is to reduce the level of interference in $\hat{r}_k^{(2)}(t)$ as compared to conventional cancellation, such that the correlator following the cancellation operation will better detect $a_1(t)$ in $\hat{r}_k^{(2)}(t)$. The main objective of this soft cancellation process, is to use the SCFs which minimize second stage BER or BER$^{(2)}$.

Thus, considering user 1 as the desired user, and seeking the set $\{\xi_l\} l \in \{2,\ldots,K\}$, such that the objective can be expressed as

$$\{\xi_l\} = \arg \left\{ \min_{\substack{0 \le \xi_l \le 1 \\ \forall l \in \{2,\ldots,K\}}} BER^{(2)}(\{\xi_l\}) \right\}, \tag{3-35}$$

yielding the BER for stage 2 of the soft interference canceller. Equation (3-35) can be expressed as

$$BER^{(2)}\left(\{\xi_l\}\right) = Q\left(\sqrt{\frac{\left(E\left[Z_{1,i}^{(2)}\middle|b_{1,i}\right]\right)^2}{Var\left[Z_{1,i}^{(2)}\middle|b_{1,i}\right]}}\right) = Q\left(\sqrt{\frac{\left(E\left[Z_{1,i}^{(2)}\middle|b_{1,i}\right]\right)^2}{E\left[\left(Z_{1,i}^{(2)}\middle|b_{1,i}\right)^2\right]-\left(E\left[Z_{1,i}^{(2)}\middle|b_{1,i}\right]\right)^2}}\right). \quad (3\text{-}36)$$

As the description and objective of the system model has been referred to above, we can now follow with an analysis of the receiver metrics used to ultimately determine the set of optimal SCFs minimizing $BER^{(2)}$ for a given system.

3.4.3 Metric Analysis Description

Before continuing with this analysis by Renucci [6], it should be noted henceforth that the index of the delay parameter τ, has been dropped, indicating that from this stage onwards, τ shall be considered as a general random delay parameter uniformly distributed over $(0,T]$, applicable to all users.

This analysis first required (as mentioned above), converting from the asynchronous case to the synchronous. It was simply done by setting $\tau = 0$ in the metric expressions of the asynchronous case. It consequently leads to $R_{l,m}(0) = 0$, thus leaving only $\hat{R}_{l,m}(0)$ to account for PN cross-correlations. Also, to make notation in subsequent analysis less cumbersome, the synchronous normalized cross-correlation of the PN code waveforms was defined as

$$\Gamma_{m,l} = \frac{1}{T}\int_0^T a_m(t)a_l(t)dt = \hat{R}_{l,m}(0),\ l \neq m \quad (3\text{-}37)$$

The original source of this definition is taken from Divsalar and Simon who have computed several moments of $\Gamma_{m,l}$,used in the second stage variance computation.

Considering the *first stage* statistic, for the asynchronous system it follows from Equation (3-15) with $\tau = 0$, that

$$Z_{1,i}^{(1)} = \sqrt{P_1}\, b_{1,i} + \sum_{l=2}^{K} \sqrt{P_l} \cos(\phi_l - \phi_1) \left[b_{l,i-1} R_{l,1}(\tau) + b_{l,i} \hat{R}_{l,1}(\tau) \right] + \eta. \tag{3-38}$$

Substituting converts to synchronism case to give

$$Z_{1,i}^{(1)} = \sqrt{P_1}\, b_{1,i} + \sum_{l=2}^{K} \sqrt{P_l}\, b_{l,i} \Gamma_{1,l} \cos(\phi_l - \phi_1) + \eta \tag{3-39}$$

Then, taking the conditional expectation of the first stage metric gives

$$E\left[Z_{1,i}^{(1)} \middle| b_{1,i} \right] = \sqrt{P_1}\, b_{1,i}, \tag{3-40}$$

NB: This is the same result as the asynchronous case, indicating that first stage metrics are unbiased amplitude estimates in the synchronous case as well.

In order to compute the conditional variance of first stage statistic, we take advantage of the statistical independence of its desired user, MAI, and noise components. Thus, the desired user contribution is zero again (as mentioned above) and the noise contribution again becomes

$$Var\left[\eta \middle| b_{1,i} \right] = \frac{N_o}{2T}. \tag{3-41}$$

The MAI is zero mean and $E\left[\Gamma_{1,m}^2\right] = 1/N$ [1]. The conditional variance of the MAI component of the first stage statistic is then computed as

$$\begin{aligned} Var\left[Z_{1,i}^{(1)} \middle| b_{1,i} \right] &= E\left[\left(\sum_{l=2}^{K} \sqrt{P_l}\, b_{l,i} \Gamma_{1,l} \cos\left(\phi_l - \phi_1\right) \right)^2 \middle| b_{1,i} \right] + \frac{N_o}{2T} \\ &= \sum_{l=2}^{K} E\left[\left(\sqrt{P_l}\, b_{1,l} \cos(\phi_l - \phi_1) \right)^2 \right] + \frac{N_o}{2T} \\ &= \frac{1}{2N} \sum_{l=2}^{K} P_l + \frac{N_o}{2T}. \end{aligned} \tag{3-42}$$

It is seen that the synchronous first stage variance is greater due to bit-synchronism on comparing Equation (3-42) with the asynchronous first stage variance in Equation (3-13). Thus for the first stage synchronous case, there is an increase in the BER observed.

Considering the second stage metric for user 1, expressed as

$$
\begin{aligned}
Z_{1,i}^{(2)} &= \frac{1}{T}\int_{iT}^{(i+1)T} \Re\left\{\hat{r}_1^{(2)}(t)\, a_1(t)\, e^{-j\theta_1}\right\} dt \\
&= \frac{1}{T}\int_{iT}^{(i+1)T} \Re\left\{\left[r(t) - \sum_{l=2}^{K} \xi_l \hat{s}_l^{(2)}(t)\right] a_1(t)\, e^{-j\theta_1}\right\} dt \\
&= \frac{1}{T}\int_{iT}^{(i+1)T} \Re\left\{r(t)\, a_1(t) e^{-j\theta_1}\right\} dt - \frac{1}{T}\int_{iT}^{(i+1)T} \Re\left\{\sum_{l=2}^{K} \xi_l \hat{s}_l^{(2)}(t) a_1(t)\, e^{-j\theta_1}\right\} dt \\
&= Z_{1,i}^{(1)} - \frac{1}{T}\int_{iT}^{(i+1)T} \Re\left\{\left[\sum_{l=2}^{K} \xi_l Z_{l,i}^{(1)} p_T(t-iT)\, a_l(t) e^{j\theta_l}\right] a_1(t)\, e^{-j\theta_1}\right\} dt \\
&= Z_{1,i}^{(1)} - \sum_{l=2}^{K} \xi_l Z_{l,i}^{(1)} \cos(\theta_l - \theta_1) \frac{1}{T}\int_{iT}^{(i+1)T} a_l(t)\, a_1(t)\, dt \\
&= \underbrace{Z_{1,i}^{(1)}}_{Conv.\,\mathrm{Re}\,c.} - \underbrace{\sum_{l=2}^{K} \xi_1 Z_{l,i}^{(1)} \Gamma_{1,l} \cos(\theta_l - \theta_1)}_{IC \quad with \quad SCF}
\end{aligned}
\tag{3-43}
$$

Substituting Equation (3-38) into Equation (3-43) gives

$$
\begin{aligned}
Z_{1,i}^{(2)} &= \sqrt{P_1} b_{1,i} + \sum_{l=2}^{K} \sqrt{P_l} b_{l,i} \Gamma_{1,l} \cos(\theta_l - \theta_1) + \eta \\
&\quad - \sum_{l=2}^{K} \xi_l \left[\sqrt{P_l} b_{l,i} + \sum_{\substack{m=1 \\ m\neq l}}^{K} \sqrt{P_m} b_{m,i} \Gamma_{l,m} \cos(\theta_m - \theta_l) + \eta\right] \cdot \Gamma_{1,i} \cos(\theta_l - \theta_1) \\
&= \sqrt{P_1} b_{1,i} + \sum_{l=2}^{K} (1-\xi_l) \sqrt{P_l} b_{l,i} \Gamma_{1,l} \cos(\theta_l - \theta_1) \\
&\quad - \sum_{l=2}^{K} \sum_{\substack{m=1 \\ m\neq l}}^{K} \left[\xi_1 \sqrt{P_m} b_{m,i} \Gamma_{1,l} \Gamma_{l,m} \cos(\theta_m - \theta_1) \cos(\theta_l - \theta_1)\right] \\
&\quad + \eta\left[1 - \sum_{l=2}^{K} \xi_l \Gamma_{1,l} \cos(\theta_l - \theta_1)\right].
\end{aligned}
\tag{3-44}
$$

The above gives the expression for the second stage statistic. The mean and variance computations are then computed in order to compare with the initial bias representations.

3.4.4 Mean and variance computations

Thus, conditioning the second stage statistic upon $b_{1,i}$ and taking the expectation, it is seen that the first term, (the desired term), in Equation (3-44) remains intact, while the last term, the noise term, vanishes. Similarly, the second term in the second stage statistic vanishes in the expectation. It is noted that the double summation term only contributes in the expectation when $m=1$, also when the cosine and PN code cross-correlation terms become squared terms. The conditional expectation therefore becomes

$$\begin{aligned} E\left[Z_{1,i}^{(2)}\middle|b_{1,i}\right] &= \sqrt{P_1}\,b_{1,i} - E\left[\sum_{l=2}^{K}\xi_l\sqrt{P_1}\,b_{1,i}\Gamma_{1,l}^2\cos^2(\theta_m-\theta_l)\middle|b_{1,i}\right] \\ &= \sqrt{P_1}\,b_{1,i} - \sqrt{P_1}\,b_{1,i}\sum_{l=2}^{K}\xi_l E\left[\Gamma_{1,l}^2\cos^2(\theta_1-\theta_l)\right] \\ &= \underbrace{\sqrt{P_1}\,b_{1,i}}_{Des.Amp.Est.} - \underbrace{\frac{1}{2N}\sqrt{P_1}\,b_{1,i}\sum_{l=2}^{K}\xi_l}_{\text{Re}\,duced\ Bias\ Term}. \end{aligned} \tag{3-45}$$

Of importance is that in the synchronous soft cancellation case the bias exists as well. Comparing Equations (3-26) and (3-45), the factor of 1/2 instead of 1/3, arose due to the change to synchronous operation. Another important difference is the presence of the summation of the SCFs of the interferers, due to the use of soft cancellation.

Equation (3-45) gives the summation of the SCFs to be always less[3] than $K-1$. Therefore, the bias magnitude in soft cancellation was less than that in conventional or brute cancellation [6].

[3] A given system will never have all SCFs minimizing $BER^{(2)}$ equal to unity, hence $\sum_{l=2}^{K}\xi_l < K-1$.

Setting all SCFs to zero would cure the system of the bias, but in doing so would in effect reduce the receiver to a conventional correlator, not cancelling any interference at all, since all MAI signal estimates would be zeroed. In general, non-zero SCFs minimize BER[(2)].

3.4.5 Second stage metric variance derivation

Defining the variance as

$$Var\left[Z_{1,i}^{(2)}\,\middle|b_{1,i}\right] = E\left[\left(Z_{1,i}^{(2)}\middle|b_{1,i}\right)^2\right] - \left(E\left[Z_{1,i}^{(2)}\,\middle|b_{1,i}\right]\right)^2. \tag{3-46}$$

$E\left[Z_{1,i}^{(2)}\,\middle|b_{1,i}\right]$ has already been computed in Equation (3-45). Hence $E\left[\left(Z_{1,i}^{(2)}\,\middle|b_{1,i}\right)^2\right]$ remains to be determined.

Using the expression for $Z_{1,i}^{(2)}$ and assigning terms, we have

$$\begin{aligned} Z_{1,i}^{(2)} &= \underbrace{\sqrt{P_1}\,b_{1,i}}_{\psi_1} \\ &\quad + \underbrace{\sum_{l=2}^{K}(1-\xi_1)\sqrt{P_l}\,b_{l,i}\Gamma_{1,l}\cos(\theta_l-\theta_1)}_{\psi_2} \\ &\quad - \underbrace{\sum_{l=2}^{K}\sum_{\substack{m=1\\ m\neq l}}^{K}\left[\xi_l\sqrt{P_m}\,b_{m,i}\Gamma_{l,m}\cos(\theta_m-\theta_l)\cos(\theta_l-\theta_1)\right]}_{\psi_3} \\ &\quad + \underbrace{\eta\left[1-\sum_{l=2}^{K}\xi_l\Gamma_{1,l}\cos(\theta_l-\theta_1)\right]}_{\psi_4}. \end{aligned} \tag{3-47}$$

The desired expectation expressed in terms of Ψ_1, Ψ_2, Ψ_3 and Ψ_4 gives

$$\begin{aligned} E\left[\left(Z_{1,i}^{(2)}\middle|b_{1,i}\right)^2\right] &= E\left[\{(\psi_1+\psi_2-\psi_3+\psi_4)\}^2\right] \\ &= E\left[\left(\psi_1\middle|b_{1,i}\right)^2\right]+E\left[\left(\psi_2\middle|b_{1,i}\right)^2\right]+E\left[\left(\psi_3\middle|b_{1,i}\right)^2\right]+E\left[\left(\psi_4\middle|b_{1,i}\right)^2\right] \\ &\quad +2E\left[\psi_1\psi_2\middle|b_{1,i}\right]-2E\left[\psi_1\psi_3\middle|b_{1,i}\right]+2E\left[\psi_1\psi_4\middle|b_{1,i}\right]-2E\left[\psi_2\psi_3\middle|b_{1,i}\right] \\ &\quad +2E\left[\psi_2\psi_4\middle|b_{1,i}\right]-2E\left[\psi_3\psi_4\middle|b_{1,i}\right] \end{aligned} \tag{3-48}$$

This subdivision was done in order to make the calculations easier. The next step is to compute each component in order of appearance in Equation (3-48). Rennuci [6], gives a detailed derivation of this.

The final computation gives the variance of the second stage metric as

$$\begin{aligned} Var\left[Z_{1,i}^{(2)}\middle|b_{1,i}\right] &= E\left[\left(Z_{1,i}^{(2)}\middle|b_{1,i}\right)^2\right]-\left(E\left[Z_{1,i}^{(2)}\middle|b_{1,i}\right]\right)^2 \\ &= E\left[\left(Z_{1,i}^{(2)}\middle|b_{1,i}\right)^2\right]-\left[\sqrt{R_1}b_{1,i}-\frac{1}{2N}\sqrt{R_1}b_{1,i}\sum_{l=2}^{K}\xi_l\right]^2 \\ &= E\left[\left(Z_{1,i}^{(2)}\middle|b_{1,i}\right)^2\right]-\left[R_1-\frac{1}{N}R_1\sum_{l=2}^{K}\xi_l+\frac{1}{4N^2}R_1\left(\sum_{l=2}^{K}\xi_l\right)^2\right]. \end{aligned} \tag{3-49}$$

Cancelling like terms finally yields

$$
\begin{aligned}
Var\left[Z_{1,i}^{(2)}\middle|b_{1,i}\right] &= \frac{1}{2N}\sum_{l=2}^{K}P_l + \frac{1}{2N}\sum_{l=2}^{K}\xi_l^2 P_l + R_1\left(\frac{9}{8N^2}-\frac{3}{4N^3}\right)\sum_{l=2}^{K}\xi_l^2 + \frac{1}{4N^2}\sum_{l=2}^{K}\sum_{\substack{m=2\\ m\neq l}}^{K}\xi_l^2 P_m \\
&+ \frac{1}{4N^2}R_1\sum_{l=2}^{K}\sum_{\substack{m=2\\ m\neq l}}^{K}\xi_l\xi_m - \frac{1}{2N^2}\sum_{l=2}^{K}\sum_{\substack{m=2\\ m\neq l}}^{K}\xi_l P_m + \frac{1}{2N^2}\sum_{l=2}^{K}\sum_{\substack{m=2\\ m\neq l}}^{K}\xi_l\xi_m P_m \\
&+ \frac{1}{8N^3}\sum_{l=2}^{K}\sum_{\substack{m=2\\ m\neq l}}^{K}\sum_{\substack{n=2\\ n\neq m,l}}^{K}P_m\xi_l\xi_n - \frac{1}{N}\sum_{l=2}^{K}\xi_l P_l - \frac{1}{4N^2}R_1\left(\sum_{l=2}^{K}\xi_l\right)^2 \\
&= \frac{N_o}{2T}\left[1+\frac{1}{2N}\sum_{l=2}^{K}\xi_l^2\right],
\end{aligned}
\tag{3-50}
$$

where the last term is the noise contribution to the variance, and all preceding terms are attributed due to MAI.

It is seen that the cancellation process generally removed more MAI than it enhanced noise, thereby making the second stage variance as a whole smaller than the first stage variance. The smaller second stage variance is indicative of second stage amplitude estimates wandering about their mean to a lesser degree than at the first stage. The positive effect of this is it allows for a high rate of correct bit estimates.

3.5 BER$^{(2)}$ of Second Stage Cancellation

As BER$^{(2)}$ is expressed in terms of the Q-function, it is found that minimizing BER$^{(2)}$ is equivalent to maximizing the Q-function argument. The optimal SCF for a given interferer $\left(\xi_K, \kappa \in \{,..., K\}\right)$ is found by taking the partial derivative of the Q-function argument with respect to ξ_k, setting it to zero, and solving for ξ_k, as denoted by

$$\{\xi_\kappa\}: \frac{\partial}{\partial \xi_\kappa}\left[\frac{\left(E\left[Z_{1,i}^{(2)}\middle|b_{1,i}\right]^2\right)}{Var\left[Z_{1,i}^{(2)}\middle|b_{1,i}\right]}\right]=0, \quad \text{where } \kappa \in \{2,...,K\}. \tag{3-51}$$

After the differentiation process, the maximum of the two extrema (minimum and maximum) was collected and was of the form

$$\xi_\kappa = \frac{\mathrm{A}}{\mathrm{B}}, \tag{3-52}$$

where

$$\begin{aligned} A = {} & 8N^3\left(P_\kappa - \frac{N_o}{2T}\right) - \sum_{\substack{l=2 \\ l\neq\kappa}}^{K} \xi_l^2\left[P_1(7N-6) + (2N-1)\left(\sum_{\substack{m=2 \\ m\neq\kappa,l}}^{K} P_m + 2NP_l\right)\right] \\ & - 2N(2N-1)\sum_{\substack{l=2 \\ l\neq\kappa}}^{K}\xi_l\left[2P_\kappa - P_l\right] - (2N-1)\left[\sum_{l=2}^{K}\sum_{\substack{m=2 \\ l\neq\kappa\ m\neq\kappa,l}}^{K}\xi_l\xi_m(P_l - P_\kappa)\right] \\ & - 4N^2\frac{N_o}{2T}\sum_{\substack{l=2 \\ l\neq\kappa}}^{K}\xi_l^2, \end{aligned} \tag{3-53}$$

and

$$B = 8N^3\left(P_\kappa + \frac{N_o}{2T}\right) - \sum_{\substack{l=2 \\ l\neq\kappa}}^{K}\xi_l\left[P_1(7N-6)+(2N-1)\left(\sum_{\substack{m=2 \\ m\neq\kappa,l}}^{K}P_m + 2NP_\kappa\right)\right]$$
$$-2N(1-2N)\left[\sum_{\substack{m=2 \\ m\neq\kappa}}^{K}P_m + (6-7N)P_1\right] - 4N^2\frac{N_o}{2T}\sum_{\substack{l=2 \\ l\neq\lambda}}^{K}\xi_l .$$

(3-54)

This is the expression for the optimal SCF used to minimize second stage BER, ($BER^{(2)}$).

The following explanation is based on Equation (3-52), with the following conditions where user 1 is still our desired user, and assigning to the κ^{th} interferer the SCF ξ_κ.

As Equation (3-52) assumed knowledge of signal and noise powers, in practice, perfect knowledge of these quantities is usually not available. According to *Moon et al* and *Celandroni et al* [6], this knowledge could be estimated in a number of ways which varied in complexity and effectiveness. It is observed that the convergence of Equation (3-52) made the implementation of the soft cancellation factor technique feasible in a digital receiver. Equation (3-52) also indicates, however, that optimal SCFs are not only functions of MAI parameters, but of noise power as well in an in-direct way, i.e. even though noise did not contribute on an average basis to MAI estimates, noise does however contribute to the oscillation of MAI estimates about their mean (basically contributing to the respective variance). Thus, as noise impacts on the variance of reconstructed MAI, it in turn impacts $BER^{(2)}(\{\xi_l\})$, therefore, hereby, optimal SCFs are able to account for noise in this manner.

Furthermore, the limiting cases analysed show the fundamental dependence of SCF upon MAI reliability. The initial insights into the behaviour of the SCFs is gained by first observing certain extreme cases.

Limiting Case 1: Consider a system with hypothetically infinite processing gain. This translates to the system having infinite immunity to MAI and will only be impaired by AWGN. With this condition, Equation (3-52) can be simplified to:

$$\lim_{N\to\infty} \xi_K = \frac{P_K - \frac{N_O}{2T}}{P_K + \frac{N_O}{2T}} \tag{3-53}$$

The SCFs depend only upon the given interferer's power and the noise power under full MAI immunity conditions. Intuitively, the more noise present in the system, the less reliable the MAI estimates become, and consequently the more MAI estimates require scaling-down. Equation (3-52) is intuitively consistent with as ξ_K decreases with increasing N_O. Also, for a given value of N_O, the stronger the interferer power P_K, the more reliable the interferer's amplitude estimate. Thus, a high-value SCF will be required to cancel the interferer.

Limiting Case 2: Considering further the above infinite processing gain system with the added hypothetical postulation of the absence of noise, this results in a system with perfect MAI estimates. This characteristic of ideal knowledge of interference uncorrupted by AWGN noise, means no MAI down-scaling would be needed. This would correspond to an SCF of unity (SCF = 1).

This is confirmed by examination of Equations (3-52) and (3-53), to obtain

$$\lim_{\substack{N\to\infty \\ N_O\to 0}} \xi_K = 1. \tag{3-54}$$

An important observation is that if the system is fully immune to MAI and there is no noise, any value of SCF (not just $\xi_K = 1$) leads to $BER^{(2)} = 0$, as the variance of the matched-filter outputs (at both stages) is zero. The fact that ξ_K approached unity under these conditions is indicative of less down-scaling needed as MAI estimates become more and more reliable.

Consider a perfect power control system where all signal powers are set equal to P. Mathematical manipulation of Equation (3-52), gave the result that under perfect power control, all interferers bore the same SCF, as determined by[4]

$$\xi = \frac{P\left(4N^2 - 2N\right) - 4N^2 \frac{N_o}{2T}}{P\left(4N^2 + 2K\left(2N-1\right) - 3N - 2\right) + 4N^2 \frac{N_o}{2T}} \tag{3-55}$$

$$= \frac{\frac{E_b}{N_o}\left(4N^2 - 2N\right) - 2N^2}{\frac{E_b}{N_o}\left(4N^2 + 2K\left(2N-1\right) - 3N - 2\right) + 2N^2}$$

When all users are received with the same power, MAI estimates across all users share the same degree of reliability, and are thus all scaled-down by the same amount. We see in Equation (3-55) the same dependence of SCF upon N_o, namely the greater the noise power, the smaller the SCF.

Another important relationship in accordance with literature (the performance of CDMA systems degrades approximately linearly with system loading), is revealed in Equation (3-55). It is that of SCF system loading: as system loading increases, SCF decreases. A plot of SCF versus loading would in fact look roughly linear.

The simulations performed by Rennuci [6], served to illustrate the fundamental dependence of SCF upon MAI reliability. It was observed that as MAI fidelity (accuracy) dropped, so did SCF, reflecting a lesser degree of reliability in MAI estimates. Also of note, was the fact that increasing the processing gain in a CDMA system, amounted to enhancing the system's inherent MAI suppression ability, i.e. when doubling the

[4] Previous analysis assumed the presence of MAI, implying $K \geq 2$. Therefore, the constraint $K \geq 2$ must also be applied to the expression of ξ for perfect power control.

processing gain for a given system load, the SCFs would only need to down-scale MAI estimates by about half as much.

Considering a cellular system, it was concluded that the system benefited from power control, and that received power variations were to be maintained rather small. On an implementation note, it was observed that for perfect power control, all users were to bear identical SCFs, i.e. regardless of the user, all users in a given system would be cancelled with a unique SCF. This implementation complexity was found to be linear in K, in contrast to the more expensive implementation which is quadratic in K, used when the signals are received with different power levels. Here, each user's SCF will be different, and it will also depend upon which user is the desired user. The former implementation scheme, using perfect power control, has been chosen in implementing the proposed P^3MUD algorithm.

The objective of this chapter has been to give a description and hopefully not an exhaustive explanation on the conventional and soft parallel interference cancellation techniques. This is to form the foundation from which the universal SCF, SCF_{UNV} can be determined.

3.6 Determining the Universal SCF

3.6.1 Motivation for the Universal SCF, SCF_{UNV}

The identification of the merits of the effect of a universal SCF has come about through studying the work done by *Renucci et al* [6]. Here, the optimal SCF values pertaining to a specific system load (number of users), were calculated. Rennuci [6], basically analysed the BER performance as the number of users K, was varied, (K=10, K=15, K=20, K=25, K=30), whilst using a specific SCF value. This study attempts to go further by analysing the behaviour of the SCF values as K is incremented by one user at a time. Equation (3-55), which minimizes second stage BER, will be used to calculate the optimal SCFs. This is in order to create a model of the optimal SCF behaviour. This model will then be used to derive the universal SCF, where $0 \le SCF_{UNV} \le 1$,which should exhibit a promising

characteristic, independent of the numbers of users K. This universal SCF will also assist in mitigating the bias effect(s) during the parallel cancellation process.

3.6.2 Methodology I

The approach taken in this dissertation study was to employ Equation (3-55) to verify the theory, as well as to be used in the calculation of the optimal SCF values. This was basically the first stage in the calculation of the Universal SCF value. It involved varying the number of users K iteratively in Equation (3-55) with $N = 31$ and SNR(E_b/N_o)=10 dB. This was done for 30 users and the magnitude of the difference between the iteratively calculated values of SCF was shown to decrease, indicating decreasing accuracy in Equation (3-55) as K approached N. This is shown in Table 3-1.

K (Users)	SCF	Delta
2	0.85774	0
3	0.83344	0.0243
4	0.81048	0.02296
5	0.78876	0.02172
6	0.76817	0.02059
7	0.74862	0.01955
8	0.73005	0.01857
9	0.71237	0.01768
10	0.69554	0.01683
11	0.67947	0.01607
12	0.66414	0.01533
13	0.64948	0.01466
14	0.63545	0.01403
15	0.62202	0.01343
16	0.60914	0.01288
17	0.59679	0.01235
18	0.58492	0.01187
19	0.57352	0.0114
20	0.56256	0.01096
21	0.55201	0.01055
22	0.54184	0.01017
23	0.53204	0.0098
24	0.52259	0.00945
25	0.51347	0.00912
26	0.50467	0.0088
27	0.49616	0.00851
28	0.48793	0.00823
29	0.47997	0.00796
30	0.47227	0.0077

Table 3-1: Tabulations of K, SCF and Delta(SCF) or ΔSCF

An accuracy of 5 decimal places was employed. These variables are graphically displayed in Figure 3-5.

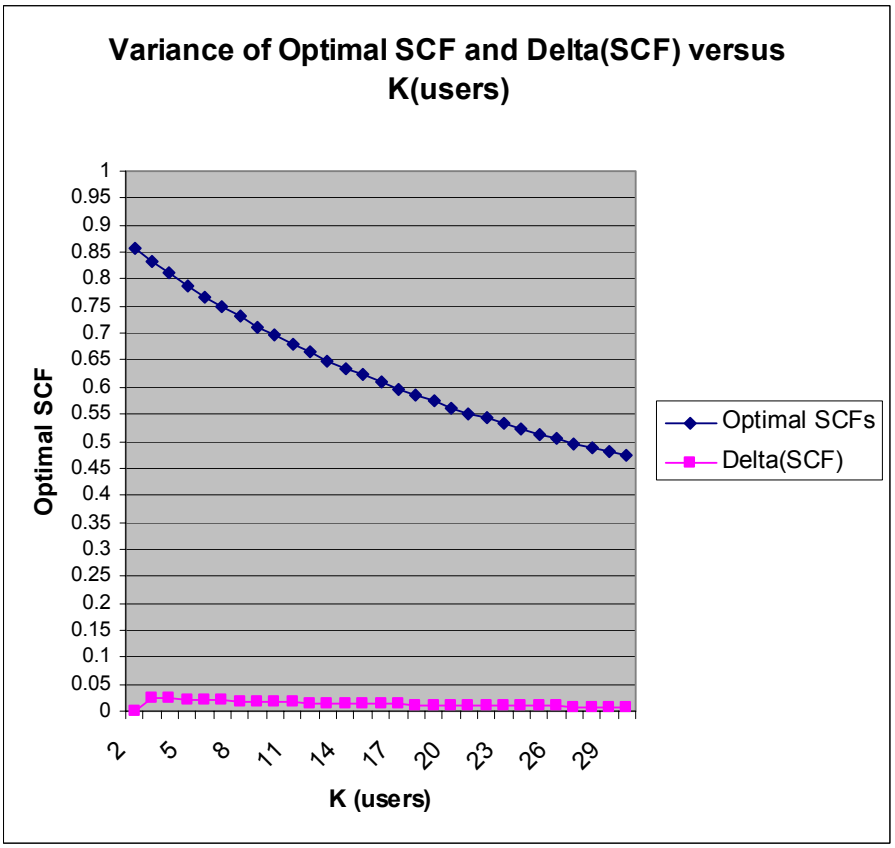

Figure 3-5: Variations of SCF and ΔSCF versus K (number of users).

The above variation agreed with the theory according to Equation (3-55). The range of optimal SCFs was shown to vary from between 0.47 up to a value of 0.87 for $2 \le K \le 30$. This indicated the inverse relationship between the SCF and K. The ΔSCF variation, i.e., the difference in magnitude in the optimal SCF value as the number of users K was progressively increased, tends to decrease as K increases.

The optimal SCF range was employed as the main guideline in the process of determining the Universal SCF. This procedure involved varying the SCF value iteratively from 0.47 to 0.86 for a given K to obtain the Probability of Error. Thus, graphical representations of the Probability of Error P_b versus the number of users for given SCF were obtained and analysed as seen in the next section.

3.7 Chapter 3 Summary

This chapter described the conventional and soft parallel interference cancellation models. It presented and analysed the receiver structures and the interference cancellation algorithm for both models. The focus was on the soft cancellation technique, and the first and second stage metrics were defined, all of which are functions of SCFs. The formulation of second stage BER, $\left(BER^2\right)$, in terms of SCFs was shown as well as deriving the set of optimal SCFs minimizing BER. It was explained how the optimal SCFs were able to reduce the bias. The motivation for the universal SCF was given, and the initial methodology to determine in which range the optimal SCFs lay, was described.

CHAPTER 4

PROBABILITY OF ERROR ANALYSIS

The focus of this chapter is to derive the probability of error expression to be used in the universal SCF, SCF_{UNV} determination. The probability of error analysis is described for the conventional receiver, which is usually stage 0, in the parallel interference cancellation process, and is also mentioned for the partial interference cancellation stage 1, which follows on from the conventional receiver. The resultant probability of error expression is used in the analysis of the behaviour of the optimal SCFs, and hence, the derivation of the Universal SCF.

4 PROBABILITY OF ERROR ANALYSIS INTRODUCTION

It was promoted by *Correal* [29], that for practical implementation purposes, multistage parallel interference cancellation was an attractive approach, both in terms of performance and computational complexity [30], as well as its robustness to moderate phase jitter and synchronization errors. In order to minimize the complexity of an interference cancellation receiver, a matched filter bank is commonly used at each stage for estimation of the transmitted bits and received signal energies. Regeneration and complete subtraction of the estimated MAI is then performed to reduce the interference affecting each user. This important fact should be noted as it differs from the bit-streaming pipelined multiuser detector, in the following chapter, where the first stage matched filter is followed by three or more stages of parallel interference cancellation.

The work done by *Correal* [29], extended the analytic approach of *Divsalar et al* , for single user multiple symbol differential decoding to derive bounds on the probability of error of multi-symbol differential partial parallel interference cancellation. Thus, an upper bound for the probability of bit error was obtained through the union bound of pairwise probabilities of error. Then, computation of the pair-wise error probabilities was performed using a technique developed by *Stein* [29] for the unified computation of the probability of error of FSK and other digital modulation techniques. Correal [29], obtained Probability of error expressions for standard differential detection,where $N_w = 2$, observation symbols, to subsequently deriving probability of error bounds for the case of $N_w = 3$, as well as asymptotic bounds for arbitrary observation lengths.

Therefore, the results obtained give an upper bound for the probability of error of the synchronous as well as the asynchronous case.

4.1 Stage 0 Probability of Error Analysis: *The Conventional Receiver*

According to Correal et al. [29], the conventional CDMA receiver, can be implemented with a bank of matched filters, or with correlation demodulators. The focus of analysis was once again reference user 1, with equal received powers being assumed.

The pairwise probability of error for standard differential detection, is thus given by :

$$P_r\left\{ |z_2|^2 > |z_1|^2 \right\} = \frac{1}{2}\left[1 - Q\left(\sqrt{\frac{2E_b}{E_b\frac{K-1}{N}+N_o}},\ 0\right) + Q\left(0,\ \sqrt{\frac{2E_b}{E_b\frac{K-1}{N}+N_o}}\right)\right]. \tag{4-1}$$

Where E_b, is the bit energy, N_o, the noise power, N, the processing gain, and K, the number of users.

In the Evaluation of Equation (4-1), advantage is taken of the following properties of the Marcum-Q function [29], where the arguments are a and b, for:

$$\begin{aligned} Q(a,0) &= 1 \\ Q(0,b) &= e^{-\frac{b^2}{2}}. \end{aligned} \tag{4-2}$$

Manipulating Equation (4-1) by these limiting forms and noting that for binary constellations, the pairwise probability of symbol error equals the probability of bit error, gives the following expression for the probability of bit error for standard differential detection:

$$P_b = \frac{1}{2}\exp\left(\frac{-E_b}{E_b\frac{K-1}{N}+N_o}\right). \tag{4-3}$$

Analysis for stage 1 and stage 2 for conventional or full interference cancellation is omitted here, but can be observed in the work done in [28]. Of interest, is the derivation of the probability of error for stage 1 employing partial interference cancellation, as it will be used in the SCF_{UNV} determination analysis. We thus move on to the partial interference cancellation analysis in the next section.

4.2 Stage 1: Probability of Error Analysis with Partial Interference Cancellation

The decision statistics at stage one are obtained by partially subtracting the estimated interference caused by the remaining users:

$$y_1^{(s=1)} = y_1^{(s=0)} - SCF_1 \sum_{u=2}^{K} y_u^{(s=0)} R_{1,u} . \tag{4-4}$$

Here, SCF_1 is the partial cancellation factor at stage 1, u is the user and $R_{1,u}$, is the signature cross-correlation. The decision statistic at stage(s=0) for user u is $y_u^{(s=0)}$.

Reiterating, the focus of analysis is user 1, as mentioned above. As before, equal received powers are assumed. Thus, using notation based on [31], the i^{th} decision statistic of user 1 in the observation window,

$y_{1,k-i}^{(s=0)}$, corresponds to:

$$y_{1,k-i}^{(s=0)} = \sqrt{E_b} e^{j\phi_{1,k-i}} + \sqrt{E_b} \sum_{u=2}^{K} R_{1,u} e^{j\phi_{u,k-i}} + n_{1,k-i} . \tag{4-5}$$

Where, in order to simplify notation, the unknown phase shift at the receiver has been accounted for in $\phi_{j,k-i}$, the phase of user j at time $k - i$, n_1, is the complex valued AWGN noise element for user 1.

Then, using Equation (4-5) to express the soft outputs of the conventional receiver, and cancelling like terms, give the decision statistics after partial interference cancellation as:

$$y_1^{(s=1)} = \sqrt{E_b}e^{j\phi_1} + \sum_{l=2}^{K}\sqrt{E_b}R_{1,l}e^{j\phi_l} + n_1 - SCF_1\sum_{u=2}^{K}\left(\sqrt{E_b}e^{j\phi_u} + \sum_{l\neq u}^{K}\sqrt{E_b}R_{l,u}e^{j\phi_l} + n_u\right)R_{1,u}. \quad (4\text{-}6)$$

Where l, is the path subscript, R_l is the path signature cross-correlation, ϕ_l , is the path phase, ϕ_u is the user phase and n_u, is user noise, $y_1^{(s=1)}$, is the decision statistic for user 1 after partial cancellation, and K , is the number of users.

Isolating and factoring common terms results in:

$$y_1^{(s=1)} = \sqrt{E_b}\left[1 - SCF_1\sum_{u=2}^{K}R_{1,u}^2\right]e^{j\phi_1} + (1-SCF_1)\sum_{u=2}^{K}\sqrt{E_b}R_{1,u}e^{j\phi_u} - SCF_1\sqrt{E_b}\sum_{u=2}^{K}\sum_{\substack{l=2\\ l\neq u}}^{K}R_{l,u}R_{1,u}e^{j\phi_l} + \left(n_1 - SCF_1\sum_{u=2}^{K}n_uR_{1,u}\right). \quad (4\text{-}7)$$

Now, to compute the pairwise probability of error, $\Pr\left\{|z_2|^2 > |z_1|^2\right\}$, we need to define the variables z_1 and z_2 , which are the multiple-symbol decision statistics as:

$$z_1 = \sum_{k=0}^{N_w-1} y_1^{(s=1)} e^{-j\sum_{m=0}^{N_w-i-2}\Delta\phi_{1,k-i-m}}. \quad (4\text{-}8)$$

and

$$z_2 = \sum_{k=0}^{N_w-1} y_1^{(s=1)} e^{-j\sum_{m=0}^{N_w-i-2}\Delta\hat{\phi}_{1,k-i-m}}. \quad (4\text{-}9)$$

Where N_w, represents the observation symbols, m is the m^{th} cancellation stage, and $k-i-m$, represents the time frame.

Proceeding, substituting in Equation (4-8) the expression given in Equation (4-7) gives:

$$z_1 = N_w\sqrt{E_b}e^{j\phi_{1,k-N_w+1}}\left[1-SCF_1\sum_{u=2}^{K}R_{1,u}^{N_w-1}\right]+\sum_{k=0}^{N_w-1}\Bigg[(1-SCF_1)\sum_{u=2}^{K}\sqrt{E_b}R_{1,u}e^{j\phi_u}$$
$$-SCF_1\sqrt{E_b}\sum_{u=2}^{K}\sum_{\substack{l=2\\ l\neq u}}^{K}R_{l,u}e^{j\phi_{l,k-i}}+(n_{1,k-i}-SCF_1\sum_{u=2}^{M}n_{u,k-i})R_{1,u}\Bigg]e^{-j\sum_{m=0}^{N_w-i-2}\Delta\phi_{1,k-i-m}}. \quad (4\text{-}10)$$

Where M, is the number of iterations.

The mean, $\overline{z_1}$, corresponds to:

$$\overline{z_1} = N_w\sqrt{E_b}\left(1-SCF_1\frac{K-1}{N}\right)e^{j\phi_{1,k-N_w+1}}. \quad (4\text{-}11)$$

It is noted that the bias in the mean has been reduced by an amount proportional to the partial cancellation factor ($0 \le SCF_1 \le 1$).

Consider the power in the non-random component S_1 as:

$$S_1 = \frac{1}{2}\left|\bar{z}_1\right|^2$$
$$= \frac{1}{2}N_w^2E_b\left(1-SCF_1\frac{K-1}{N}\right)^2. \quad (4\text{-}12)$$

The noise power after cancellation corresponds to:

$$N_s = \frac{1}{2}E\left\{\left|\sum_{i=0}^{N_w-1} y_{1,k-i}\, e^{-j\sum_{m=0}^{N_w-i-2}\Delta\phi_{1,k-i-m}} - N_w\sqrt{E_b}\left(1+SCF_1\frac{K-1}{N}\right)e^{j\phi_{1,k-i}N_w+1}\right|^2\right\}. \tag{4-13}$$

Then, substituting for $y_{1,k-i}$ as given in (4-7) results in:

$$\begin{aligned}
N_s = {} & \frac{1}{2}E\left\{\left|\sqrt{E_b}SCF_1\sum_{i=0}^{N_w-1}\left(\frac{K-1}{N}-\sum_{u=2}^{K}R_{1,u}^2\right)e^{j\phi_{1,k-N_w+1}}\right|^2\right\} \\
& + \frac{1}{2}E\left\{\left|\sqrt{E_b}(1-SCF_1)\sum_{i=0}^{N_w-1}\sum_{u=2}^{K}\sqrt{E_b}R_{1,u}e^{j\phi_{u,k-i}-j\sum_{m=0}^{N_w-i-2}\Delta\phi_{1,k-i-m}}\right|^2\right\} \\
& + \frac{1}{2}E\left\{\left|\sqrt{E_b}SCF_1\sum_{i=0}^{N_w-1}\sum_{u=2}^{K}\sum_{\substack{l=2\\ l\neq u}}^{K}R_{l,u}R_{1,u}e^{j\phi_{l,k-i}-j\sum_{m=0}^{N_w-i-2}\Delta\phi_{1,k-i-m}}\right|^2\right\} \\
& + \frac{1}{2}E\left\{\left|\sum_{i=0}^{N_w-1}\left(n_{1,k-i}-SCF_1\sum_{u=2}^{K}n_{u,k-i}R_{1,u}\right)e^{-j\sum_{m=0}^{N_w=i=2}\Delta\phi_{1,k-i-m}}\right|^2\right\}.
\end{aligned} \tag{4-14}$$

Where N_s, is the equivalent noise power.

The evaluation of the expectations is readily performed to give,

$$\begin{aligned}
N_s = {} & \frac{1}{2}N_w{}^2E_bSCF_1{}^2\left(\frac{2(K-1)}{N^2}\right) \\
& + \frac{1}{2}N_wE_b(1-SCF)^2\frac{K-1}{N} \\
& + \frac{1}{2}N_wSCF_1{}^2(K-1)(K-2)\frac{1}{N^2} \\
& + \frac{1}{2}N_w\left(N_o-2N_oSCF_1\sum_{u=2}^{K}E\{R_{1,u}^2\}+\sum_{u=2}^{K}N_oSCF_1{}^2E\{R_{1,u}^2\}\right).
\end{aligned} \tag{4-15}$$

The direct evaluation of Equation (4-15) is possible by assuming that $E\{R_{1,u}^2\} = \frac{1}{N}$. This is the variance of the signature cross-correlations.

Therefore:

$$\begin{aligned} N_S &= \frac{1}{2} N_w^2 E_b SCF_1^2 \left(\frac{2(K-1)}{N^2} \right) \\ &+ \frac{1}{2} N_w E_b (1 - SCF_1)^2 \frac{K-1}{N} \\ &+ \frac{1}{2} N_w E_b SCF_1^2 (K-1)(K-2) \frac{1}{N^2} \\ &+ \frac{1}{2} N_w N_o \left(1 - 2 SCF_1 \frac{K-1}{N} + SCF_1^2 \frac{K-1}{N} \right). \end{aligned} \tag{4-16}$$

4.3 Computation of probability of error

Now consider the standard differential receiver ($N_w = 2$). The parameters a and b of the Marcum-Q function are given by:

$$\begin{Bmatrix} a \\ b \end{Bmatrix} = \begin{Bmatrix} 0 \\ \frac{S_1}{N_S} \end{Bmatrix}. \tag{4-17}$$

where, S_1 and N_s are given in Equations (4-12) and (4-16) respectively.

Continuing, by substituting (4-12)and (4-16) into (4-18) yields the pairwise error probability of choosing $\Delta\hat{\phi}_j$,(the estimated information sequence), when $\Delta\phi_j$,(the reference information sequence), is transmitted, is obtained. From the previous definitions, the pairwise error probability $P_r\{\hat{\eta}_j > \eta_j | \Delta\phi_j\}$ is equivalent to $\Pr\{|z_2|^2 > |z_1|^2 | \Delta\phi\}$. Calculation of the pairwise probability of error will be performed based on the results by

Etten [29] and applied in work by *Divsalar et al* [29] to the single user problem. Thus, the pairwise error probability can be evaluated according to *Divsalar et al* [29]:

$$\Pr\left\{\left|z_2\right|^2 > \left|z_1\right|^2\right\} = \frac{1}{2}\left[1 - Q(\sqrt{b},\sqrt{a}) + Q(\sqrt{a},\sqrt{b})\right] \tag{4-18}$$

where

$$Q(a,b) = \int_b^\infty \exp\left(-\frac{a^2+x^2}{2}\right) I_O(ax)dx. \tag{4-19}$$

is the Marcum-Q function, with arguments determined according to:

$$\left\{\begin{matrix} a \\ b \end{matrix}\right\} = \frac{1}{2N_s}\left\{\frac{S_1 + S_2 - 2|\rho|\sqrt{S_1 S_2}\cos(\theta_1 - \theta_2 + \phi)}{1-|\rho|^2} \mp \frac{S_1 - S_2}{\sqrt{1-|\rho|^2}}\right\}. \tag{4-20}$$

Where S_1 and S_2 represents power in non-random components z_1 and z_2, respectively, and θ_1 and θ_2 are the respective phases, and ρ, is the correlation coefficient,

Therefore, since for $N_w = 2$ and binary signaling, the pairwise probability is equivalent to the probability of bit error, then:

$$\Pr\{\left|z_2\right|^2\} > \left\{\left|z_1\right|^2\right\}^{(s=1)} =$$
$$\frac{1}{2}\exp\left(\frac{-E_b\left(1 - SCF_1\frac{K-1}{N}\right)^2}{\left(E_b 2SCF_1^2\frac{2(K-1)}{N^2} + (1-SCF_1)^2\frac{K-1}{N} + SCF_1^2(K-1)\frac{K-2}{N^2}\right) + N_o\left(1 - 2SCF_1\frac{K-1}{N} + SCF_1^2\frac{K-1}{N}\right)}\right). \tag{4-21}$$

Alternatively, in a slightly more compact notation:

$$P_b^{(s=1)} = \Pr\left\{ |z_2|^2 > |z_1|^2 \right\}^{(s=1)}$$

$$= \frac{1}{2}\exp\left(\frac{-E_b\left(1 - SCF_1\frac{K-1}{N}\right)^2}{E_b\frac{K-1}{N}\left(SCF_1{}^2\frac{K+2}{N} + (1-SCF_1)^2\right) + N_o\left(1 - SCF_1\frac{K-1}{N}(2 - SCF_1)\right)} \right). \quad (4\text{-}22)$$

For $SCF_1 = 1$*, Equation (4-22) evaluates to the probability of bit error for the full cancellation approach [29]. For* $SCF_1 = 0$ *it evaluates to the probability of error of the conventional receiver.*

To note also, is that the signature sequence cross correlations are uncorrelated, but not independent, random variables. It was shown in Appendix E of [29] that the variance of signature cross-correlations is:

$$E\{R_{i,j}R_{j,m}R_{i,m}\} = \frac{1}{N^2}. \quad (4\text{-}23)$$

Thus, this fact should be taken into consideration in order to augment the expressions employed in the computation of the probability of error. This is in order to account for quadratic terms that arise due to expressions of the form of Equation (4-23).

Therefore, Equation (4-13) is augmented to obtain an expression for the equivalent noise power. The resultant process involves adding the appropriate terms, to obtain;

$$
\begin{aligned}
N_s &= \frac{1}{2} N_w{}^2 E_b SCF_1{}^2 \left(\frac{2(K-1)}{N^2} \right) \\
&+ \frac{1}{2} N_w E_b (1 - SCF_1)^2 \frac{K-1}{N} \\
&+ \frac{1}{2} N_w E_b SCF_1{}^2 (k-1)(K-2) \frac{1}{N^2} \\
&- \frac{1}{2} N_w E_b SCF_1 (1 - SCF_1) \frac{(K-1)(K-2)}{N^2} \\
&+ \frac{1}{2} N_w N_o \left(1 - 2SCF_1 \frac{K-1}{N} + SCF_1{}^2 \left(\frac{K-1}{N} + \frac{(K-1)(K-2)}{N^2} \right) \right).
\end{aligned}
$$

(4-24)

Then the probability of error reduces to:

$$
P_b^{(s=1)} = \frac{1}{2} \exp \left\{ \frac{- E_b \left(1 - SCF_1 \frac{K-1}{N} \right)^2}{E_b \frac{K-1}{N} \left(SCF_1{}^2 \left(\frac{K+2}{N} \right) + (1 - SCF_1)((1 - SCF_1) - 2SCF_1 \frac{K-2}{N}) \right) + \cdots} \right.
$$

$$
\left. \frac{}{\cdots + N_o (1 - SCF_1) \frac{K-1}{N} \left(2 - SCF_1 (1 + \frac{K-2}{N}) \right)} \right\}
$$

(4-25)

Comparisons of the analytic results produced with the augmented expression, along with simulation and analytical results using the independent Guassian assumption for the user cross correlations was done by Correal [29]. It was seen that the augmented expression produced optimistic results when compared to simulation results. This was alluded to the fact that, in addition to the quadratic terms, there are consequential higher order terms that have not been accounted for.

A further addition from Divsalar et al. [31], was that a more accurate expression was derived for the bit-energy to noise spectral density ratio for stage 1. This expression, based

on the analytical averages of the binomially distributed signature sequence cross correlations, results in a re-written formula:

$$P_b^{(s=1)} = \frac{1}{2}\exp\left\{\frac{-E_b\left(1-SCF_1\frac{K-1}{N}\right)^2}{E_b\frac{K-1}{N}\left(SCF_1^2\left(\frac{K+2}{N}+\frac{K^2-5K+2}{N^2}\right)+(1-SCF_1)((1-SCF_1)-2SCF_1\frac{K-2}{N})\right)+\cdots}\right.$$

$$\left.\frac{}{\cdots+N_o(1-SCF_1\frac{K-1}{N}\left(2-SCF_1(1+\frac{K-2}{N})\right)}\right\} \quad (4\text{-}26)$$

Where SCF_1, is the optimum partial cancellation factor, K, is number of users, N is the processing gain, E_b, is the bit energy and N_o is the noise.

Comparisons done by Correal [29], between modelling the cross correlations as independent Gaussian random variables and the results based on the binomial distribution for the cross correlations, indicated that the curve for the binomially distributed cross correlations appeared more accurate compared to the Gaussian model curve.

During Stage 2 analysis, not mentioned here the decision statistics obtained in stage 1 (s = 1) are used to partially remove the interference caused by the remaining users. The detailed explanation can be seen in [29]. The expression of Equation (4-26) is now used in the SCF_{UNV} determination in the following section.

4.4 Calculation of Universal SCF

4.4.1 Methodology II

A detailed analysis of the behaviour of the SCF values as measured by the Probability of Error when K was varied, was done.

According to Equation (4-26), the probability of error was calculated and tabulated for each value of SCF in the range from 0.47 to 0.86, as K was varied from 2 to 30. The values of $N = 31$ and $E_b / N_o = 10dB$ were used in the calculations. The results are indicated in Figures 4-1 to 4-8, including the zoomed views of the area of interest.

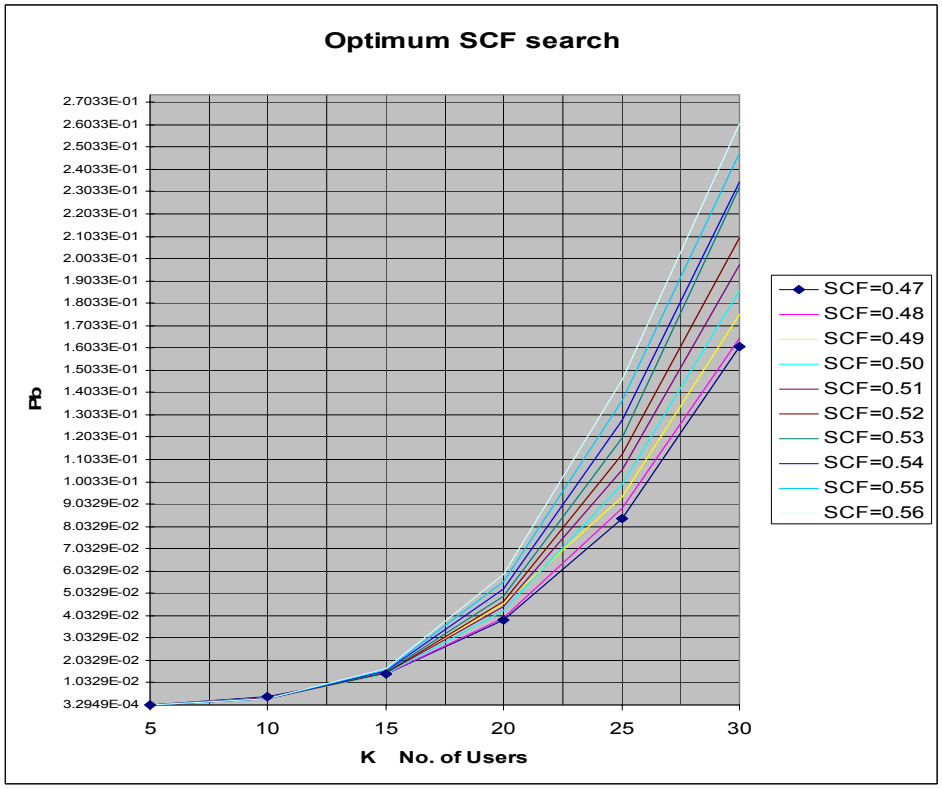

Figure 4-1: Graphical representation for SCF range 0.47 to 0.56

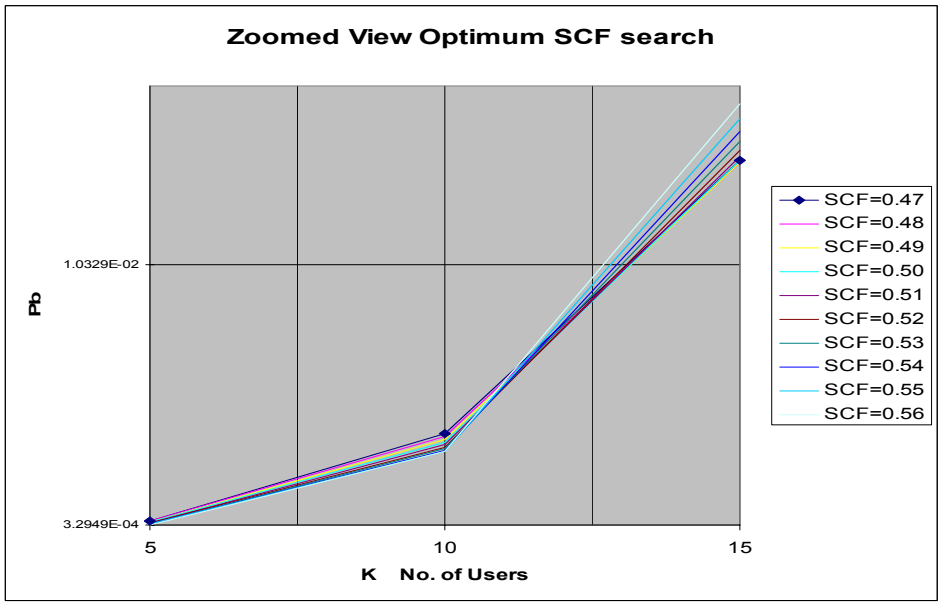

Figure 4-2: Zoomed Graphical representation for SCF range 0.47 to 0.56

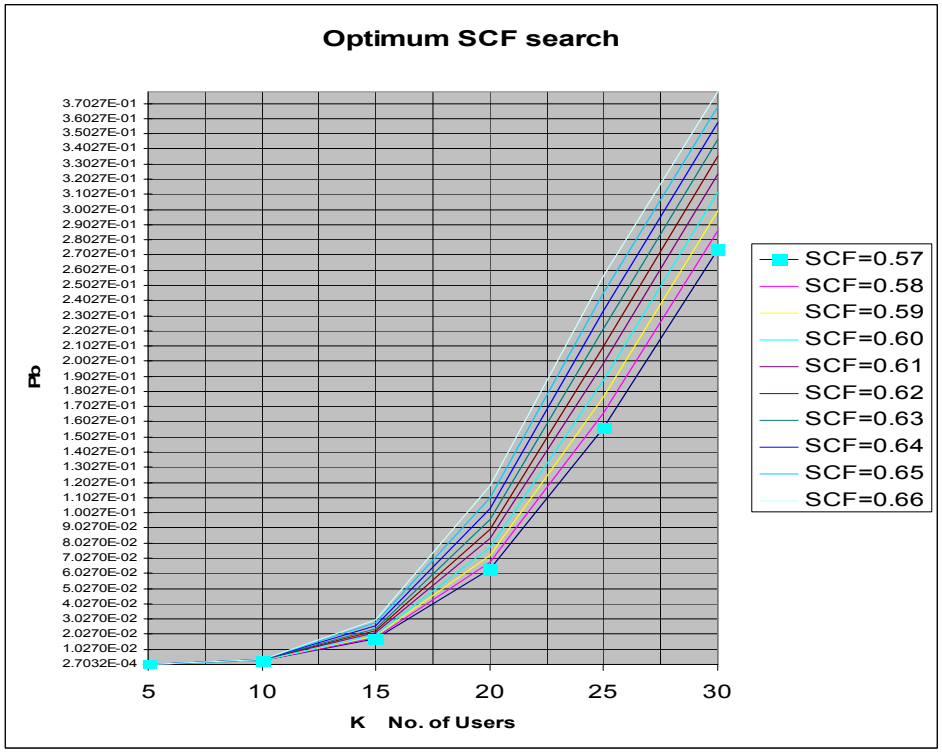

Figure 4-3:Graphical representation for SCF range 0.57 to 0.66

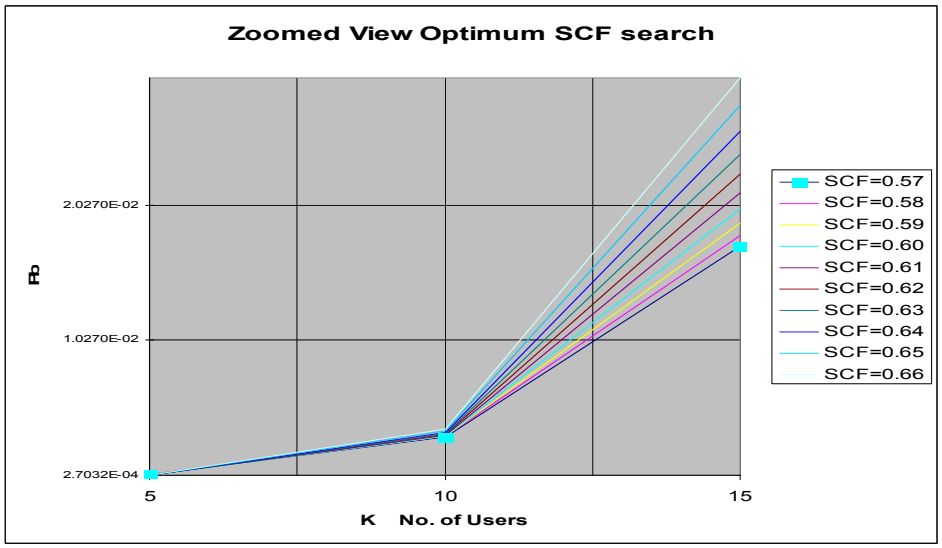

Figure 4-4: Zoomed Graphical representation for SCF range 0.57 to 0.66

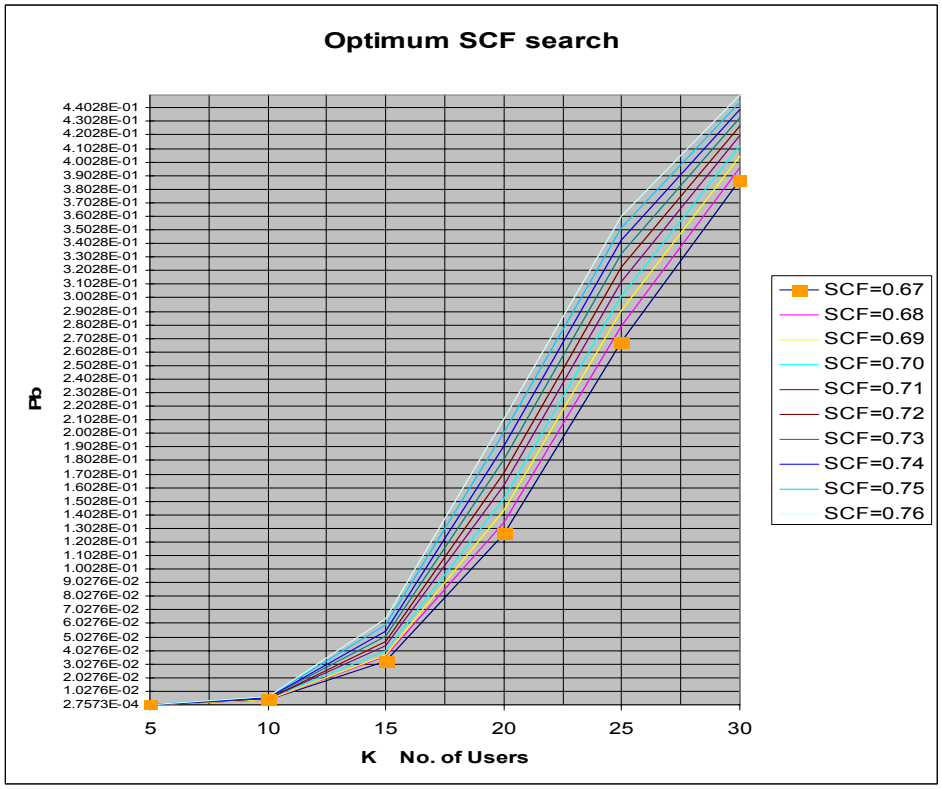

Figure 4-5:Graphical representation for SCF range 0.67 to 0.76

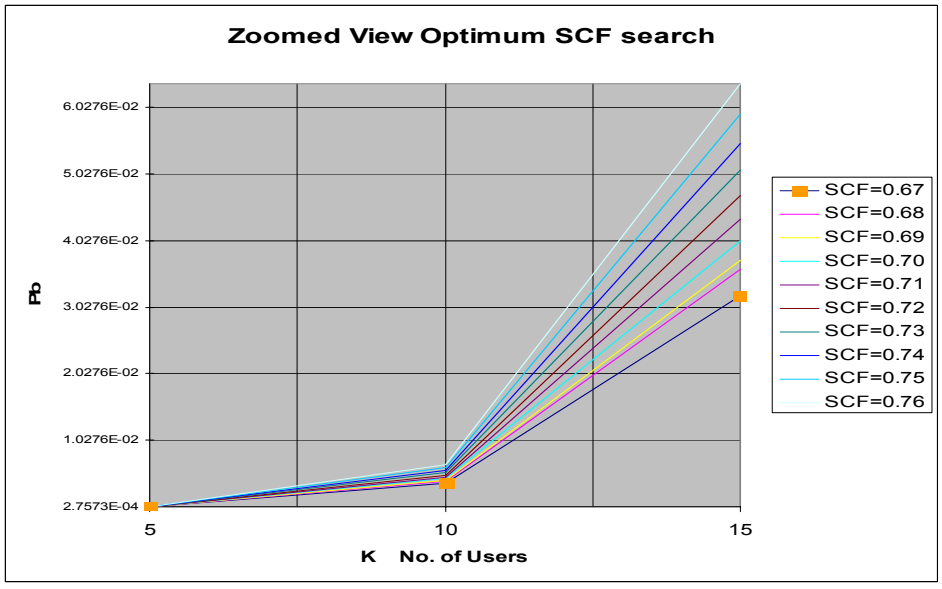

Figure 4-6: Zoomed Graphical representation for SCF range 0.67 to 0.76

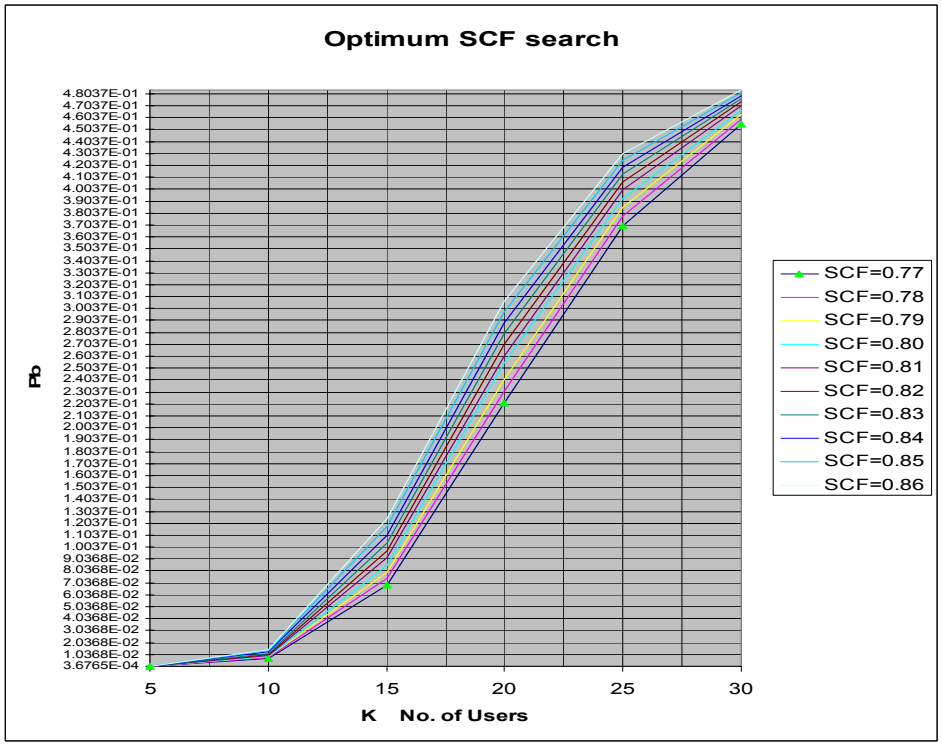

Figure 4-7:Graphical representation for SCF range 0.77 to 0.86

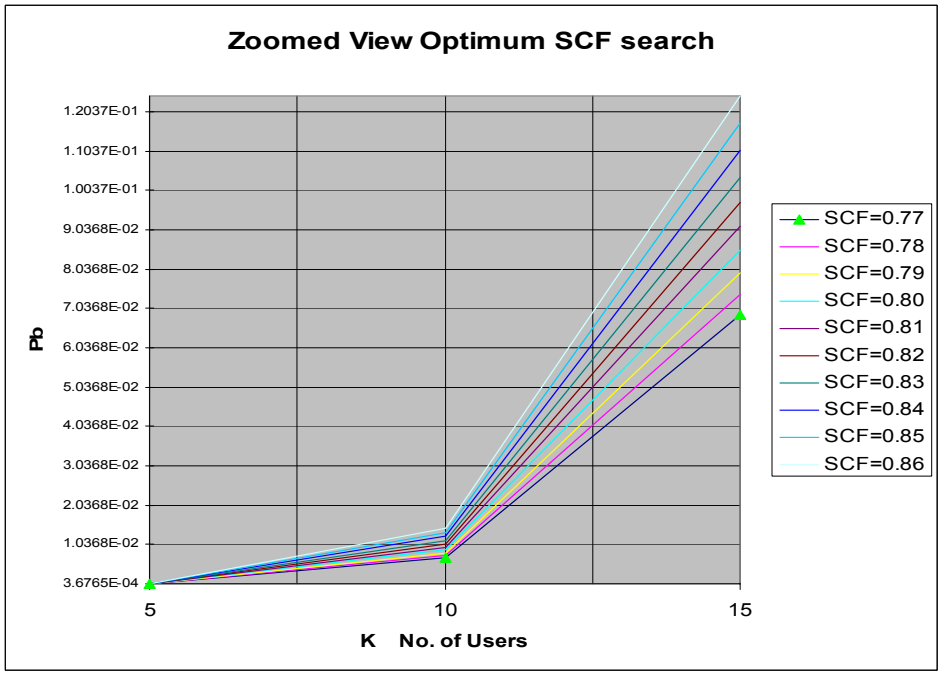

Figure 4-8: Zoomed Graphical representation for SCF range 0.77 to 0.86

4.4.2 Observation and Possible Explanation

The observed trend in the behaviour of optimal SCF values is that when the number of users is small,(k =2,3..etc), the particular SCF indicates a high BER. As the number of users is gradually increased, the BER characteristic will tend to increase slowly, up and until a certain threshold point. It is at this point that the BER characteristic switches to a lower value, i.e. the high initial BER characteristic now becomes a characteristic with a lower BER variation as K increases. This trend is repeated right through from SCF = 0.47 to SCF = 0.86. This behaviour appears to be in agreement with the work done by Rennuci [6], in that the smaller SCF values tended to have good BER characteristics for a large K, whilst the larger SCF values tended to have good characteristics for smaller K. This also agrees with theory in Rennuci [6] and Correal [29], in that the small K will produce a small MAI and bias. As it will not require a large down-scale, a large value of SCF will be required. The inverse is true for the large K case.

4.4.3 P_b Variance and Determination of Universal SCF

The multiple observations noted in the detailed analyses of the graphs reinforced that indicated in the analyses over the various ranges of SCF. Here, from $5 \le K \le 10$, the variance in P_b is $3.858026 \times 10^{-3} \le \mathrm{P}_b \le 1.4645548 \times 10^{-2}$. Thus, the magnitude of the variance is

$$\Delta \mathrm{P}_b = 1.0787521 \times 10^{-2}, \tag{4-27}$$

according to observation.

But, for the range $10 \le K \le 30$, this shows a marked variance in P_b, and this is highlighted clearly by the graphs for the different SCF ranges, Figures 4-1 to 4-8. The variance is given by $3.8580265 \times 10^{-3} \le \mathrm{P}_b \le 4.8353523 \times 10^{-1}$,

and the magnitude is:

$$\Delta P_b = 4.796772 \times 10^{-1}. \tag{4-28}$$

Thus, according to Equation (4-27), the SCFs displays a low variance in this range $5 \le K \le 10$, that they could each be used interchangeably. Therefore, it is decided to take the mean of the SCFs given by

$$\sum_{SCF=0.47}^{SCF=0.86} SCF \quad /40 = 0.665. \tag{4-29}$$

The SCF value of 0.47 exhibits a low overall P_b throughout the range $5 \le K \le 30$, according to observation, and this fact is utilised in the Universal SCF calculation.

Thus, continuing with our calculation, the Universal SCF value can be given by:

$$SCF_{UNV} = \frac{(0.665 + 0.47)}{2} = 0.5675 \approx 0.57. \tag{4-30}$$

The so called Universal SCF value, should be expected to exhibit reasonable behaviour over the total range as K varies. It has basically been determined by taking the low P_b characteristics of the SCF(0.47) and combining them with the mean SCF between $5 \le K \le 10$ range, due to low variance of P_b, to obtain a Universal SCF value. Figures 4-9 and 4-10 illustrate the SCF variations, especially that of the Universal SCF which can also be approximated to the characteristic for $SCF = 0.57 \approx SCF_{UNV}$. This SCF_{UNV} will be tested in the multistage Parallel Interference Cancellation Algorithm in the next section. The observations noted during this current exercise will provide input to areas of modification of the algorithm.

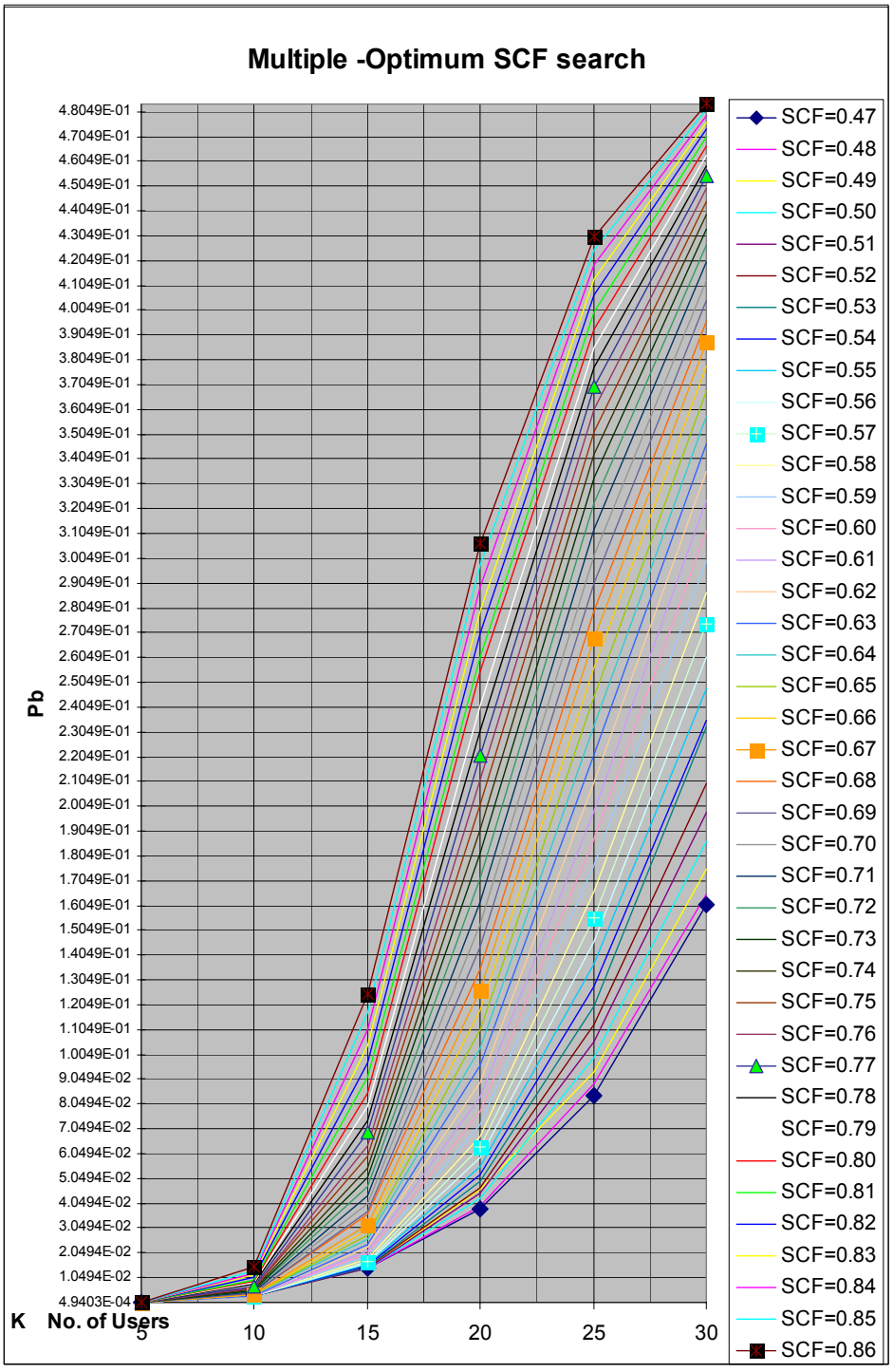

Figure 4-9: Graphical representation for SCF range 0.47 to 0.86

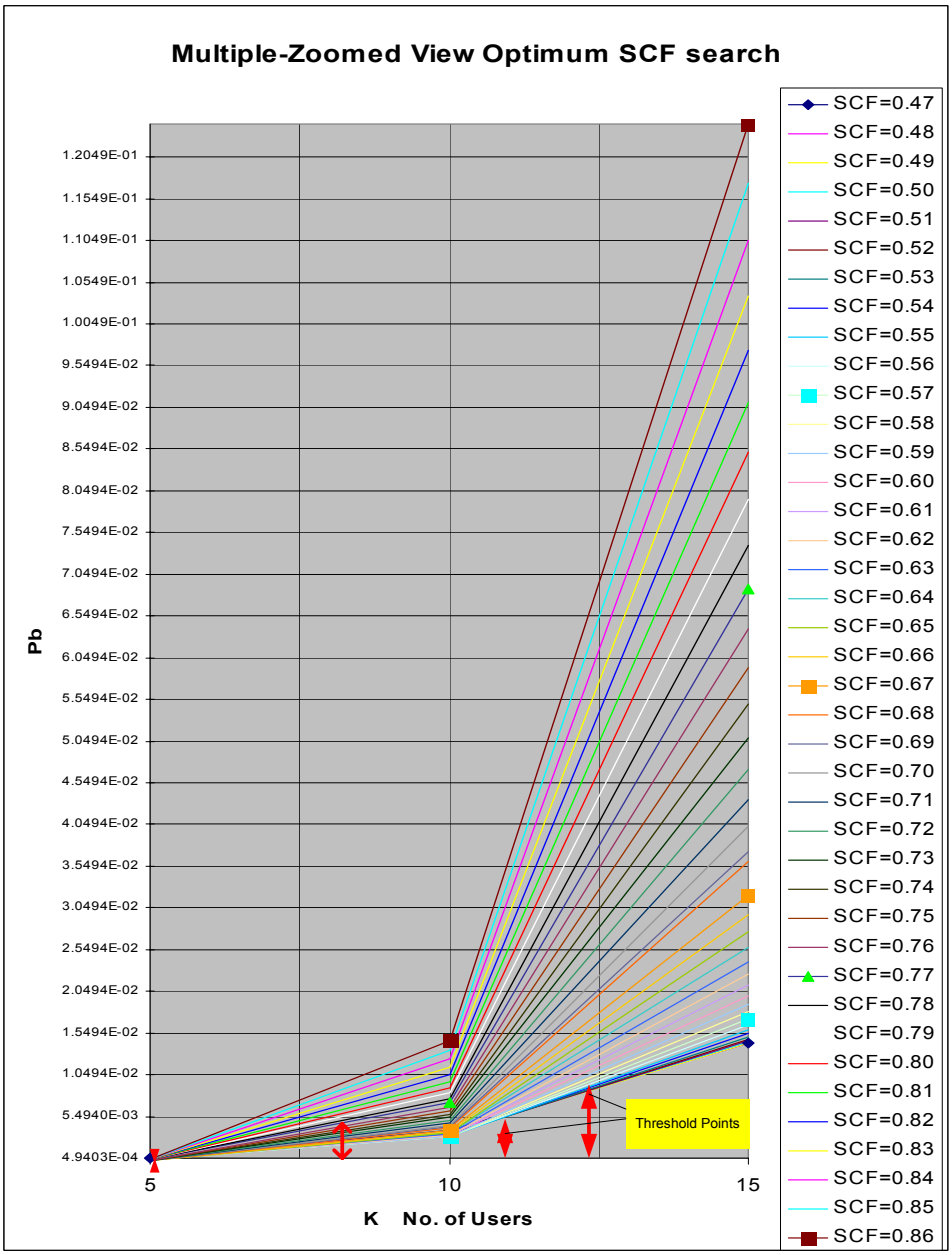

Figure 4-10: Zoomed Graphical representation for SCF range 0.47 to 0.86

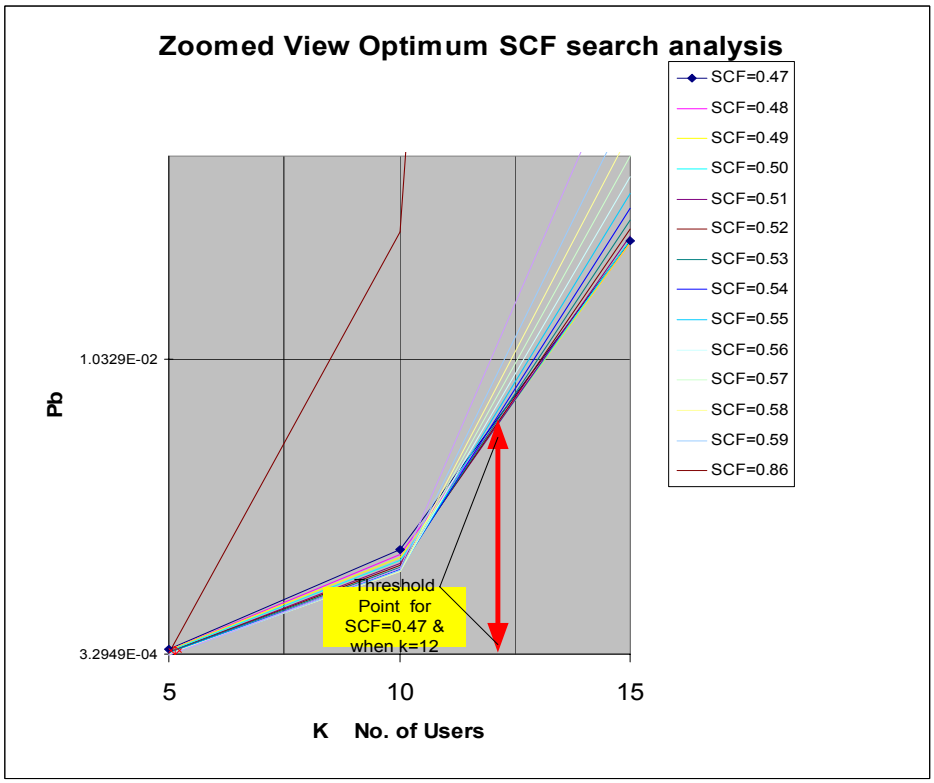

Figure 4-11: Focus on SCF = 0.47 variation showing the threshold point

Figure 4-11, attempts to describe the threshold points as mentioned above displayed by the optimal SCFs in the '*threshold crossing*' phenomenon. This threshold may be defined as a point or a plane across which the behaviour of the SCF variations may be described. The observed variation when SCF = 0.47, is a clear example of how, as K was incremented, the graph initially possessed the highest BER of all the SCF variations, and then at a point, (threshold point), of approximately $K = 12$, as indicated clearly in Figure 4-11, it crossed the graphs it had preceded to eventually end up with the lowest observed BER for the rest of the K variation. This was observed for all SCF variations, with each appearing to have it's own characteristic threshold point. As the value of SCF tended to increase, the corresponding threshold point tended to decrease as shown in Figure 4-10.

4.5 Discussion and Conclusion

The proposed method and approach differs from Rennuci [6], in that the obtained universal SCF's aim is to process a wider range of users in the parallel interference cancellation process. This value of SCF, SCF_{UNV}, has come about due to the modelling of the behaviour of the optimal SCFs. The method used in the derivation of SCF_{UNV} appears to be consistent with the analytical observations. In the analysis in Rennuci [6], optimal SCFs were assigned to a particular number of users, and Renucci proposed that this type of setup would require a lookup table structure storing these SCFs, in order to process the users in the multiuser detection. This study on the other hand, aims to implement the SCF_{UNV} in the multistage algorithm, with the assistance of the proposed compensator mechanism.

Considering the threshold phenomenon. The main conclusion that can be drawn from this is that each SCF has an ideal operating range as regards K variation, and that once this range is passed, according to the threshold point phenomenon, the SCF will tend to behave in a non-ideal manner. Thus, in the case of SCF = 0.47, the ideal behaviour can be observed for $K \geq 12$, whilst the non-ideal behaviour can be observed for $K < 12$. Also, for SCF = 0.86, the ideal behaviour, (lowest initial BER value), can be observed for $K \leq 5$, whilst the non-ideal behaviour, (highest overall BER value), is for $K > 5$. This type of observational analysis is true for all optimal SCF value graphs.

4.6 Chapter 4 Summary

The probability of error expression was derived and used in the universal SCF, SCF_{UNV} determination. This factor will be tested in the proposed Partial Parallel Pipelined Multiuser Detector.

CHAPTER 5

PIPELINED MULTIUSER DETECTOR ,PREREQUISITE TO PARTIAL PARALLEL PIPELINED MUD - P^3*MUD*

The second part of the research involves the conventional parallel pipelined detector. This Chapter gives a background overview of the detector and an understanding of the processes involved. It describes the channel estimation and subsequent multiuser detection stages. This is vital to an understanding of the incorporation of the universal SCF into this conventional detector to propose the Partial Parallel Pipelined MUD in Chapter 6.

5 INTRODUCTION TO PIPELINED MULTIUSER DETECTOR

This solution employs the advantages of two directions of research as regards our multiuser detection for wireless communication receivers.

Multiuser detection is a capacity enhancing feature in the WCDMA standard. As mentioned in the previous chapter, combining different IC strategies into a hybrid scheme appears to be a realistic way to achieve a reliable MUD, overcoming the limitations of the investigated schemes. Hence, the overall objective of the study is to describe such a (new) scheme which should comply as much as possible with the requirements and standards. The results of the study will be a description of the proposed scheme(s) in detail, accompanied by related simulation(s).

5.1 Background to the Partial Parallel Pipelined Multiuser Detector – PPPMUD or P^3MUD

This has been brought about by the initial and extensive work done by *Rajagopal et al*. [7], who were motivated by the proposed algorithms for WCDMA communication systems which had extremely high performance requirements. The focus was on both the different processing and precision requirements for the multiuser channel estimation and detection algorithms. The computational complexity associated with the asynchronous multiuser detection method involved multishot detection characterised by block-based computations and matrix inversions. Thus, extensive research was done by Rajagopal [7], on iterative based suboptimal schemes to decrease this complexity and eliminate the need for matrix inversions, with an added advantage of avoiding multishot detection if the scheme started from a matched filter estimate. This resulted in the ability to have the stages of the iteration pipelined and the bits processed in a streaming fashion using this bit-streaming,

pipelined architecture. It was shown that the implementation scheme could reduce the latency of the bits by the detection window length $D/2$ at the same time assisting the DSP implementation by eliminating the storage requirements for block computation. The edge-bit computation effects could be avoided using this scheme, reducing the computation per detection stage by $2/D$. The advantage of using the scheme was indicated by the DSP simulations that showed that data rates of 800 Kbps for a single user to 50 Kbps for 32 users could be processed in real-time with additional FPGAs in a pipelined fashion. This was achieved using a spreading gain of 31, which gave an increase in speed of at least 4 times over a single DSP implementation. The software implementation of the pipelined detector was carried out on a Texas Instruments TI TMS320C6701 DSP at 167 MHz, with the pipelining of the multistage detector carried out in hardware using a high density FPGA per stage [7].

A description of this detector is vital to an understanding of the parallel interference cancellation process employed. The P^3MUD simulations have been done using Matlab Code, [7], where the original algorithm and code has been modified to take into account the presence of a partial parallel interference cancellation constant, in this case the SCF_{UNV}.

5.2 Channel Estimation and Pipelined Multistage Detector

The uplink channel estimation scheme uses a pilot or preamble (a sequence of bits known at the receiver), which is time-multiplexed with the data. The channel causes changes in the preamble as the signal passes through the channel. Thus at the receiver, by comparing the received bits with the known preamble, the channel parameters (delays and amplitudes) can be extracted from the signal. The channel parameters are assumed to remain static until

the end of the frame. These estimates are then passed on to the pipelined multistage detector. The pipelined multistage detector performs the interference cancellation stage by stage until the algorithm converges. The channel estimation and detection algorithms essentially consider multi-path and multiuser effects. The assumptions made are that the static or slow fading channel (existing for the duration of the frame) has a single sensor at the receiver. Also, the algorithms process a short repeating spreading sequence system (short codes).

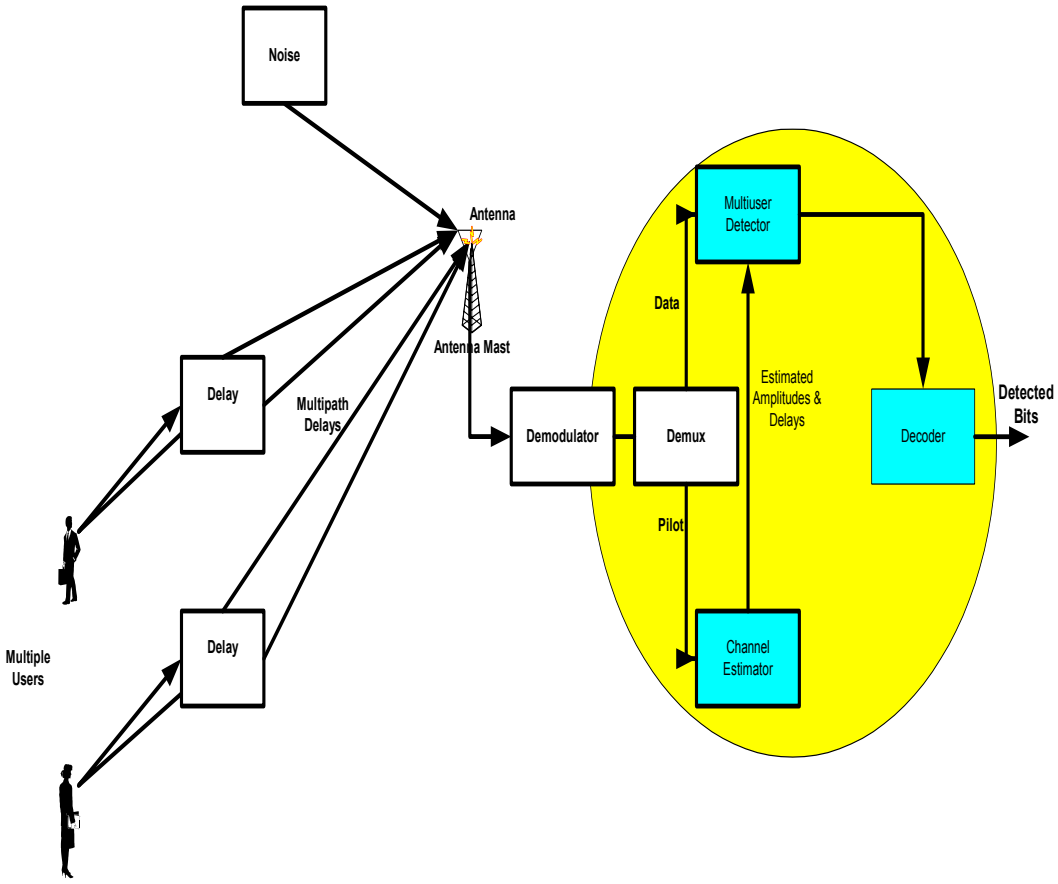

Figure 5-1: Base Station Receiver for the uplink Estimation and Detection Scheme.

5.3 Maximum Likelihood Channel Estimation Overview

The maximum likelihood estimation method has been adopted, mainly as a result of the channel having unknown a priori statistics. The information contained in the received pilot signal is the basis for the extraction of the channel parameters. Thus, the observation vector r_i depends on the channel whose a priori statistics are unknown, and is a function of the channel vectors z_k, the noise covariance matrix K, which is assumed unknown and the transmitted bits b_i. It is assumed that the bits b_i are known. This is accomplished in the acquisition phase by requiring that all users transmit training pilot sequences. The maximum likelihood method can be characterized by the following steps.

Maximum Likelihood Steps

$$R_{rr} = \frac{1}{L}\sum_{i=1}^{L} r_i r_i^H \quad . \tag{5-1}$$

$$R_{br} = \frac{1}{L}\sum_{i=1}^{L} b_i r_i^H \quad . \tag{5-2}$$

$$R_{bb} = \frac{1}{L}\sum_{i=1}^{L} b_i b_i^H \quad . \tag{5-3}$$

$$\mathrm{Y} = R_{br} R_{bb}^{-1} . \tag{5-4}$$

$$\mathrm{K} = R_{rr} - \mathrm{Y} R_{br}^H \quad . \tag{5-5}$$

$$z_k^H = \left(Y_{2k-1}^H K^{-1} U_k^R + Y_{2k}^H K^{-1} U_k^L\right) \times \left(U_k^{R'} K^{-1} U_k^R + U_k^{L'} K^{-1} U_k^L\right)^{-1} . \tag{5-6}$$

where:

R_{rr} is the autocorrelation of the observation vector,

R_{br} is the cross- correlation between the observation vector and the preamble bits,

R_{bb} is the autocorrelation of the preamble bits,

K the noise covariance matrix,

Y is the estimate of UZ,

U is the matrix of codes

Z is the channel impulse response matrix.

A detailed description is given in Rajagopal [24].

Then, the strongest **P** paths are extracted by performing a least squares fit of z_k. Thus, for each pair of adjacent coefficients of z_k, local values of amplitudes, α, and delays are obtained, using the following optimization,

$$[\alpha_q, \gamma_q] = \arg\min \left\| z_{k,q} - (1-\gamma)\alpha \right\|^2 + \left\| z_{k,q+1} - \gamma\alpha \right\|^2 . \quad (5\text{-}7)$$

Next, searching for the global maxima to obtain the strongest path :

$$q = \arg\max |\alpha_q|, \tau = (q + \gamma_q)T_c, \alpha = \alpha_q . \quad (5\text{-}8)$$

where:

γ is the fractional part of the delay,

q is the integer part of the delay,

τ is the estimated delay

α is the estimated amplitude.

Finally, the estimated path is subtracted from z_k and the process is repeated to find the next strongest path, until a specified number of paths have been identified.

5.4 Matched Filter and Pipe-lined Multistage Detector Overview

The stages following channel estimation are Matched Filter and Pipe-Lined Multistage Detection and both of these stages comprise the Multiuser Detection process. The multiuser detection techniques use the output of the matched filter bank and the cross-correlation information of all users in the system. The process flow is illustrated in Figure 5-2.

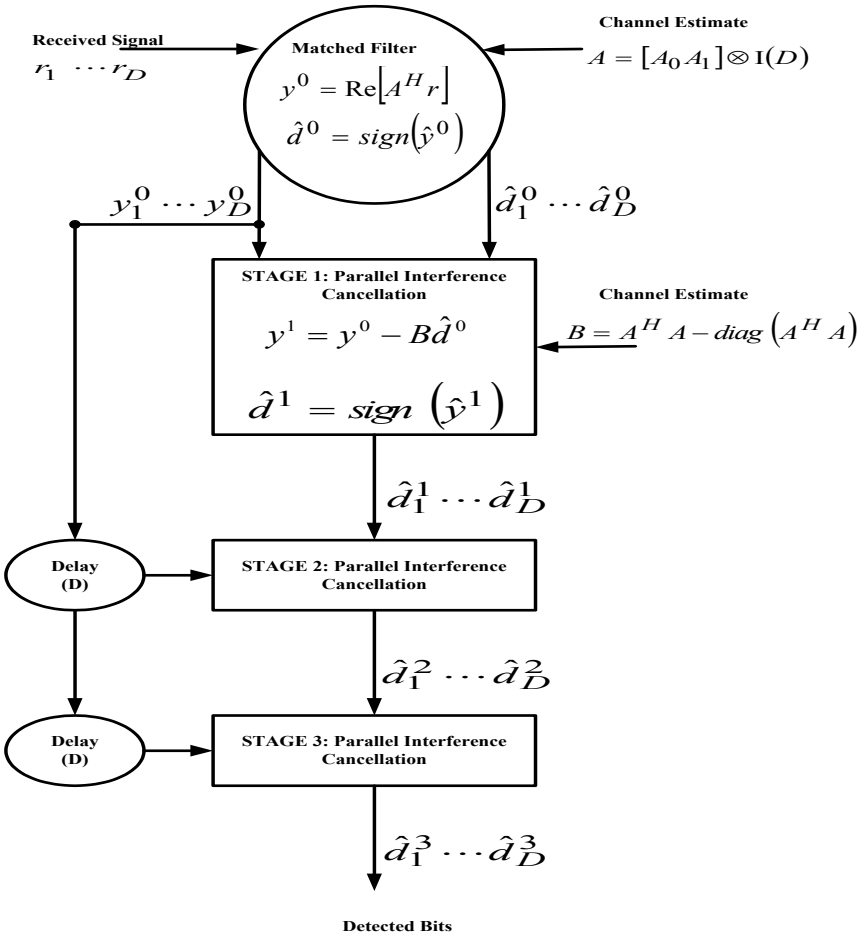

Figure 5-2: Multistage Multiuser Detection process overview

A Matched Filter is assigned per user, and the collection of Matched Filters forms a Bank of Filters, which is usually the first stage in the baseband signal detection. Here, the data bits are passed through the matched filter bank to detect each user's signal. Then, the matched filter output, given below, is sent through the pipe-lined multiuser detector where the parallel interference cancellation is done in stages. After M_{iter} iterations, it is most likely that $\hat{d}^{(l+1)} = \hat{d}^l$, which reflects the convergence of the PIC algorithm, (this is not a very effective way to investigate/verify convergence of the multistage algorithm).

The implementation of this PIC process differs from that in chapter 3 section 3.4.2 [6,29],

The matched filter output is represented by the expression

$$y = R\mathrm{A}d + \eta\,. \tag{5-9}$$

where:

y is the output of the matched filter bank

d represents the transmitted user data bits,

R is the cross correlation matrix of the synchronized spreading codes

A is a diagonal matrix containing the amplitudes of the users.

Alternatively, the cross correlation matrix R can also be split into three parts, given by

$$R = D + S + S^T\,, \tag{5-10}$$

$$B_R = \left(S + S^T\right)\mathrm{A}\,. \tag{5-11}$$

where:

$$D = diag\left(R\right) = \mathrm{I}\ , \tag{5-12}$$

S is the lower triangular part of matrix R .

B_R is used to simplify the notation in the non-linear multistage detection algorithm.

The structure of $\mathrm{A}^H\mathrm{A} \in C^{KD\times KD}$ is as shown:

$$\begin{bmatrix} \mathrm{A}_0^H\mathrm{A}_0 & \mathrm{A}_0^H\mathrm{A}_1 & 0 & 0 \\ \mathrm{A}_1^H\mathrm{A}_0 & \mathrm{A}_0^H\mathrm{A}_0+\mathrm{A}_1^H\mathrm{A}_1 & \mathrm{A}_0^H\mathrm{A}_1 & 0 \\ \vdots & \ddots & \ddots & \vdots \\ 0 & 0 & \mathrm{A}_1^H\mathrm{A}_0 & \mathrm{A}_0^H\mathrm{A}_0+\mathrm{A}_1^H\mathrm{A}_1 \end{bmatrix}. \quad (5\text{-}13)$$

Rajagopal et al. [7], exploited the tri-diagonal block-Toeplitz nature (assumption of the static nature of the channel during the detection window, whilst other multiuser detectors based on matrix inversions lose their block-Toeplitz structure due to matrix inversions and hence, cannot be pipelined), of the matrix in equation (5-13) for reducing the complexity and pipelining the algorithm effectively.

5.5 Detailed System Model Description

The detailed system model is now described covering the three main stages of Channel estimation, Matched-Filter Detection and Pipelined Multistage Detection.

Considering an asynchronous system: Assuming Binary Phase Shift Keying (BPSK) modulation in the uplink. The channel estimate can be given as $\mathrm{A}_0, \mathrm{A}_1 \in C^{N\times K}$, corresponding to partial correlation information for the successive bit vectors $d_{i-1}, d_i \in \{+1,-1\}^K$, which are to be detected. The spreading gain is represented by N ,and K represents the number of users in the system. In vector form, the received signal is given by:

$$r_i = \begin{bmatrix} \mathrm{A}_0 \mathrm{A}_1 \end{bmatrix} \begin{bmatrix} d_{1,i-1} \\ \vdots \\ d_{K,i-1} \\ d_{1,i} \\ \vdots \\ d_{K,i} \end{bmatrix} + \eta_i . \quad (5\text{-}14)$$

Where, the bits, d_i, of the K users to be detected lie between the received signal r_i and r_{i-1} boundaries. Thus, the matched filter detector, according to Moshavi [21], and Verdu [32], does a single user detection for each user. This process neglects the effects of other users. The representation of the matched filter detector after substitution can be given by

$$\hat{d}_i = sign\left(\Re\left[\mathrm{A}_1^H r_{i-1} + \mathrm{A}_0^H r_i \right] \right). \tag{5-15}$$

Equation (5-15) represents the hard decision output of the matched filter, which inherently becomes the input to the pipe-lined multistage detector. The causal nature (characteristic exploited in pipelining the multistage detector), of the matched-filter detector means it does not require succeeding bits of other users to produce an output estimate.

The PIC performed iteratively in stages for the multistage detector [8, 33] and required multishot detection. Multishot detection (cancelling the interference due to the succeeding/future bits of the users) required extending the model to include multiple bits. Considering D bits at a time $(i = 1,2,\ldots,D)$. ,the multishot received vector $r \in R^{ND}$ was formed by concatenating D vectors $\left(r_i, i = 1,2,\cdots,D\right)$, expressed by

$$r = \begin{bmatrix} \mathrm{A}_0 & \mathrm{A}_1 & 0 & 0 \\ 0 & \mathrm{A}_0 & \mathrm{A}_1 & 0 \\ \vdots & \ddots & \ddots & \mathrm{A}_1 \\ 0 & 0 & 0 & \mathrm{A}_0 \end{bmatrix} \begin{bmatrix} d_{1,1} \\ \vdots \\ d_{K,1} \\ \vdots \\ d_{1,D} \\ \vdots \\ d_{K,D} \end{bmatrix} + \eta_i . \tag{5-16}$$

Where:

$\mathrm{A} \in C^{ND \times KD}$ represents the new multishot channel matrix.

Also

$$y^{(0)} = \Re\left[\mathrm{A}^H r\right] \tag{5-17}$$

$$\hat{d}^{(0)} = sign\left(y^{(0)}\right). \tag{5-18}$$

Where the initial soft decision outputs $y^{(0)} \in R^{KD}$ and hard decision outputs $\hat{d}^{(0)} \in R^{KD}$ of the detector were obtained from the matched filter using the channel estimates.

According to Rajagopal et al [7], during multi-user detection, the desired user's bits receive interference from the past or future overlapping symbols of different users along with their current symbols because they are asynchronous. Thus, the Pipelined Multistage Detection algorithm they proposed is based on the principle of Parallel Interference Cancellation (PIC), where the scheme cancels the interference from different users, successively in stages. It has been shown to have computational complexity linear with the number of users. The pipelined effect can best be described by Figure 5-3, where an example highlighting the calculation of bit 3 in the detector is shown.

An initial estimate of the received signal is done using a matched filter detector, which depends only on the current and the past received bits. The stages of the multiuser detector need bits 2 and 4 of all users to cancel the interference for bit 3. Hence, the first stage can cancel the interference only after the bits 2 and 4 estimates of the matched filter are available. The other stages have similar structure. Hence, while bit 3 is being estimated from the final stage, the matched filter is estimating bit 9, the first stage bit 7 and the second stage bit 5. By avoiding edge bit computations, we get $2/D$ savings in computation per detection stage, where D is the detection window length. Also, instead of detecting a block of bits, each bit is detected in a streaming fashion with a latency of 2 bits, reducing the latency by the detection window length to $D/2$ and eliminating the storage requirements of block computation.

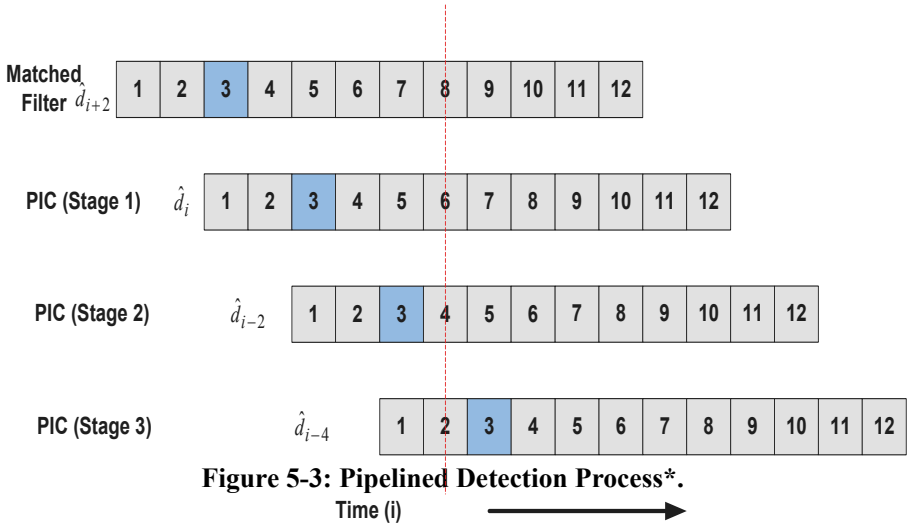

Figure 5-3: Pipelined Detection Process*.

**The detection process can be streamlined to work on a bit basis rather than in blocks. As soon as the immediate future bits are available, the next iteration of detection is carried out. Bit 3 is highlighted as an example.*

Also, the computations are reduced to work on smaller matrix sets due to the block Toeplitz nature of the matrix $\hat{\mathrm{A}}^H\hat{\mathrm{A}}$ in (5-13). The computations performed on the intermediate bits reduce to

$$L = \Re\left[\hat{\mathrm{A}}_1^H\hat{\mathrm{A}}_0\right]. \tag{5-19}$$

$$C = \Re\left[\hat{\mathrm{A}}_0^H\hat{\mathrm{A}}_0 + \hat{\mathrm{A}}_1^H\hat{\mathrm{A}}_1 - diag\left(\hat{\mathrm{A}}_0^H\hat{\mathrm{A}}_0 + \hat{\mathrm{A}}_1^H\hat{\mathrm{A}}_1\right)\right]. \tag{5-20}$$

$$y_i^{(l)} = y_i^{(0)} - L\hat{d}_{i-1}^{(l-1)} - C\hat{d}_i^{(l-1)} - L^T\hat{d}_{i+1}^{(l-1)}. \tag{5-21}$$

$$\hat{d}_i^{(l)} = sign\left(y_i^{(l)}\right). \tag{5-22}$$

where $y_i^{(l)}$ and $\hat{d}_i^{(l)}$ are the soft and hard decisions respectively, after each stage of the multistage detector. These computations are iterated for $l = 1,2,\cdots,M_{iter}$ where M_{iter} is the

maximum number of iterations chosen for PIC algorithm convergence (typically $M_{iter} = 3$ stages of the detector, with one iteration per stage, successfully). The P^3MUD, proposed detector attempts to reduce the convergence stage of the algorithm to one or two, as reflected by the BER simulations.

Continuing with the discussion, equation (5-21) represents subtracting the interference from the past bit of users, who have more delay, and the future bits of the users, who have less delay than the desired user.

Also,

L, the left matrix stands for the partial correlation between the past bits of the interfering users and the desired user,

L^T, the right matrix stands for the partial correlation between the future bits of the interfering users and the desired user.

C, the center matrix is the correlation of the current bits of interfering users and the diagonal elements are made zeros since only the interference from other users, represented by the non-diagonal elements, needs to be canceled.

The lower index, i, represents time, while the upper index, l, represents the iterations. The initial estimates are obtained from the matched filter. The equations (5-21)-(5-22) represent bit-streaming computations.

Equation (5-21), forms the foundation of the proposed Partial Parallel Pipelined Multiuser Detector –PPPMUD or P^3MUD, as seen in the next section.

5.6 Chapter 5 Summary

A description of the conventional Pipelined Multiuser Detector, a prerequisite to Partial Parallel Pipelined MUD, P^3MUD, was given in order to provide a vital understanding of the parallel interference cancellation process employed.

CHAPTER 6

PROPOSED P^3MUD

This chapter is the culmination of the study, tying together the themes discussed previously, and most importantly, proposing the Partial Parallel Pipelined Multiuser Detector (P^3MUD). It describes the motivation behind the proposed detector, and gives the proposed algorithm architecture. The simulation software implementation is mentioned, as well as the simulation parameters used. Of importance is the proposed P^3MUD algorithm analysis procedure. The compensator mechanism is described as well. The simulation outputs for the various detector configurations are shown, and observations and a discussion are made.

6 PROPOSED PARTIAL PARALLEL PIPELINED MULTIUSER DETECTOR ALGORITHM –PPPMUD OR P^3MUD

The description of the two main lines of research has been made above. The dissertation so far has involved determining the universal SCF, which will now be employed in the proposed P^3MUD algorithm. It has also involved describing the workings of the three-stage conventional pipelined multiuser detection method, which has been reduced to two stages according to the P^3MUD, proposal. This is in accordance with the aims of the study where the advantages of the various existing interference cancellation schemes would be used to formulate an improved scheme. This improved scheme would be tested and compared against the existing ones to measure the extent of improvement, if at all.

Before deriving the system model for the Proposed Partial Parallel Pipelined Multiuser Detector Algorithm, an insight into the motivation for the methodology used is given.

6.1 Motivation for Proposed Partial Parallel Pipelined Mud Algorithm

The motivation towards the possibility of combining the best features of the various research work to produce an improved algorithm as regards multiuser detection, has been brought about by the work done by *Correal et al.* [34]. According to *Correal* [34], a simple yet effective way to mitigate the effect of the bias (mentioned in Chapter 3), and improve the performance of a parallel multistage interference cancellation receiver, is based on multiplying the channel gain estimates before signal reconstruction by a partial-cancellation factor $0 \le SCF_K^{(s)} \le 1$ that varies with the stage of cancellation s and system loading k.

Thus, the decision metric could be represented in the following equation:

$$\hat{s}_j^{(s)}(t) = \frac{2SCF_K^{(s)}}{T} a_j(t)\cos\left(\omega_c t + \phi_j\right) \sum_{i=-\infty}^{\infty} Z_{j,i}^{(s)} p_T(t - iT). \quad (6\text{-}1)$$

Where $\hat{s}_j^s(t)$ corresponds to the estimated reconstructed signal for user j at stage s, and $p_T(t)$ is a unit pulse function of duration T equal to the bit period, a_j is spreading waveform, and $Z_{j,i}^{(s)}$, is the decision metric [34].

This is interpreted as modifying the complete cancellation scheme to include the partial-cancellation factor $SCF_K^{(s)}$ as follows:

$$\hat{r}_k^{(s)}(t) = r(t) - SCF_K^{(s)} \sum_{j \neq k} \hat{s}_j^{(s)}(t). \quad (6\text{-}2)$$

Explained further, the first step involves creating the first stage decision statistic for bit 1 of each user, (see Figure 6-1a). This is to be stored and used as an estimate of each user's data bit and received power in the cancellation process, i.e., the overlap between bit 1 of user k and bit 2 of any user j, where $j < k$ (assuming users are numbered according to increasing delays).

According to *Correal et al*. [34], the first-stage decision statistics of each user are needed for bit interval 2, (see Figure 6-1b), before proceeding with cancellation, so that, once stage 1 correlation over bits 1 and 2 is completed for each user, cancellation over bit interval 1 may proceed, (see Figure 6-1c). This is done by first multiplying the correlation result by the factor SCF_K and the spreading code of each user, and then using the resulting signal estimate to subtract out each estimated signal from the received signal, (refer to equation (6-2)). The residual signal is then input to the next stage (stage 2). The next step is to perform correlation over bit interval 3, (see Figure 6-1d), followed by stage 1 cancellation on bit 2 of each user, as seen in Figure 6-1e. Finally, stage 2 processing could now be performed on bit 1, (see Figure 6-1f). The stage 2 residual signal is correlated with the spreading code of each user to obtain a correction factor which is added to the correlation score of the first stage. The result is then used as the decision statistic, and the process is repeated if additional stages are used.

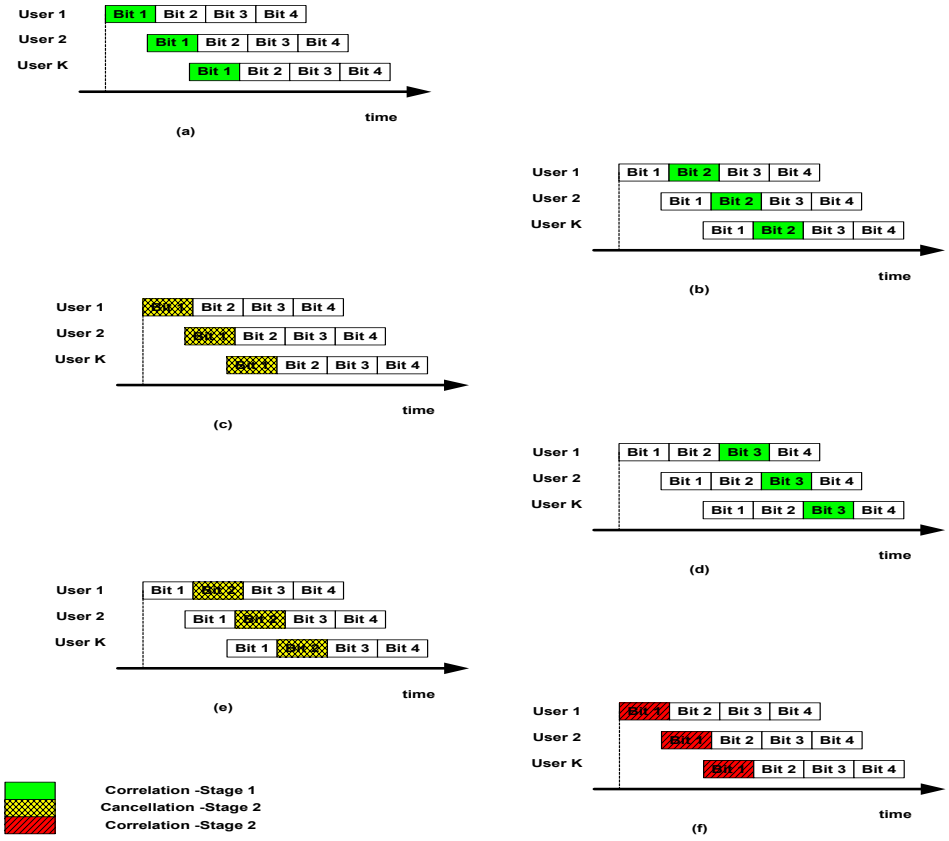

Figure 6-1: P^3MUD **Process flow description using a timing diagram**

Thus, the similarities of equations (6-2) and (5-21) are apparent in that the future soft decision estimates are obtained by subtracting the estimates of the interfering users from the received signal input. It is in this manner that the formulation of the pipelined multistage detector soft decision estimate output is done. The SCF constant is incorporated into equation (5-21) to give:

$$y_i^{(l)} = y_i^{(0)} - (SCF)L\hat{d}_{i-1}^{(l-1)} - (SCF)C\hat{d}_i^{(l-1)} - (SCF)L^T\hat{d}_{i+1}^{(l-1)} . \qquad \textbf{(6-3)}$$

Where the symbol definitions can be found in Chapter 5, section 5.4 and 5.5.

This addition is similarly reflected in the modified pipelined multistage algorithm of *Rajagopal* [7], which has an additional compensation mechanism (adjusting the Universal

SCF accordingly), that takes into account the number of users and adjusts the SCF so that the accuracy in the multiuser detection process is increased. When the number of users k approaches the processing gain N, the algorithm effectiveness begins to degenerate.

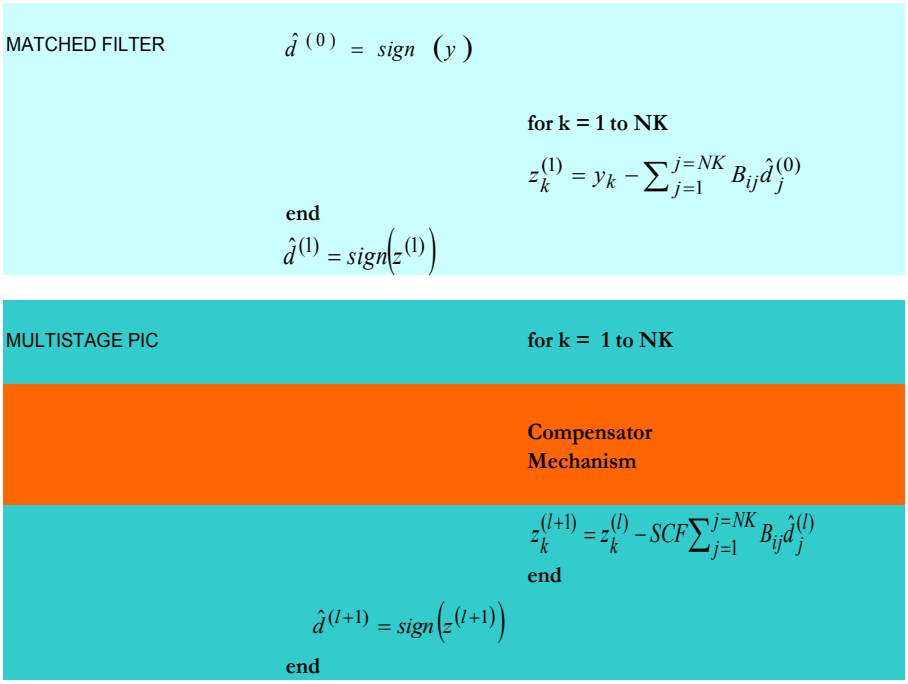

Figure 6-2: Steps in the Multistage Detector Algorithm

The detector takes in the matched filter estimates y_i and the hard decisions, $\hat{d}_i$. The partial correlation matrices L, C (channel estimates) are also loaded. The detector subtracts the interference iteratively in stages from the matched filter output. Each stage of the detector sends a delayed-by-2 match-filtered estimate and the updated hard decisions to the next stage of the detector.

6.2 Proposed Algorithm Architecture Differences

The proposed pipelined architecture differs from the conventional one *Rajagopal* [7], by the presence of the SCF constant, which enhances the possibility of the multistage

detection algorithms being reduced to at least two stages instead of three. It also differs by the presence of the SCF compensation mechanism which results in the algorithm being able to process effectively a large number of users *k*. Thus, the third stage is indicated by red dashed lines and arrows, signifying that convergence can occur in the second stage of the P^3MUD algorithm.

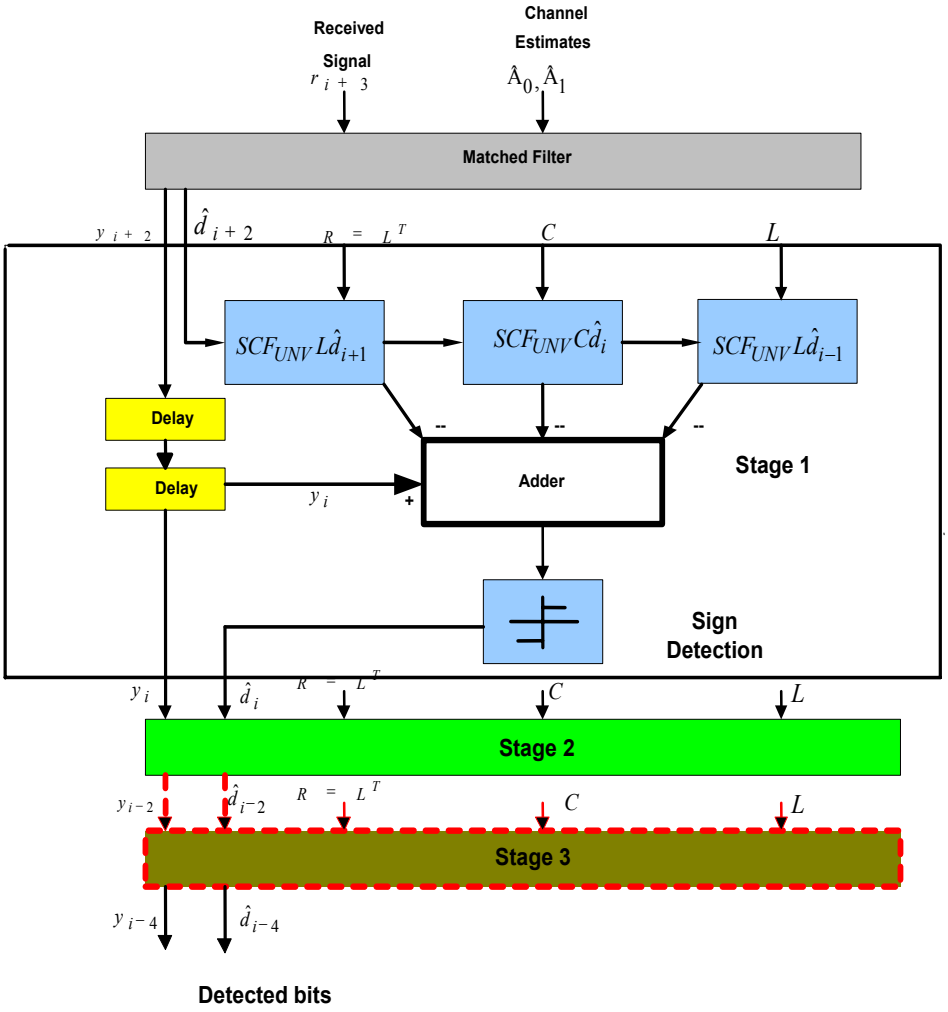

Figure 6-3: Partial Parallel Pipelined multiuser detector $\left(P^3MUD\right)$ architecture.

6.3 Simulation Software implementation

The simulation software has been implemented using Matlab (ver 6). The code has been based on that used by Rajagopal [7], for the conventional pipelined detector. The four main modifications or additions made are:

- The restructuring and optimization of the original code. The code, the original version and the amended/modified version, can be seen in Addendum A.
- The incorporation of the SCF_{UNV} constant into the algorithm.
- The addition of the compensator mechanism for the SCF_{UNV} constant.
- The creation of a user friendly Graphical User Interface (GUI) which incorporates a dual-output presentation for the BER ver SNR and BER ver *k* (Number of users) on a single screen. This also makes it easier for comparison purposes. This is seen below in Figure 6-4.

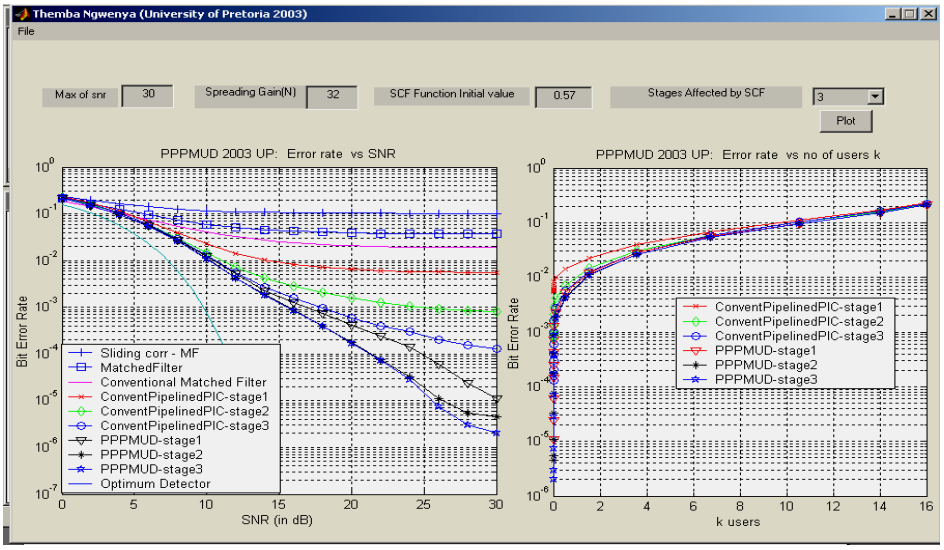

Figure 6-4 :Layout of PPPMUD or P^3MUD Graphical User Interface

6.3.1 The Conventional Matched Filter Receiver and Optimum Detector Bounds

A measure or sense of accuracy in the graphical outputs of the proposed P^3MUD detector has been the introduction of the conventional matched filter bound, represented by the Gaussian approximation of a k-user system, [35], and the optimum detector (single-user) bound originally defined by Verdu, [35].

Gaussian Approximation for Conventional Matched Filter

The Gaussian expression for probability of error of k^{th} user is given by,

$$\tilde{P}_K^C(\sigma) = Q\left[\frac{A_K}{\sqrt{\sigma^2 + \sum_{j\neq k} A_j^2 \rho_{jk}^2}}\right] \tag{6-4}$$

where $\tilde{P}_k^c(\sigma)$ denotes the probability of error when a conventional receiver is used; A_k, is the received amplitude from the k^{th} user, and A_j^2, is the j^{th} user energy, ρ_{jk} is the cross correlation between the signature waveforms of j^{th} and k^{th} users, and σ, is the noise level. This Gaussian approximation is good for low SNR, but highly unreliable at high SNR [35]. It also states that the probability of error goes to a non-zero limit for high SNR. The Matlab code for the approximation is found in Addendum A.

Single-User Representation for Optimum Detector

The optimum detector representation for probability of error for single user bound is given by

$$P_k^c(\sigma) = Q(A_k / \sigma) \tag{6-5}$$

Thus, the probability of error $P_1^c(\sigma)$ for user one, (single-user), versus normalized amplitude of user one A_1/σ, is plotted. The Matlab code for the optimum detector is found in Addendum A.

Reseachers have and are still using the optimum detector bound derived by Verdu, as a guide to the accuracy of their work.

6.4 Simulation Parameters Used

The simulation code used certain parameters in the main program file as well as the sub-programs. The PPPMUD or P^3MUD GUI (see Figure 6-4), shows four of these input parameters and these are explained as follows.

- Maximum SNR, input the signal-to-noise parameter (by code structure is also in-put for maximum *k*, number of users)
- Spreading Gain, input, typically 32
- SCF coefficient or SCF start value = SCF_{UNV} in this case = 0.57
- Stages required for algorithm to be processed, 1, 2 or 3

Addendum A in the Addendum section contains the simulation code. Converting from E_b/N_0 *to SNR,* $E_b/N_0 = 10.^{(SNR/10)}$*, has been used.*

6.5 P^3MUD AlgorithmTest Analysis

The P^3MUD was then tested by plotting the BER graphs against SNR and also against K (the number of users). The output graphs were able to show a comparison between the conventional pipelined algorithm and the proposed P^3MUD algorithm. The Sliding Correlator and Matched Filter Detector outputs, *Rajagopal* [7], where left in for comparison purposes, as well as those of the Conventional Pipelined Multiuser Detector.

Multiuser detection will cancel the interference from other users to improve the error rate performance. This is in comparison with traditional single user detection using only a matched filter [7]. In this process, the desired user's bits receive interference from the past

or future overlapping symbols of different users along with their current symbols, because they are asynchronous, according to explanation in Figure 6-5.

The assumption that the delays of the different users are coarsely synchronized within one symbol duration is taken here.

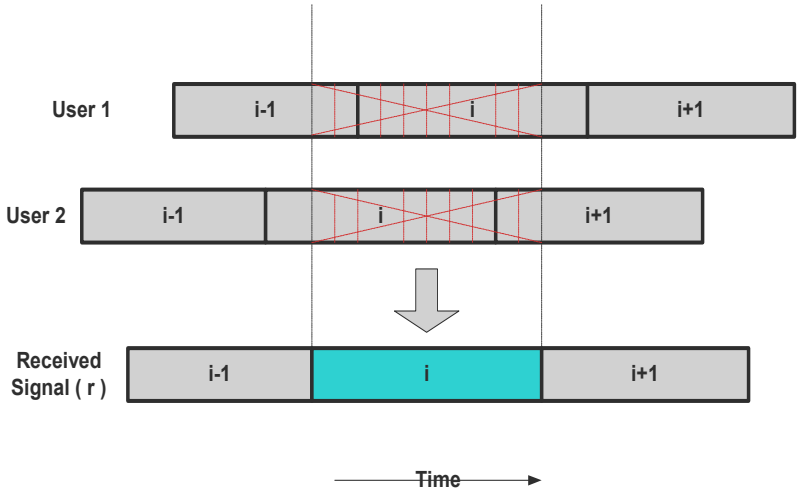

Figure 6-5 : Graphical representation of Multiple Access Interference, showing the interference from past, current and future bits (each shaded differently) of other users.

6.6 Methodology III

6.6.1 P^3MUD Algorithm Analysis Objectives and Methodology

The objectives of the test analysis was to determine the performance behaviour of the P^3MUD algorithm. This involved:

- A graphical analysis where the impact of the P^3MUD algorithm was compared to the conventional pipelined detector, as the SCF value was varied.
- A graphical analysis when the SCF compensator mechanism was activated and the SCF_{UNV} value of 0.57 used. This was also compared to the non-compensator outputs.

This is indicated in Figures 6-6 to 6-11.

6.6.1.1 Simulations without SCF_{UNV} and Compensator Mechanism

This is represented by Figures 6-6 to 6-10, as the SCF varies from 0.47 to 0.87, for all three stages of the multiuser detection algorithms.

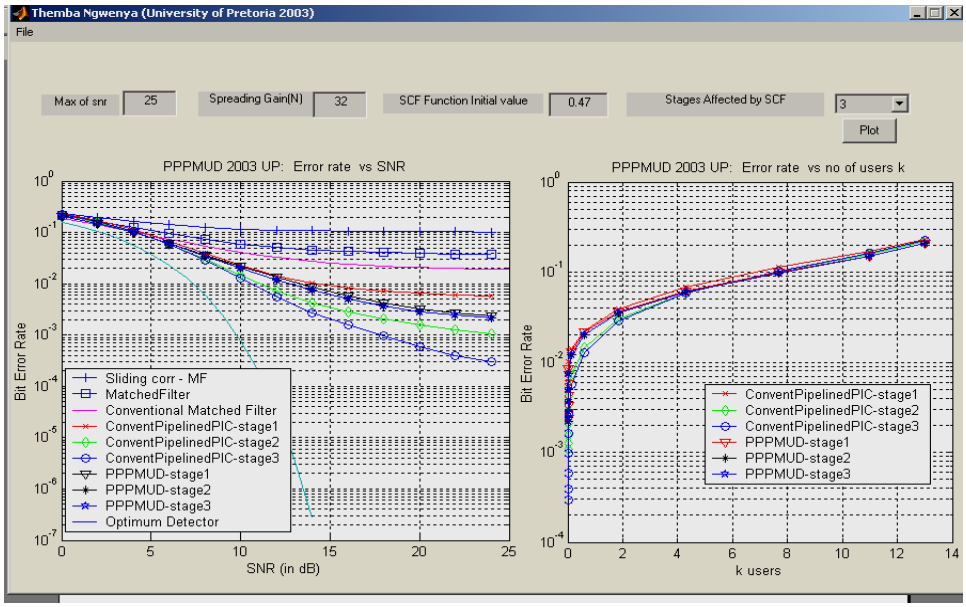

Figure 6-6 : A 3-stage analysis with SCF = 0.47 at constant k(k=13) on left, and constant SNR(SNR=25), on right

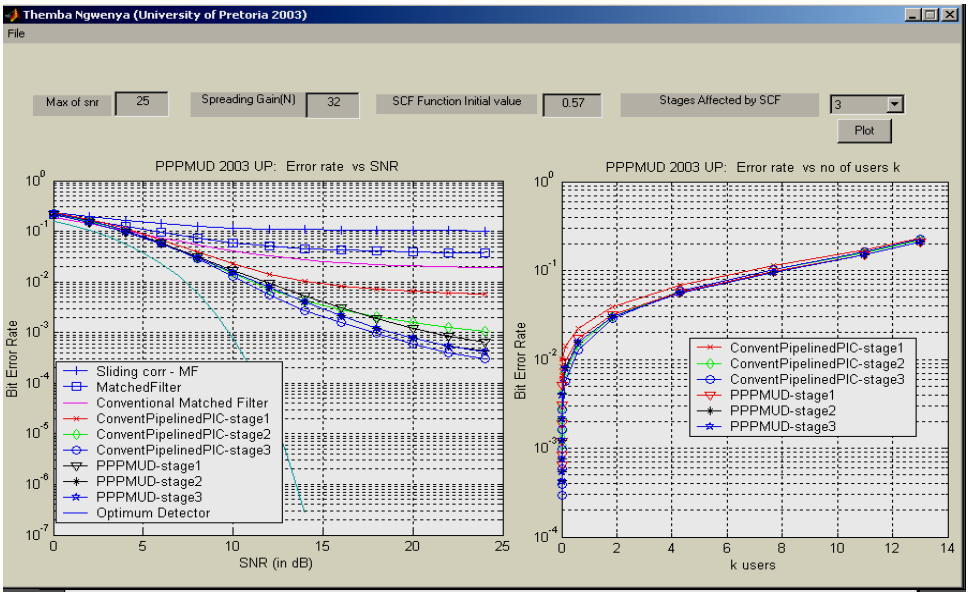

Figure 6-7 : A 3-stage analysis with SCF = 0.57 at constant k(k=13) on left, and constant SNR(SNR=25), on right

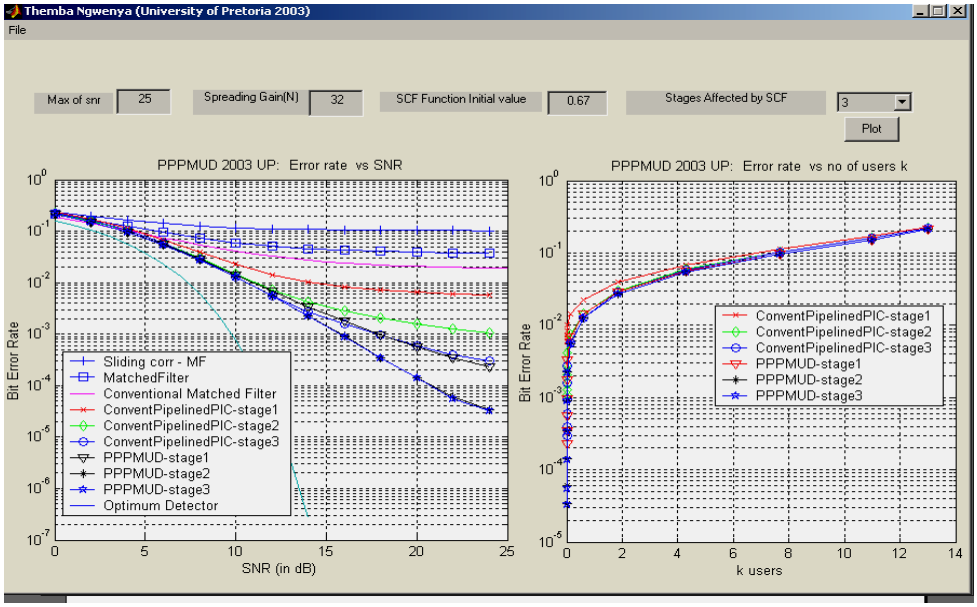

Figure 6-8 : A 3-stage analysis with SCF = 0.67 at constant k(k=13) on left, and constant SNR(SNR=25), on right

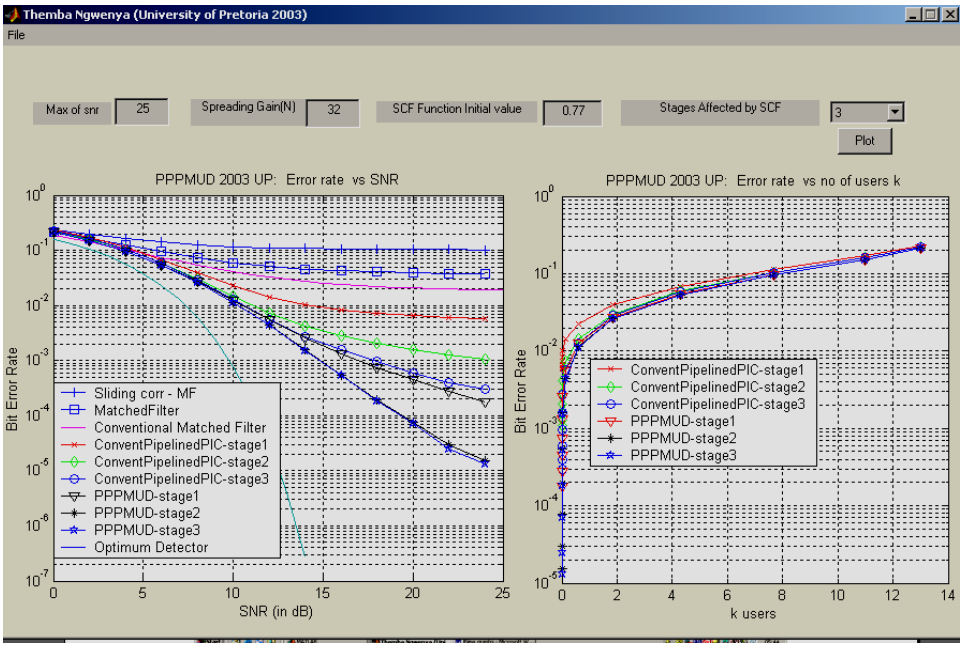

Figure 6-9 : A 3-stage analysis with SCF = 0.77 at constant k(k=13) on left, and constant SNR(SNR=25), on right

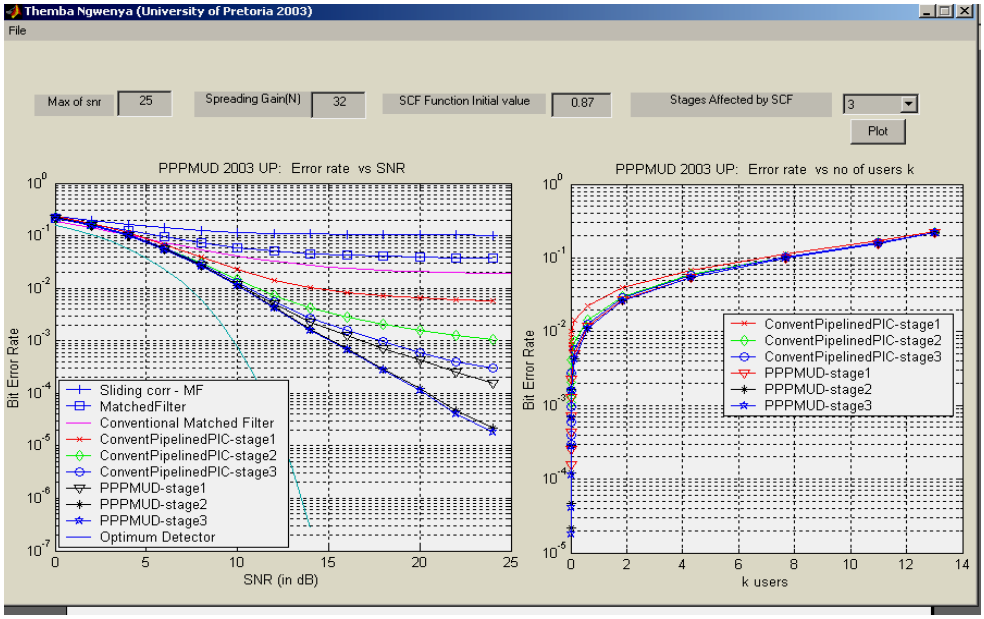

Figure 6-10 : A 3-stage analysis with SCF = 0.87 at constant k(k=13) on left, and constant SNR(SNR=25), on right

6.6.1.2 Compensated SCF_{UNV} Output

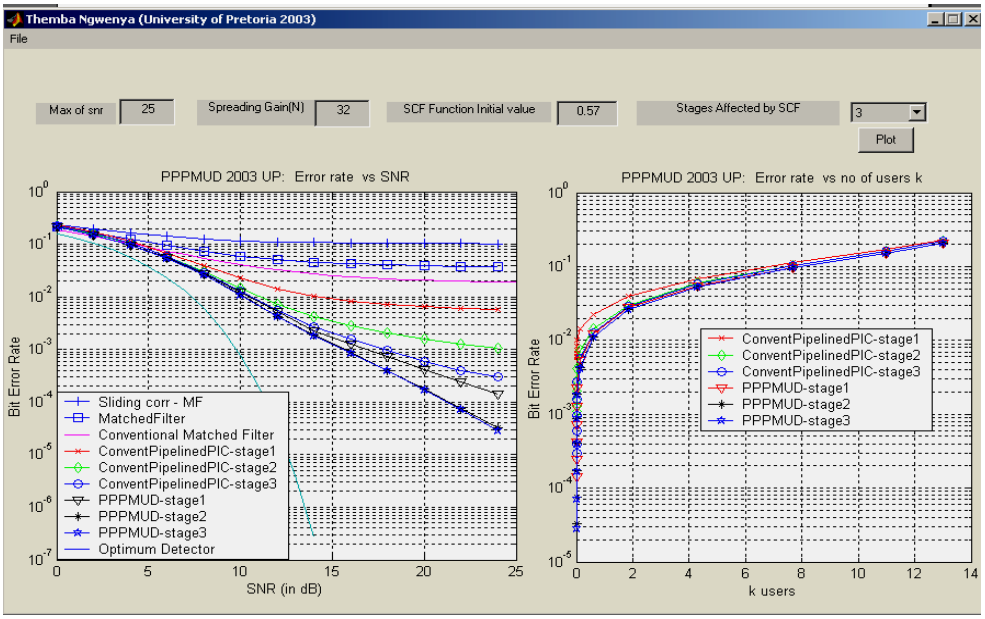

Figure 6-11 : A 3-stage analysis with $SCF_{UNV} = 0.57$ with compensator at constant k(k=13) on left, and constant SNR(SNR=25), on right

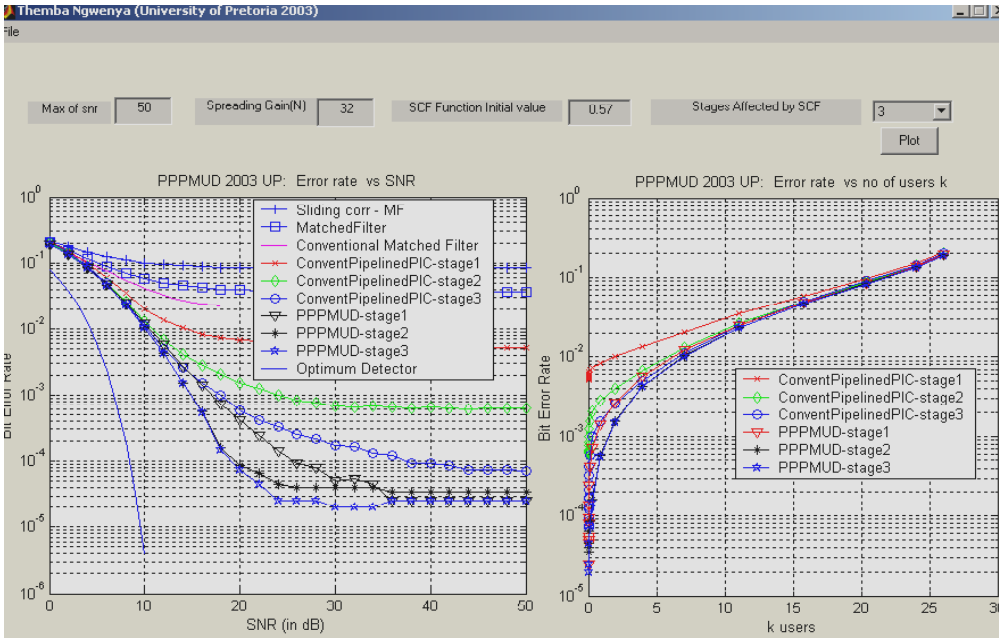

Figure 6-12 : A 3-stage analysis with $SCF_{UNV} = 0.57$ with compensator at constant k(k=26) on left, and constant SNR(SNR=50), on right

Figure 6-12 indicates the behaviour of the P^3MUD at high system loads.

6.6.2 SCF_{UNV} Compensator Mechanism

The structure of the compensator mechanism is as shown below:

Where *k* refers to the number of users, and *r*, is a function, (*see SCF.m in Addendum A*), which takes into account parameters such as *k*, SNR, the number of stages (1,2 or 3) of the Algorithm, and returns an adaptively adjusted SCF value depending on the number of users present.

```
if  k > 2 & k <= 8
    r = r + 0.1;

elseif  k>2 & k<=12
      r = r + 0.2;

elseif   k > 2 & k <=35
      r = r + 0.3;
else
      r=r;
end
```

Figure 6-13 : Structure of Compensator Mechanism

The compensator has come about due to the optimal SCF modeling exercise of Chapter 4. The modeling exercise indicated by how much an optimal SCF could be incremented or de-cremented based on the integer-variation of *k* in order to produce a good BER characteristic. Thus, the aim of the use of the compensator is to assist the P^3MUD algorithm in automatically adjusting the SCF_{UNV} in order to cope with sudden increases in the number of simultaneous users *k*. The mechanism, through the script above, will be able to adjust the SCF_{UNV} value accordingly.

6.7 Observations and Discussion

It is observed from Figures 6-6 to 6-10 that, for 3-stage analysis when the number of simultaneous users is 13, the rise in the SCF value used tends to give a good corresponding lower overall BER. This possibly means that for the value of SCF = 0.87, the operation of the algorithm in those conditions would be efficient if compared to the lower SCF values. The observations also indicate that as the number of users, *k*, rises, the BER will correspondingly increase, according to theory. Importantly, the results indicate that the incorporation of the SCF into the pipelined multiuser detector to produce the P^3MUD algorithm appears to be successful. It is also observed from Figure 6-10, that the 1-stage P^3MUD graph, (as well as the subsequent stage graphs), actually has a lower overall BER characteristic as compared to the conventional pipelined PIC graph. This again indicates the improvements offered by the P^3MUD algorithm.

The use of the SCF_{UNV} in conjunction with the compensator mechanism in Figure 6-11, show the improvement in overall BER as compared to the conventional pipelined PIC. An interesting note, is that the SCF_{UNV} -Compensator outputs are almost identical to that of Figure 6-10, when SCF = 0.87. This result concludes first of all that the compensator mechanism does work, and if written based on the results of the optimal SCF modeling, according to Figure 6-12, it will enhance the processing ability of the P^3MUD algorithm. This means that the SCF_{UNV} based system can also be modeled to mimic a system that offers low overall BER during the multiuser detection process. This translates into an overall performance improvement due to the low BER observed as compared to the conventional Bit-Streaming PIC.

CHAPTER 7

PROPOSED 2-STAGE P^3MUD

The simulation analysis in Chapter 6 has brought about an observation which motivates for a two-stage algorithm as opposed to the conventional three-stage process. This chapter justifies this observation with further analysis being performed. Once again, observations and a discussion are made of the proposed two-stage system.

7 PROPOSED 2-STAGE P^3MUD ALGORITHM IMPLEMENTATION

7.1 Motivation for 2-Stage P^3MUD

This has been motivated by the observations of the algorithm as it processes the various parallel interference cancellation stages. The analysis involved producing graphical outputs for non-compensated SCF at values 0.57 and 0.87. Then, additional outputs using the SCF compensator and the SCF_{UNV}. Also, outputs showing the variation of signal-to-noise ratio SNR, as well as the number of users k, were obtained for the 2-stage implementation. These are shown in Figures 7-1 to 7-8.

It should be noted that due to the time-frame of this dissertation, the MATLAB output code was not modified to reflect a particular cancellation stage process, i.e. at 1-stage cancellation, only the graphs pertaining to that particular stage(stage-1) should be shown to avoid any confusion when analyzing the results. Thus for stage 2 processing, only stage 1 and stage 2 graphs would be output, and so on.

7.1.1 Observations at Varying Detector Stages (1, 2 and 3) for SCF=0.57 & SCF=0.87 without Compensator Mechanism

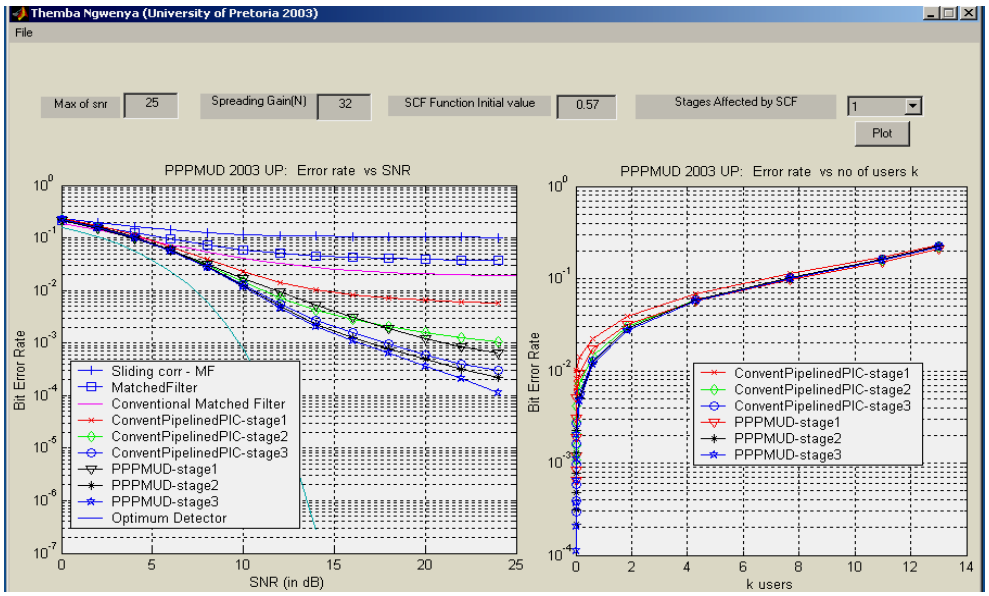

Figure 7-1 : A 1-stage analysis with SCF = 0.57 at constant k(k=13) on left, and constant SNR(SNR=25), on right

Centre For Radio & Digital Communication (CRDC)
Department of Electrical, Electronic & Computer Engineering
University of Pretoria

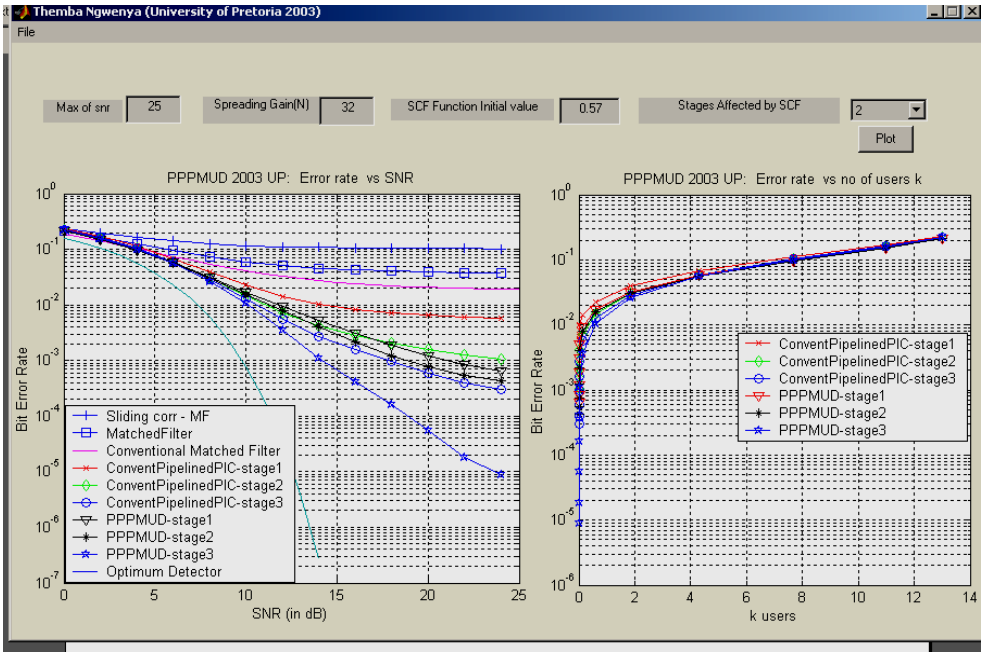

Figure 7-2 : A 2-stage analysis with SCF = 0.57 at constant k(k=13) on left, and constant SNR(SNR=25), on right

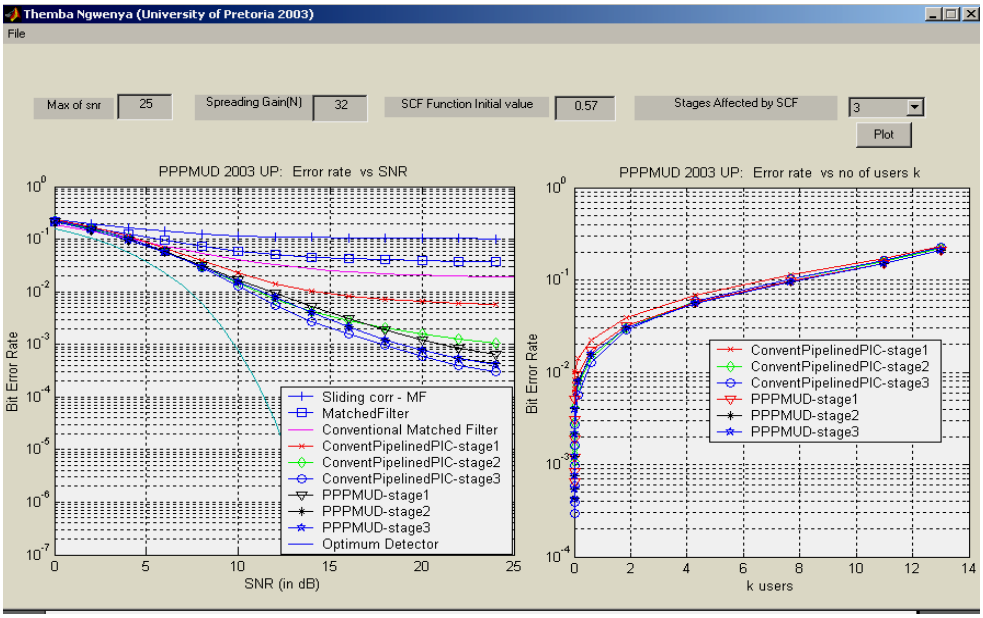

Figure 7-3 : A 3-stage analysis with SCF = 0.57 at constant k(k=13) on left, and constant SNR(SNR=25), on right

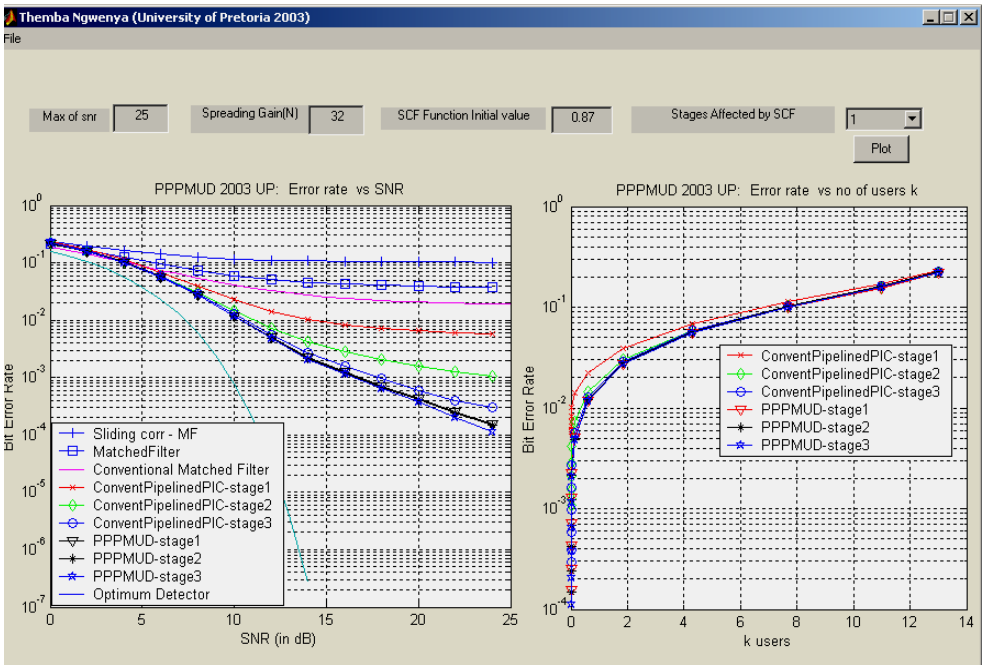

Figure 7-4 : A 1-stage analysis with SCF = 0.87 at constant k(k=13) on left, and constant SNR(SNR=25), on right

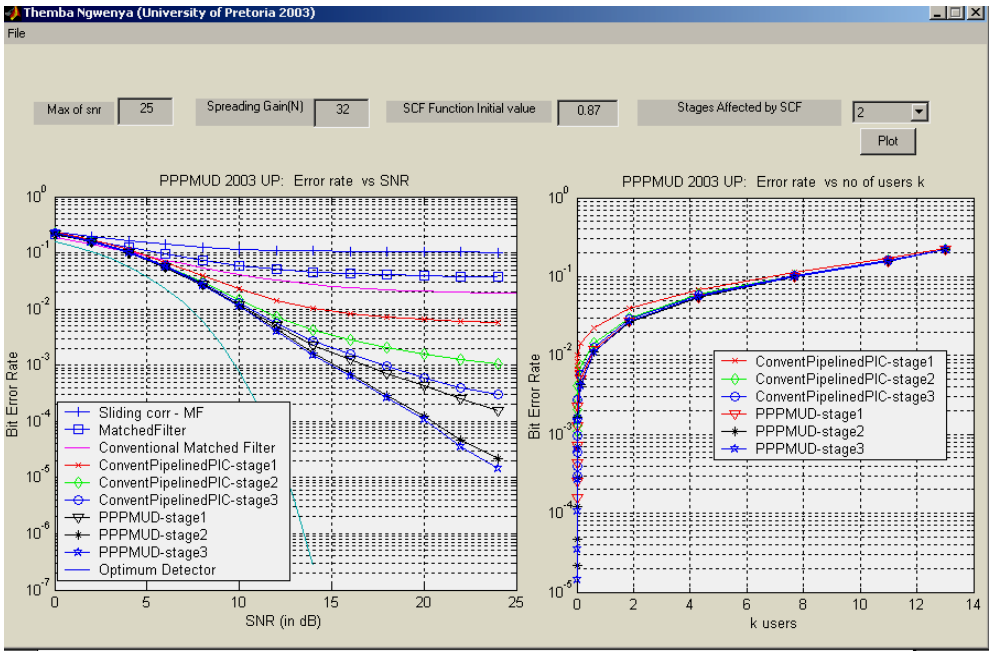

Figure 7-5 : A 2-stage analysis with SCF = 0.87 at constant k(k=13) on left, and constant SNR(SNR=25), on right

Centre For Radio & Digital Communication (CRDC)
Department of Electrical, Electronic & Computer Engineering
University of Pretoria

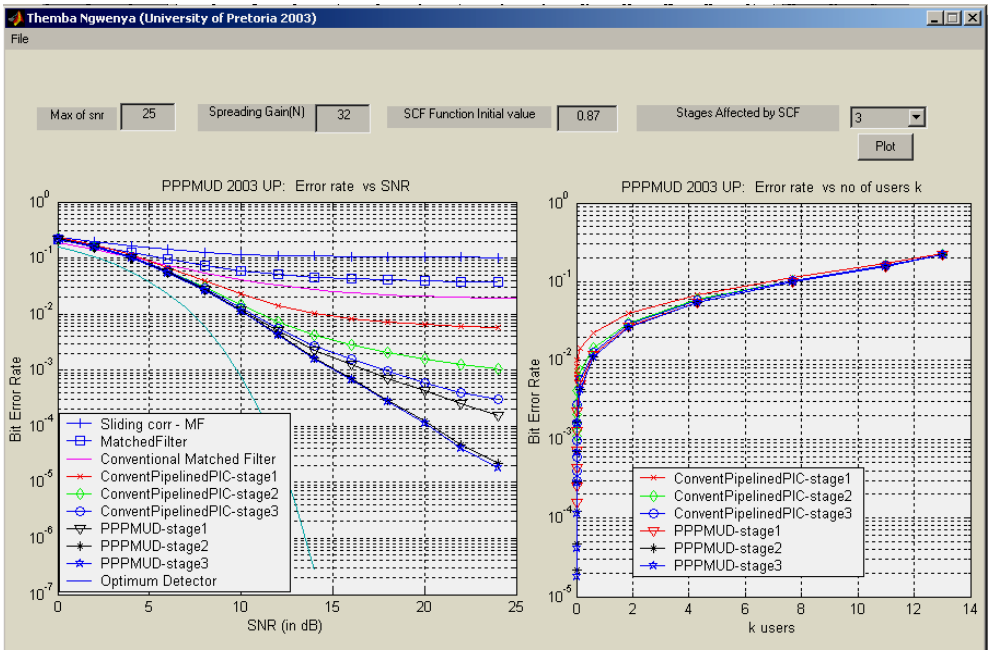

Figure 7-6 : A 3-stage analysis with SCF = 0.87 at constant k(k=13) on left, and constant SNR(SNR=25), on right

Centre For Radio & Digital Communication (CRDC)
Department of Electrical, Electronic & Computer Engineering
University of Pretoria

7.1.2 Observed Compensated SCF_{UNV} Outputs as Detector Stages vary (1,2 and 3)

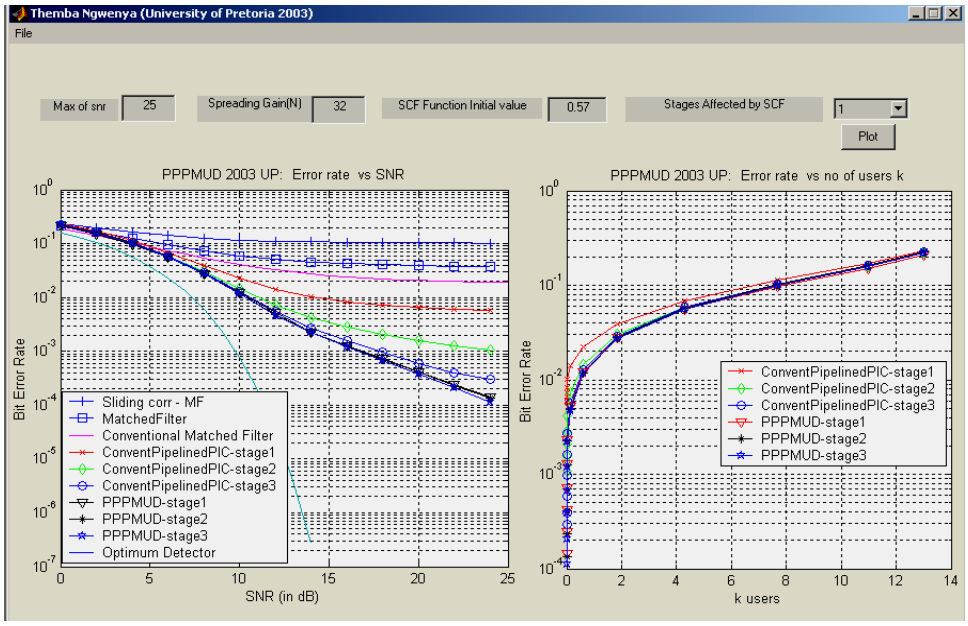

Figure 7-7 : A 1-stage analysis with $SCF_{UNV} = 0.57$ with compensator at constant k(k=13) on left, and constant SNR(SNR=25), on right

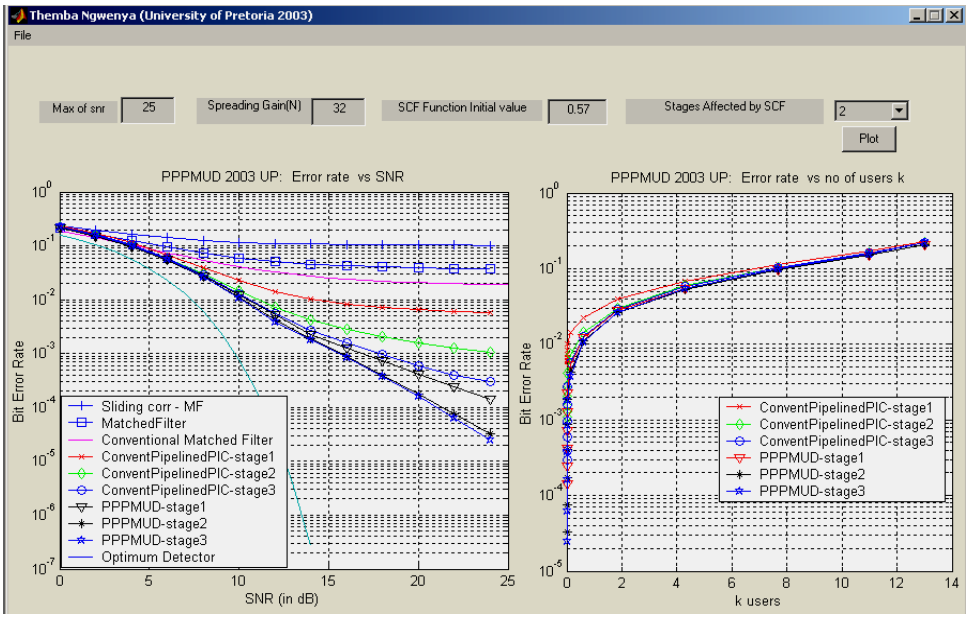

Figure 7-8 : A 2-stage analysis with $SCF_{UNV} = 0.57$ with compensator at constant k(k=13) on left, and constant SNR(SNR=25), on right

Centre For Radio & Digital Communication (CRDC)
Department of Electrical, Electronic & Computer Engineering
University of Pretoria

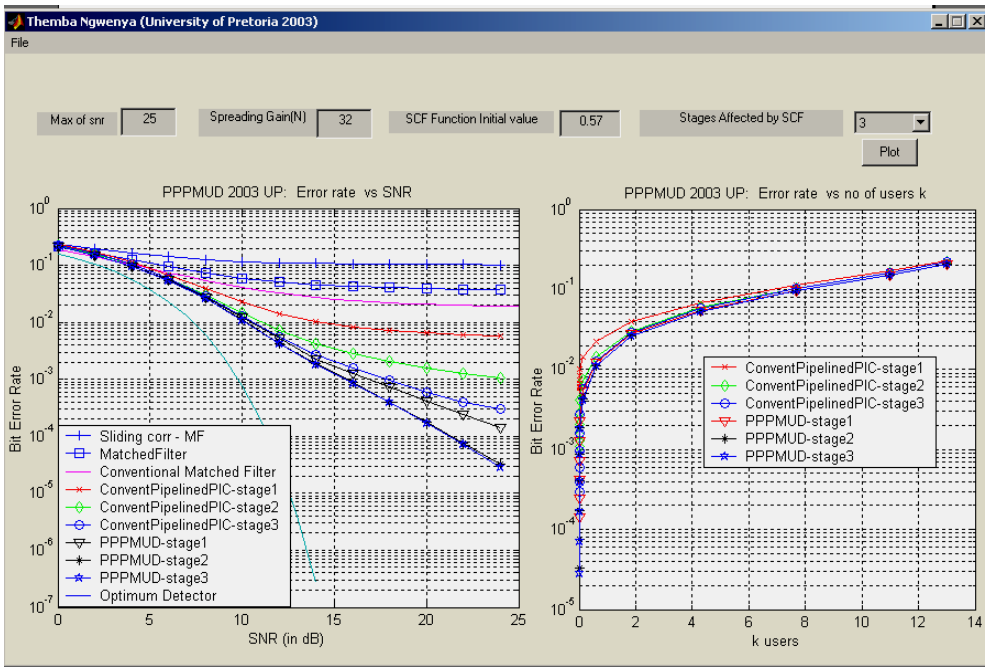

Figure 7-9 : A 3-stage analysis with $SCF_{UNV} = 0.57$ with compensator at constant k(k=13) on left, and constant SNR(SNR=25), on right

Figure 7-9, again indicated the apparent ineffectiveness of the third cancellation stage. The SNR and *k* was varied for the proposed two-stage P^3MUD, as shown in Figures 7-10 to 7-13.

Centre For Radio & Digital Communication (CRDC)
Department of Electrical, Electronic & Computer Engineering
University of Pretoria

7.1.3 Observed Compensated SCF_{UNV} with Varying SNR and *k* , for proposed 2-Stage Detector

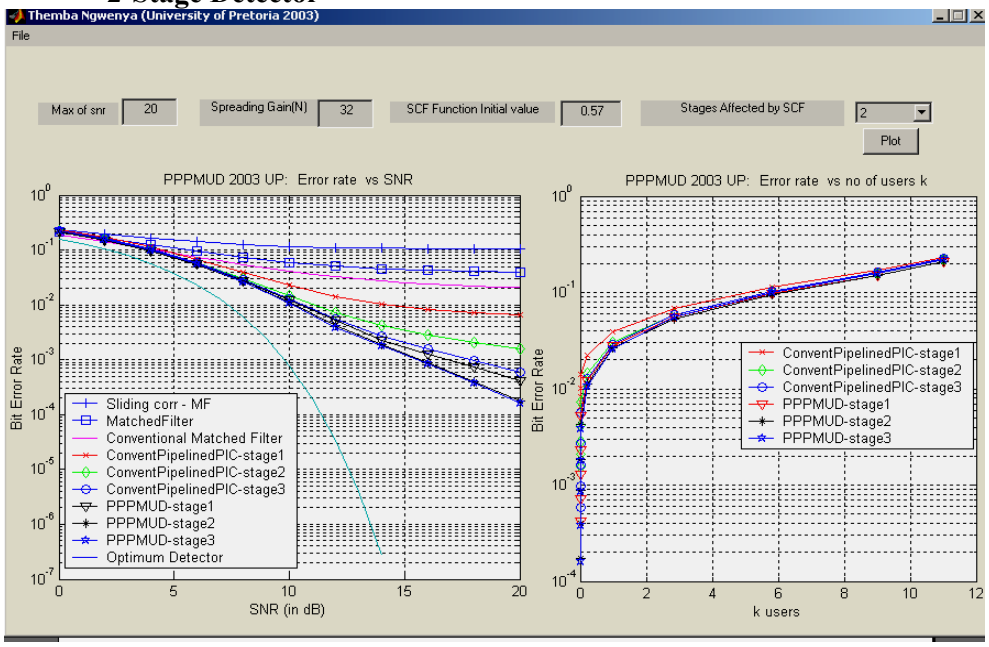

Figure 7-10 : A 2-stage analysis, $SCF_{UNV} = 0.57$ with compensator at constant k(k=11) on left, and constant SNR(SNR=20), on right

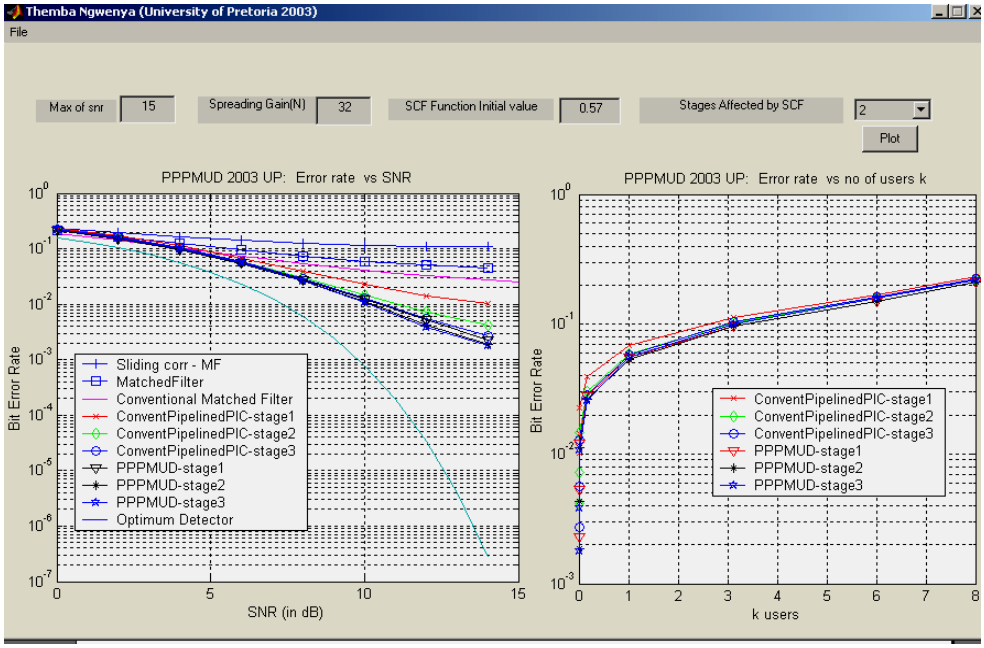

Figure 7-11 : A 2-stage analysis, $SCF_{UNV} = 0.57$ with compensator at constant k(k=8) on left, and constant SNR(SNR=15), on right

Centre For Radio & Digital Communication (CRDC)
Department of Electrical, Electronic & Computer Engineering
University of Pretoria

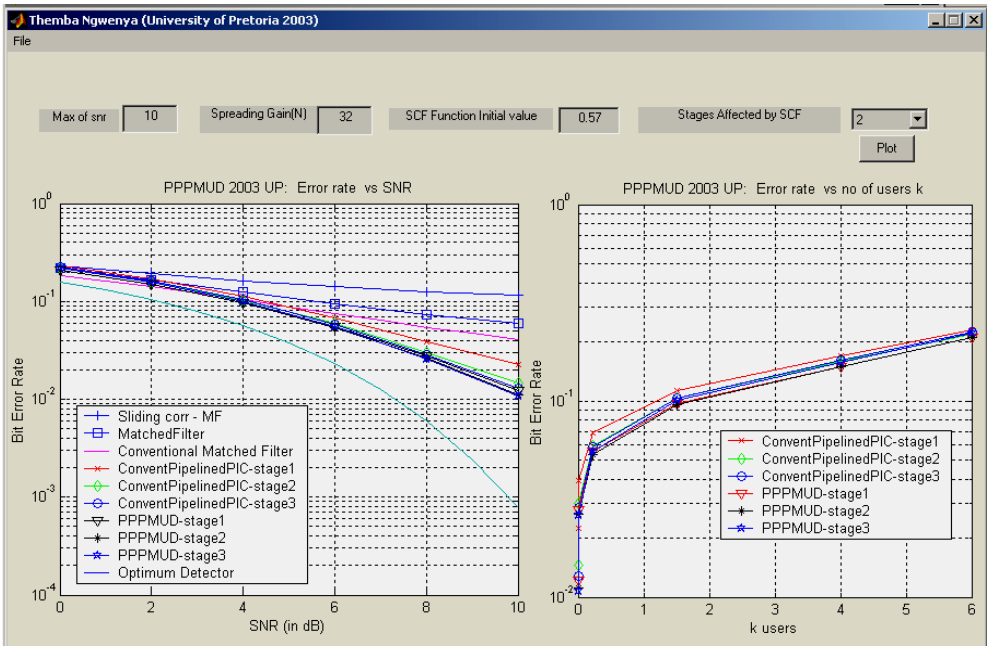

Figure 7-12 : A 2-stage analysis, $SCF_{UNV} = 0.57$ with compensator at constant k(k=6) on left, and constant SNR(SNR=10), on right

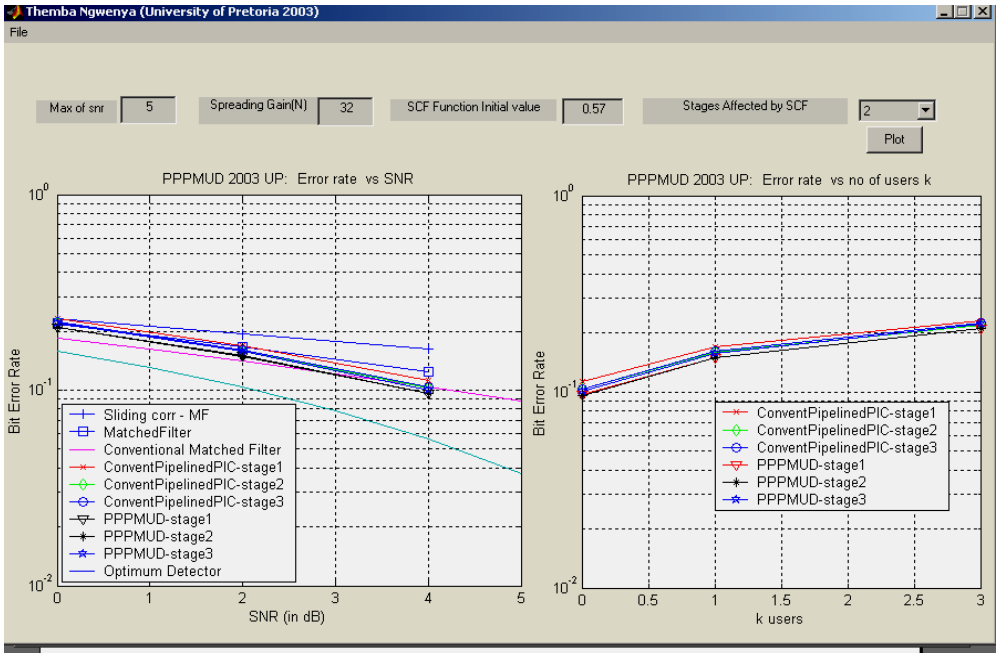

Figure 7-13 : A 2-stage analysis, $SCF_{UNV} = 0.57$ with compensator at constant k(k=3) on left, and constant SNR(SNR=5), on right

Centre For Radio & Digital Communication (CRDC)
Department of Electrical, Electronic & Computer Engineering
University of Pretoria

7.2 Observations and Discussion

Comparing the outputs when SCF= 0.57 and when SCF = 0.87, for varying stages (1,2 or 3) of algorithm processing, indicated for both cases how the third –stage affected the process. In both cases, it does not appear to add much to the overall multiuser detection process, (see Figures 7-1 to 7-6). The compensated outputs when using SCF_{UNV} and the compensator mechanism appeared to indicate the apparent in-effectiveness of the third-stage in the multiuser detection algorithm, (see Figures 7-7 to 7-9). This agrees with theory in that the algorithm has converged by the second-stage, and third-stage processing is futile or will not produce any significant changes in the detector output. Simulations were also done for 2-stage analysis for SCF_{UNV} with varying maximum SNR and maximum k, (see Figures 7-10 to 7-13).

On the whole, it is seen that the P^3MUD 2-stage output graphs produce lower overall BER as compared to the conventional 2-stage outputs. Figure 7-13 shows the ideal stage when BER is almost non-existent due to the small number of users, (3 in this case). The overall conclusion is that the P^3MUD algorithm can do most of the multiuser processing in the first stage, with the second-stage available to reinforce or enhance the process. The third-stage appears not to contribute much to the multiuser detection process, and thus is the foundation for the motivation of a 2-stage P^3MUD implementation. The new approach therefore has the advantage of considerable savings in computational complexity, with corresponding benefits in terms of less costly multiuser detection without performance loss compared to 3-stage P^3MUD schemes.

Centre For Radio & Digital Communication (CRDC)
Department of Electrical, Electronic & Computer Engineering
University of Pretoria

CHAPTER 8

SUMMARY , CONCLUSIONS AND RECOMMENDATIONS

This final chapter mainly summarises the overall study exercise, makes conclusions from the observations seen in Chapters 6 and 7, and in the future work discussion, makes possible recommendations of the way forward as regards the proposed P^3MUD algorithm.

8 SUMMARY OF DISSERTATION

This study exercise can be summarised by figure 8-1. The original SCF was mainly obtained to assist in decreasing the MAI during the PIC process. The proposed SCF_{UNV} does the same, but is implemented by being dynamically adjusted by the Soft Cancellation Mechanism or Compensator. A look-up table implementation had been proposed for the original SCF method [6].

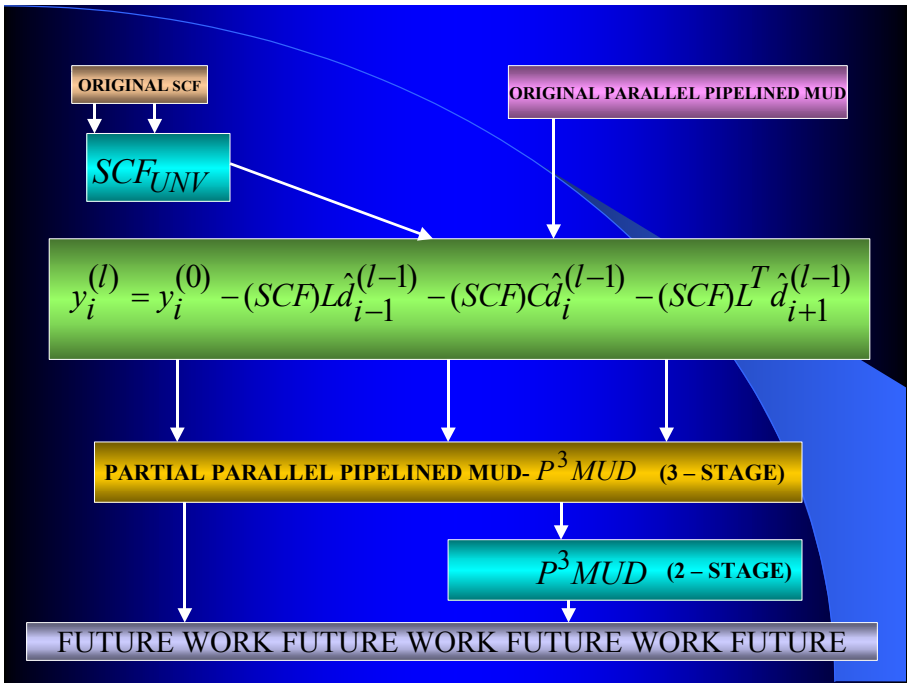

Figure 8-1 : Summary of Dissertation

The original Bit-Streaming Parallel Pipelined MUD was chosen to implement and test the SCF_{UNV} because it offered a computational advantage detector as compared to the computational complex matrix inversion earlier detectors [7]. Hence, the Partial Parallel Pipelined MUD or P^3MUD was created.

Centre For Radio & Digital Communication (CRDC)
Department of Electrical, Electronic & Computer Engineering
University of Pretoria

The simulations observed indicate that the presence of a soft cancellation factor in the conventional PIC algorithm does assist in improving the overall BER during the 3-Stage PIC detection process. It is also observed that the 3-Stage PIC BER is almost similar to 2-Stage PIC BER for the proposed P^3MUD ,thus 2-Stage P^3MUD is also proposed. Before the future work and recommendations is discussed, conclusions on the observations made in Chapters 6 and 7 are follow next.

8.1 Conclusions on 3-Stage P^3MUD (Chapter 6) Observations

The simulation results indicate that the presence of the P^3MUD algorithm, including the compensator mechanism, has helped improve the overall BER results for a 3-stage software implementation of the algorithm, as compared to conventional pipelined multiuser detection implementation. The initial aims of the study were to investigate the possible improvement techniques for WCDMA using multiuser detection and interference cancellation. The creation of the P^3MUD algorithm is a culmination of the original goals, as simulation analyses indicate an improvement offered to the multiuser detection process. As these tests alone may not be conclusive enough to test the integrity of this proposed algorithm implementation, a further suite of tests can be created, such as analyzing the effect of the multiuser detection process on an identified user, as the user's signal is processed, as opposed to the current simulation implementation where the strongest user or user of interest is randomly chosen. A possible hardware implementation of the P^3MUD algorithm would be to incorporate the code into the DSP and FPGA implementations of *Rajagopal* [7]. It would be interesting to see what the P^3MUD method would have on the hardware-software implementation, especially with the data rate requirements per user. According to this present study, the effect of the SCF in the Pipelined Multiuser Detector has been to lower overall processing BER. Thus, according to this theory, the data rates per user should also be increased in the hardware-

software implementation. This falls within the WCDMA requirements to provide higher data rates per user by enhancing the multiuser detection process.

Further work, as mentioned above, would be required before the practical implementation of the P^3MUD became feasible. This practical implementation of the P^3MUD algorithm could have far reaching effects, as already seen by the promising simulation results of this current study, in that the system would be able to absorb a large number of simultaneous users, and effectively process each of them without the processing algorithms failing, due to saturation of users. Currently, due to the enhanced processing power achieved in FPGA implementation over DSP, it is the favored implementation. In a practical WCDMA cellular system this would translate to the ability of the service provider to offer a wider range of high data rate services to a wider population, and hence increase the income base. Thus, the importance of the efficiency of the multiuser detection algorithms is noted as regards the effect it has on the overall improvements to the WCDMA system. Research, present and future, will be centered around how best to implement this process. This will also affect the successful implementation of the 4G (All IP), systems [12].

8.2 Conclusions on 2-Stage P^3MUD (Chapter 7) Observations

The analysis of the proposed 2-stage P^3MUD algorithm initially indicates the apparent in-effectiveness of the third-stage's contribution to the multiuser detection process. The advantages of a proposed 2-stage implementation is that it enhances the algorithm implementation, and practically, it does away with unnecessary processing power requirements using the same hardware. Thus, processing time is saved, which on the surface may appear minute, but in cases where algorithm processors have to deal with very large numbers of simultaneous users[5], this constitutes a significant saving. This effect adds to the overall improvement in WCDMA system performance.

[5] The more users a system is able to process will mean the individual data rates of the users is low, whilst the opposite is true in the case of few users in the system.

On the whole, it appears that the 2-stage P^3MUD detector is a possibility. Thus, not only is this study proposing the P^3MUD algorithm, but also the 2-stage P^3MUD detector, which should offer performance improvements over the conventional pipelined multiuser detector algorithm.

8.3 Recommendations and Future Work

A possible start would be to practically implement the P^3MUD algorithm to see how it compares to the hardware-software implementation of Rajagopal [7], and also to establish how practically realisable it would be to reduce the number of multistage algorithm stages from three to two.

Another key area for further work should be to investigate the performance of P^3MUD in a multipath channel environment using the recommended WCDMA channel models.

A lookup-table implementation, Rennuci [6], of the SCF part of the P^3MUD algorithm would be interesting, to see how it compares to the compensator method used in this present study.

Another implementation path would be using the differential multistage detector Rajagopal *et al.* [36], to implement the P^3MUD algorithm. The differencing multistage differs from the multistage algorithm in that, instead of dealing with each estimated bit vector $\hat{d}^{(l)}$, we calculate the difference of the bits in two consecutive stages, i.e the input of each stage becomes, $\hat{x}^{(l)} = \hat{d}^{(l)} - \hat{d}^{(l-1)}\left(j = 1.2,\ldots,K\right)$, where $\hat{x}$ is called the differencing vector.

Further work could evolve around implementing the algorithm such that a single user's signal can be analyzed from a background of multi-user signals. This would assist in determining the effect of the algorithm per user.

A neural network implementation could also be possible, as it would involve designing/training the multiuser detector so that it responds according to sets of input asynchronous user/training data.

The suppression of MAI in the UMTS multi-path propagation environment could also be another area of possible future work.

The possibility of further work in this research appears endless, which further enhances the importance that has been attached to the study of this section of the receiver architecture.

The overall goal of this and similar type research would be to improve the performance of WCDMA systems.